Functionalization of Biomaterials with Atomic Layer Deposition for Tunable Performance Enhancements

By

Arghya Kamal Bishal

B. Tech., Haldia Institute of Technology, West Bengal University of Technology, India, 2013

THESIS

Submitted as partial fulfilment of the requirements
for the degree of Doctor of Philosophy in Bioengineering
in the Graduate College of the
University of Illinois at Chicago, 2018

Chicago, Illinois

Defense Committee:

Christos G. Takoudis, Chair and Advisor

Cortino Sukotjo, Department of Restorative Dentistry

Michael A. Stroscio

Salman R. Khetani

Mathew T. Mathew, Department of Biomedical Sciences, UIC College of Medicine at Rockford

Gregory Jursich

This thesis is dedicated to

my mother, Mala Bishal

my father, Arup Kumar Bishal

and to my beloved wife, Anindita Sarkar

without whom it would never have been accomplished. Their constant encouragement, unconditional support and love have motivated me throughout my journey.

ACKNOWLEDGMENTS

First and foremost, I want to thank my advisor and dissertation chair, Dr. Christos G. Takoudis for all his insightful guidance and mentorship he provided throughout my graduate studies. He encouraged and motivated me to push myself beyond my ability and thus enable me to perform my best. His openness to “any new idea” and “collaborations” facilitate all my interdisciplinary projects to be completed successfully at an elite level. I would like to thank my co-advisor, Dr. Cortino Sukotjo for all his support and helpful discussions. He helped me to understand the real clinical problems which could be solved through engineering and this added a great value to my research by having direct medical applications. I would also like to thank my other committee members, Dr. Michael A. Stroscio, Dr. Salman R. Khetani, Dr. Mathew T. Mathew and Dr. Gregory Jursich for their thoughtful assistance and for taking time out of their busy schedules to serve on my graduate committee.

I thank my group alumni Dr. Sathees K Selvaraj, Dr. Arman Butt and all AMReL and IBTN lab members for their generous help and support during my doctoral study. Thanks to bioengineering departmental staffs, Susan Lee, Jessica Mejia and a special cordial thanks to Lukasz Zientara, for all kind help. I thank UIC Physics Shop, UIC Glass Shop for custom-built apparatus and supplies, and I also thank UIC Research Resource Center for their characterization facilities.

Financial support from the UIC Department of Bioeingeering and the National Science Foundation (NSF CBET 1067424 and DMR 1307052) is gratefully acknowledged.

CONTRIBUTION OF AUTHORS

Chapter 1 is a brief introduction and overview of research technique used in this dissertation. Chapter 2 are adapted from the manuscripts where I am the primary author. Section 2.1 is under review for publication, where Dr. Alvin G. Wee contributed in raw sample preparation and color measurements presented in TABLE I, Dr. Valentim A R Barão helped in artificial aging experiment, Dr. Judy Chia-Chun Yuan contributed in statistical analysis of data and Dr. Richard Landers helped to collect data plotted in Figure 5. Section 2.2 is adapted from my published manuscript (1) for which I am the primary author. Section 2.3 is under review for publication, where Dr. Jacob R Jokisaari and Dr. Robert F Klie helped in collecting data for Figure 14. For Section 2.4, Nickolas Anderson helped in collecting data of electrical measurements presented in TABLE V and Figure 25, Dr. Ahyeon Koh and Sai Ken Ho Hung helped in collecting data presented in Figure 26. Section B. 1 is adapted from my published manuscript (2) for which I am the primary author. For Section B. 1 and B. 2 John Grotberg helped in sample polishing.

As a primary author, I performed all other experiments and wrote the manuscripts. Dr. Takoudis helped with project planning, supervising, continuous discussions and correcting of manuscripts. Co-advisor, Dr. Cortino Sukotjo contributed through helpful discussions, design of biological experiments and reviewing manuscripts. Committee member, Dr. Mathew T. Mathew were also instrumental in reviewing and correcting manuscripts.

TABLE OF CONTENTS

TABLE OF CONTENTS (Continued)

CHAPTER **PAGE**

LIST OF TABLES

TABLE **PAGE**

LIST OF FIGURES

LIST OF FIGURES (Continued)

FIGURE **PAGE**

LIST OF FIGURES (Continued)

FIGURE **PAGE**

LIST OF FIGURES (Continued)

FIGURE **PAGE**

LIST OF FIGURES (Continued)

FIGURE **PAGE**

SUMMARY

Biomaterials are engineered to interact with biological systems for a variety of therapeutic and diagnostic clinical purposes. The biomaterial surface plays a significant role in its interaction process with surrounding living environments. Therefore, successful use of a biomaterial relies on appropriate functionalization of the surface. The surface of biomaterials can be modified utilizing different surface treatments in order to obtain desired tunable surface properties for improved functionality. Among the different available surface engineering techniques, Atomic Layer Deposition (ALD) is a unique and powerful approach of nanotechnology to functionalize surfaces through deposition of very thin (few Å or nm thick) films of metal/metal oxide.

ALD was developed in the 1960s and it was primarily focused on depositing thin films for applications in semiconductor industries. ALD technique often uses higher temperature than that required for biomaterial substrate and applications. However, ALD is increasingly becoming an important technique to enhance surface properties of biomaterials since low temperature ALD has become increasingly used. Low temperature ALD facilitates deposition of metal and/or metal oxides thin film on biomaterial surface to functionalize the surfaces at the nanometer length scale without causing thermal damage/alteration of the original materials.

This Thesis focuses on the development and optimization of low temperature ALD processes to improve functionalities of different biomaterials by depositing thin film of metal/metal oxides at lower substrate temperature (i.e., room or near room temperature), various surface characterizations to investigate the physico-chemical properties of the resulting ALD functionalized biomaterials, and some preliminary applications to study the enhanced performance of those surface-functionalized biomaterials.

A near room temperature ALD was established to deposit thin film of titanium dioxide (TiO_2) on a biopolymer, polydimethylsiloxane (PDMS), widely used in extra-oral maxillofacial implants. ALD-TiO_2 thin film was deposited on pigmented PDMS surface to protect the color degradation of this polymer from weathering especially ultra violet exposure. PDMS specimens were subjected to artificial aging, and color measurements were performed before and after ALD-TiO_2 deposition, and before and after aging. A color-stable PDMS was achieved using ALD-TiO_2 nano-coating and this coated PDMS showed 44% less discoloration compared to control PDMS.

A room temperature ALD process was developed to deposit TiO_2 thin film on commercially available collagen barrier membranes, used in dentistry for bone grafting procedure. A liner growth at a growth rate of 0.06 nm/cycles was achieved at this room temperature ALD-TiO_2 process. Chemical analysis revealed that the pure TiO_2 thin film was amorphous in nature. The fibers of the collagen membranes were uniformly and conformally coated by TiO_2 using this room temperature TiO_2-ALD process; thus, the fiber became thicker which made the membrane denser. Bioactivity of this ALD-TiO_2 coated membranes was also studied. TiO_2 coated collagen membrane showed enhanced biocompatibility and biomineralization capability when compare to non-coated control collagen membranes.

Low temperature ALD of platinum (Pt) thin film was studied on collagen membranes with a goal of achieving conductive biomaterials for potential applications in biosensors. A thin, continuous and conductive Pt film was achieved at 150°C. A buffer layer of ALD-TiO_2 thin film was found to improve the nucleation and surface coverage of Pt film on collagen, thereby turning collagen into a conductive biomaterial. Electrical measurements confirmed the ALD-Pt coated

collagen to be conductive and its average volume resistivity was stable after bending the sample over different radii of curvature ranging from 10.5 cm to 1.7 cm and straining the samples with 2000 to 16000 microstrain. Therefore, this flexible, conductive biomaterial could be used in the fabrication of implantable biosensors.

1. INTRODUCTION

Biomaterials are being broadly utilized in medical devices and modern medicines. These biomaterials can be synthesized in laboratory or can directly be derived from natural resources. The biomaterials constitute whole or part of a biomedical device or a living structure which can be utilized to execute, improve or restore a natural function. The surface of a biomaterial largely control the series of interactions occur between the surface of biomaterial and the surrounding living environment after the implantation of biomaterial. (3)

1.1. Surface Functionalization – Thin Film

Primarily, most of the available biomaterials do not have the appropriate surface functions and properties suitable for desired functionality. Therefore, appropriate surface modifications and functionalization are required to enhance the performance of biomaterials. (4) In modern surface science, nanotechnology is a potent tool to nano-functionalize the surface incorporating nano-structural features into materials. As a result, it is significant to investigate the potential of nanotechnology in nano-functionalizing surface, and to characterize the improved properties of surface-functionalized biomaterials.

Thin films and coatings can be deposited as a surface modification technique to nano-functionalize the surface of biomaterials. (5) Based on the nature of deposition process, the available surface coating or thin film deposition techniques can be broadly categorized into two main groups (Figure 1): physical (e.g. sputtering, spraying, evaporation etc.) and chemical (e.g. sol-gel in liquid phase, chemical vapor depositions in gas phase). (5) Among these techniques, ALD offers unique aspects in depositing very thin film of metal and/or metal

oxides, nitrides chemically, with precision control at atomic or molecular level to functionalize complex nanostructure of materials. (6) In this thesis ALD was used to deposit thin film of metal oxide and metal on surfaces of different biomaterials to render desirable properties.

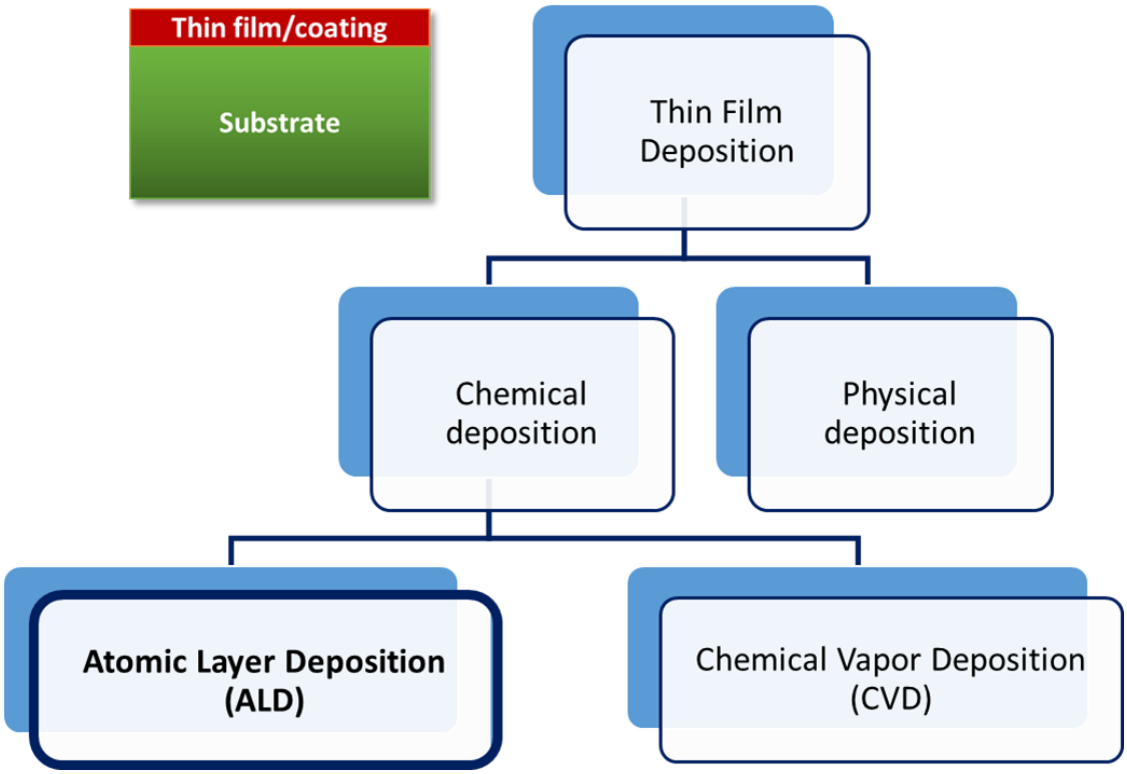

Figure 1: ALD thin film for surface functionalization of substrate over the other available deposition techniques.

1.2. History of ALD

Two different research groups independently developed the ALD technique back in 1960s and 1970s. (7) The first concept of ALD was introduced in 1960s by Prof. Aleskovski et al in Russia and at that time ALD was named as “Molecular Layering”. (8) In 1974, Dr. Tuomo Suntola and his colleagues independently developed this same thin film deposition method under the name “Atomic Layer Epitaxy” in Finland, with the focus of improving zinc sulfide

(ZnS) films quality to be used in thin-film based electroluminescent flat-panel displays, was first lit in 1982 in the display board at Helsinki Airport. (9-11) More than 2 million electroluminescent displays have been produced since the development of ALD. (9) In 1980s, great efforts were made to prepare epitaxial compound semiconductors and III-IV compounds through application of ALD, however no real progress/benefits were obtained using ALD since group III alkyl compounds and group V hydrides being chemically unstable. (12) For more than two decades the industrial applications of ALD remained marginal. (13) After this lag period, the large take-off of ALD began in the middle 1990s and the semiconductor industry was the major driver behind this renaissance of ALD. (12; 13) A new thin film deposition method was required to facilitate the miniaturization of device dimension and increasing aspect ratios in integrated circuits (IC). With high precise control over film thickness and tunability in chemical composition of film at atomic level, ALD gained the most focus to cater to the needs of silicon-based microelectronics processing. (12)

1.3. Atomic Layer Deposition Process

ALD is an innovative approach of nanotechnology which offers unique aspects in depositing thin film, over the other available surface modification techniques. ALD enables us to deposit conformal, uniform thin film layer by layer and provides a precise control over film thickness and composition due to the self-limiting chemical reactions. (6) A layer can be grown as thin as one atom thick to few nanometers using ALD. Moreover, to uniformly deposit a thin film around complex, high aspect ratio, three-dimensional (3D) nanostructure ALD possibly the only legitimate approach. (14)

ALD is a vapor phase chemical deposition process of thin film and in this cyclic process substrate surface is exposed to the reactant molecules sequentially. One complete ALD cycle consists of four sub-steps, in case of ALD with 2 reactants (Figure 2): precursor exposure (pulse), precursor purge, oxidizer exposure (pulse) and oxidizer purge. Deposition temperature, precursor temperature, reactor chamber pressure, pulse and purge time of precursor and oxidizer – all these parameters of ALD can be tuned accordingly to obtain optimal film growth rate. Due to the cyclic manner of ALD process, deposited film growth rate is directly related to the number of ALD cycle and typically the film thickness increases linearly with the increase in number of ALD cycle. Appropriate selection of precursor – oxidizer system is also required considering optimal nucleation and saturation of coating material on the surface of the selected substrate.

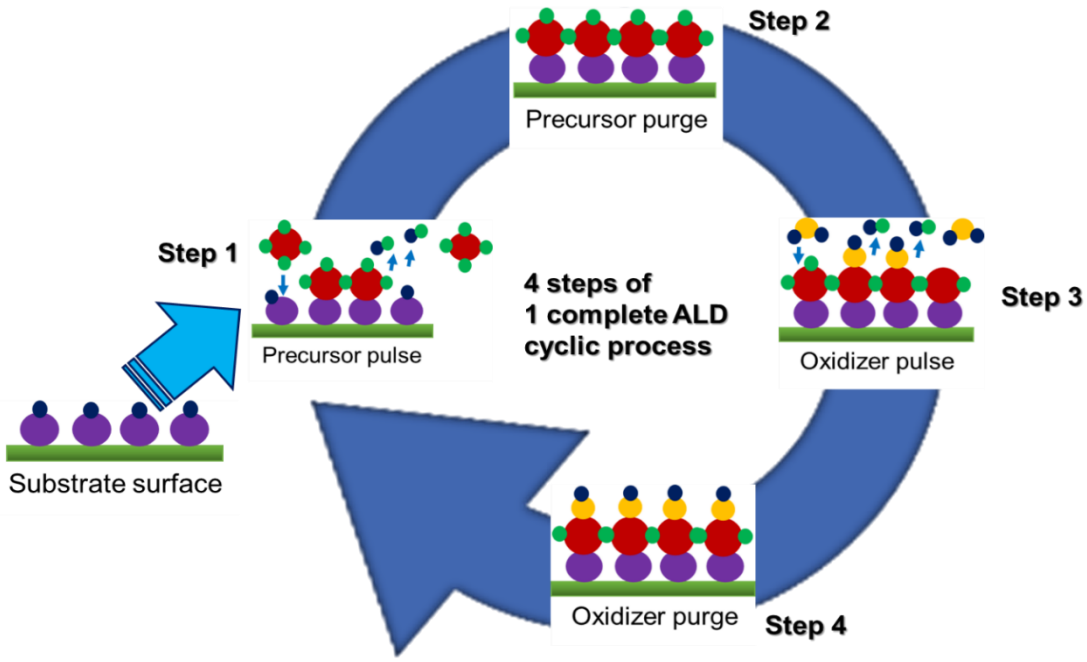

Figure 2: A schematic representation of the basic principle of a ALD cyclic process consists of four steps.

ALD is a modified version of the CVD process. The gas phase chemical reactions of ALD relies on the chemisorption process. Unlike physisorption process where the weak van deer Waals forces keep the precursor molecules and substrate surface groups together (15), in this process a strong ionic or covalent bond is formed between reactive groups present on the substrate's surfaces and the precursor molecule, and thus this process is "independent of line-of-sight" which enables to deposit thin film uniformly and conformally on complex nanostructures. (16-18) The microstructure of deposited thin film and the growth rate is tunable using reaction temperature, pressure and saturation of the reactants. (16-18)

1.4. Low Temperature ALD for heat-sensitive organic substrates

ALD is being widely used in semiconductor industries. In those applications, ALD is performed typically at higher temperature to obtain high purity and optimal film growth. On the other hand, biomaterials or biological substrates are heat fragile and they denature at high temperature. For these kind of heat-sensitive materials, low (room or near room) temperature ALD is needed to deposit thin film for their surface modification. Appropriate metal precursor and oxidizer system is required which allows the low temperature thin film deposition through ALD. (19) For each cyclic chemical reaction of ALD certain amount of activation energy is required and typically that energy is supplied from heat energy in case of thermal ALD. Metallo-organic precursors typically have low binding energy and as a results it requires less substrate temperature to initiate the chemical reactions. (20-22) Precursors with adequate volatility, high reactivity, completely self-limiting surface reactions are necessary to achieve pure ALD film at low temperature. (12; 23-25) Among the metallo-organic precursors, metal amides (e.g. alkyl amides) are highly reactive towards hydroxylated surface (-OH) compared

to metal halides as metal-nitrogen bond is significantly weaker compared to metal-halide bond. (23; 26)

First low temperature ALD was reported to deposit Al_2O_3 on polymer bottle at 33°C. (27) But so far to deposit TiO_2, the lowest ALD deposition temperature was reported 70°C. (28; 29) Previously, ALD on different biological fibrous substrate such as cellulose fibers from cotton(30) and paper, (31) spider silk, (32) egg shell membrane (28; 29) were reported and the lowest deposition temperature was 60°C. The room temperature ALD is generally facilitated with plasma enhanced or radical enhanced. As per my best knowledge, a room temperature ALD of TiO_2 was developed for the first time from a novel alkylamide titanium precursor and ozone oxidizer using a custom ALD reactor. (1)

1.5. Thesis Overview

This thesis is divided into two sections. The first section (Introduction) describes the evolution, basic principles of ALD and low temperature ALD process, and the second section (Results and Discussion) describes the application of low temperature ALD to functionalize the surfaces of different biomaterials. Chapter 2.1 summarizes the low temperature ALD of TiO_2 thin film on PDMS polymer surface to protect the surface from color degradation while exposed to aging. Chapter 2.2 presents the development of a room temperature TiO_2-ALD process and its application to modify the surfaces of collagen membranes. The investigation on the biocompatibility and biomineralization capability of this room temperature ALD-TiO_2 coated collagen membrane has been included in Chapter 2.3. Finally, Chapter 2.4 discusses the low temperature ALD process to deposit Pt thin film on collagen membrane followed by surface characterizations.

2. RESULTS AND DISCUSSION

2.1. ALD of TiO_2 on Polydimethylsiloxane (PDMS) polymer

2.1.1. Introduction

Silicone, also known as polydimethylsiloxane (PDMS), is one of the widely used polymers in the biomedical industry.(33) It is popular for its inertness, high thermal stability and usability (at least from −100°C up to +100°C),(34) unique flexibility (the shear modulus between 100 kPa and 3 MPa),(35) high gas permeability, high compressibility and normally non-toxic nature.(36) In biomedical science, it is used in different applications such as from facial prostheses to parts of a biomedical implant and devices like catheter, artery regeneration due to its inertness and good cellular responses. Over 50 years, these silicone elastomers are materials used in fabricating extra-oral maxillofacial prostheses; one option currently available to rehabilitate patients with craniofacial defects occurred due to surgical treatment of cancer, trauma or birth defects on those facial regions.(37-41) However, the principal concerns of clinicians and patients who undergo this prosthetic approach of rehabilitation are the longevity and maintenance of these facial prostheses.(37-40) The mean life span of silicon-based facial prosthesis ranges from 1.5 to 3 years, while only 4.8% of prostheses last longer than 2 years.(38; 42-45) The most common reason behind replacement of facial prostheses is the discoloration of the silicone elastomers.(38; 46-48) This color deterioration of the silicone elastomers is primarily caused by exposure to weather conditions as the external environmental factors like solar radiation, temperature and water.(37; 38; 49-53) Despite being a smaller portion of solar radiation, the ultraviolet

(UV) radiation has a large impact on the color degradation of extra-oral maxillofacial materials.(41)

For facial skin, color, a phychophysical sensation in the eyes provoked by visible light and interpreted by brain, is the most pronounced appearance attribute.(54) The three dimensions of color are defined as hue (color name), value (lightness, from black to white) and chroma (color strength, from pale to strong).(54) Color notations are frequently defined using CIELAB system developed by CIE (Commission Internationale de L'Eclairage, International Commission of Illumination) where the overall color difference attributed from all the color coordinate differences, is denoted as ΔE*.(55) The clinical significance of the color-difference can be determined by two types of judgments: one is "can the color difference be seen?"-denoted as "Perceptibility", and the other one is "is the difference in color acceptable?"-denoted as "Acceptability".(54) Therefore, in dental research it is essential to evaluate perceptibility and acceptability thresholds to determine the color-difference of maxillofacial prosthesis with respect to the established thresholds. For maxillofacial prosthetic silicone with light skin-colored, the perceptibility and acceptability thresholds was found to be ΔE of 1.1 and 3.0 respectively,(54) which were used in this study for determining the color differences of silicone elastomers.

In industry, nano-oxides such as titanium dioxide or titania (TiO_2), zinc oxide (ZnO), cerium oxide (CeO_2) are widely used as inorganic UV absorbers because the particle size of these nano-oxides are smaller compared to the wavelength of UV light (290-400 nm). Thus, these nano-oxides are capable of reducing harmful damage from UV rays by absorbing and scattering the incident UV light.(53) Besides these nano-oxides, organic UV

absorbers, the ultraviolet light absorbers (UVA) and hindered amine light stabilizers (HALS) are also used in color stability. This is due to UVA can absorb harmful UV radiation by dissipating it as heat and HALS can act as free-radical scavenger, preventing polymer degradation thereby.(53) Several studies were conducted to evaluate the effects of nano-oxides, UVAs, HALS and opacifiers in protecting the color of silicone facial prosthesis materials subjected to accelerated artificial aging involving different environmental factors especially UV.(41; 56; 57) Han et al reported that the nano-oxides particularly 1% nano-CeO_2 and around 2-2.5% nano-TiO_2 was effective in preventing color change of the silicone A-2186 materials.(41) The effect of UVA and HALS on color stability of silicone A-2186 was evaluated by Tran et al, and they reported that the color stability was improved by using the UVA and HALS.(56) The effect of opacifiers on color stability of a maxillofacial elastomer (MDX4-4210) was also investigated in a similar study. The authors found that the opacifiers protected silicone from color degradation and titanium white opacifier was the most color stable.(57) However, the safety of using these UVA and HALS in maxillofacial silicone prostheses for prolonged contact with skin and mucous membrane has not yet been established through clinical research.(53) On the other hand, on those previous studies the nano-oxide particles were directly incorporated into bulk materials during fabrication, whereas the surface of a material first faces all the challenges of weathering induced degradations.

Currently, no published literature was found on the effect of Atomic Layer Deposition (ALD) mediated nano-coating preventing color degradation on pigmented silicone elastomer subjected to artificial aging. Therefore, this investigation mainly focused on a

study of surface nano-oxide coating deposited using ALD, in the color stability of a pigmented silicone elastomer A-2000. TiO_2 has been reported to be an effective color stabilizer due to its UV shielding capability based on both the scattering and absorption of the UV light for its higher refractive index and semiconductive properties.(58) Considering these capabilities of TiO_2, the surface of the silicone elastomer or PDMS was coated with a nano layer of TiO_2 using the ALD technique, a novel and powerful chemical vapor deposition tool of nanotechnology. ALD offers unique approach to deposit conformal, uniform and very thin (few nanometers thick) film of metal oxides on three-dimensional, complex, porous, nano-structual materials at relatively lower process temperature, and it provides with precise control over the chemical composition and thickness of the nano-coatings.(58-61) For this study, the null hypotheses tested were: ($H_0$1) Color difference between coated and non-coated silicone specimen would be below perceptibility threshold, and ($H_0$2) there would be no difference between the color change after aging of non-coated and coated silicone, from their baseline color prior to aging.

2.1.2. Materials and Methods

Platinum-catalyzed, vinyl-terminated poly (dimethyl siloxane) elastomer (A-2000; Factor II, Inc.) combined with functional intrinsic pigments (FI-SK: Functional Intrinsic Skin Colors - Silicone Coloring System; Factor II, Inc.) was used for this study. The elastomer was combined with a polymethyl hydrogen siloxane cross-linking agent at a 1:1 ratio by weight. Once elastomer components were thoroughly mixed, pigments were added to resemble human skin color. The elastomer - pigment combination was placed under 5×10^{-3} Torr vacuum for 10 minutes to remove air from the system, then poured into three

disk-shaped molds with diameter of 34 mm. The molds were placed into a convection oven and held at 98°C for 1 hour to achieve full polymerization. The molds were removed and allowed to cool to room temperature; a biopsy punch was used to core the specimens resulting in 2.5mm diameter sample (N=20). After color test$_0$, 10 specimens were randomly selected for coating process and the remaining 10 specimens served as control (non-coated). Diagram of the experiment was described in detail in Figure 3.

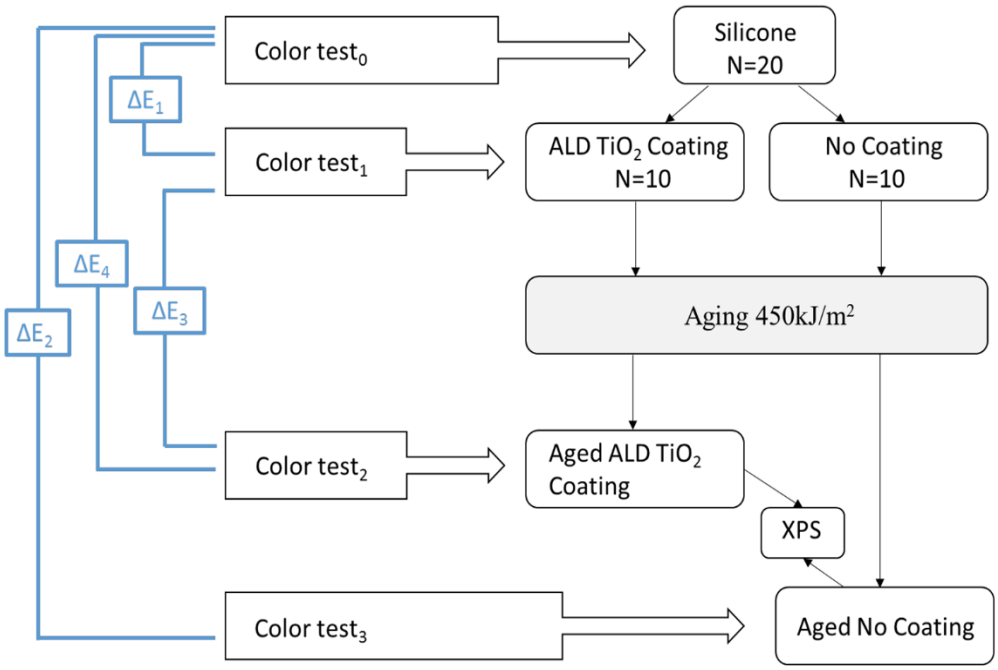

Figure 3: Schematic of color measurements experiment plan involving TiO_2-ALD coating and artificial aging; Color test$_0$ implies the color measurements of baseline or control specimens, color test$_1$ implies the color measurements of specimens after TiO_2 coating, and color test$_2$ and color test$_3$ is the color measurements after artificial aging performed for TiO_2-coated and non-coated specimens, respectively.

Thin film of TiO_2 was deposited on the specimen surface using the ALD technique in a custom ALD reactor.(62) Specimens were pre-treated with oxygen plasma (Plasma Etch) for 1min at 400W power, to make the surface hydrophilic prior to ALD process. The sequence of the ALD experiment was described in Figure 4. The deposition was carried out at 65-70°C reactor temperature and the deposition pressure was 500 mTorr. Tetrakis(dimethylamino)titanium (TDMAT) was used as titanium (Ti) source and ozone was used as oxidizer source for this TiO_2-ALD process. A reference silicon (Si) wafer was used during the deposition on the silicone elastomer specimens and the thickness of the deposited oxide was measured on the reference si-wafer using a spectral ellipsometer (model M44; J.A. Woollam Co., Inc).

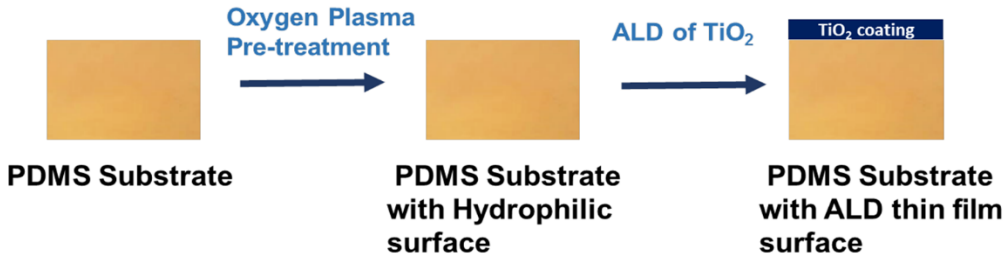

Figure 4: Schematic of the TiO_2-ALD coating process on silicone elastomer surface

Color measurements of the specimens were performed before (color test$_0$) and after ALD coating (color test$_1$), and after the aging of coated (color test$_2$) and non-coated (color test$_3$) specimens. A spectroradiometer (PR 650; PhotoResearch Inc) was fixed on a composite breadboard laboratory table (Edmund Optics) with a height adjustable metric lab jack (Edmund Optics) positioned beneath it. One illuminator (FO-150; Chi Technical Corp) was positioned at a 45-degree angle from the horizontal plane of the specimen. This assembly provided an optical configuration of 0-degree observance and 45-degree illumination to the specimen without any aperture between specimen and light/sensor.(63) After warming up the illuminator for 15 minutes, the spectroradiometer was calibrated with a white standard (Reflectance Standard SRS-3; PhotoResearch).(63) Color measurements (2.4 mm diameter measurement area) performed in this study were obtained from a 380 to 780 nm spectral reflectance with a 5-nm interval (SpectraWin2; Photo Research Inc) before conversion to Commission Internationale d'Eclairage L*a*b* (CIELAB) values. The converted CIELAB values were based on the standard of using D65 illumination and 10-degree observer. These L*, a* and b* values were used to calculate the color change (ΔE*) using the formula: $\Delta E^* = \sqrt{(\Delta L^*)^2 + (\Delta a^*)^2 + (\Delta b^*)^2}$, where ΔL^* = lightness difference (light or dark), Δa^* = difference in a* values (green to red coordinate), and Δb^* = difference in b* values (blue to yellow coordinate).

Specimens were aged according to American Society for Testing and Materials (ASTM) G154 specification(64) for 450 kJ/m^2 total exposure.(41) An artificial aging chamber (EQUV; Equilam) containing an UV-A lamp (340 nm of wavelength) with a typical irradiance of 1.55 W/m^2/nm was used. Each exposure cycle was 8 hours of UV at 70±3°C

black panel temperature and 4 hours of condensation at 50±3°C black panel temperature. Ten cycles were performed to provide a total exposure of 450 kJ/m^2, adequate energy to verify the color stability of silicone materials.

X-ray photoelectron spectroscopy (XPS) was used to study the chemical composition of the specimen surface. A high-resolution x-ray photoelectron spectrometer (VSW HA100; Vacuum Scientific Workshop) equipped with an Al Ka (1486.6 eV) x-ray source operating at 12 kV and 15 mA was used for this study.

Means and standard deviation of all L, a, b values of all specimens were calculated. The color differences (ΔE) as color difference after coating (ΔE_1), color difference after aging without coating (ΔE_2), color difference after aging with coating (ΔE_3 and ΔE_4), and their standard deviations were calculated. Data were analyzed using independent t-tests to compare the potential color difference between groups. One-sample t test was used to compare the potential difference between the recorded color difference to perceptibility threshold (ΔE = 1.1) and acceptability threshold (ΔE = 3.0).(54) The estimate effect size was tested using Partial Eta Squared (η_p^2). With a minimum of 8 samples per group, a large size effect (η_p^2>0.26) was obtained for ΔE (η_p^2=0.292, *P*=.027), ΔL (η_p^2=0.790, *P*<.001), Δa (η_p^2=0.508, *P*=.001), and Δb (η_p^2=0.741, *P*<.001). All statistical analyses were performed using a statistical software (IBM SPSS statistics v22.0; IBM Corp). The level of significance was set at α=0.05.

2.1.3. Results

A nano-coating of TiO_2 was deposited successfully on silicone specimens using ALD technique. Total 300 ALD cycles were performed to deposit the TiO_2 nano-coating and

this resulted in approximately 16nm-thick TiO_2, as measured on the reference Si-wafer surface experienced exact same process condition while ALD was performed on silicone specimens.

Specimens	**L**	**a**	**b**	**ΔE**	**Perceptibility threshold = 1.1 (54) (*P*-value)**	**Hypothesis**
Non-coated	73.3 ±0.5	10.5 ±0.4	22.3 ±0.8	ΔE_1=3.4 ±1.4	*P*=.001	$H_0$1
TiO_2-coated	70.7 ±0.7	11.7 ±0.5	23.8 ±0.7			
Non-coated	73.4 ±0.5	10.5 ±0.4	22.4 ±0.6	ΔE_2=2.5 ±0.7	*P*=.001	$H_0$2
Aged Non-coated	71.4 ±0.4	10.5 ±0.3	23.8 ±0.7			
TiO_2-coated	70.9 ±0.5	11.5 ±0.3	23.6 ±0.6	ΔE_3=1.4 ±0.6	*P*=.167	
Aged TiO_2-coated	70.5 ±0.8	11.3 ±0.4	24.8 ±0.7			
Non-coated	73.3 ±0.5	10.5 ±0.4	22.4 ±0.8	ΔE_4=3.8 ±1.3	*P*<.001	N/A
Aged TiO_2-coated	70.5 ±0.8	11.3 ±0.3	24.8 ±0.7			

TABLE I. Means ±standard deviations (SD) values of L, a and b of non-coated and TiO_2-coated specimens before and after aging, and statistical analysis of color difference (ΔE) values with respect to perceptibility threshold (54)

The means and standard deviations of L, a, b values, the color differences (ΔE) among evaluated specimen groups are presented in TABLE I. It is observed from the demonstrated results that all the evaluated specimen groups experienced a chromatic alteration (ΔE>0) to some extent due to oxide coating as well as exposure to artificial aging. A significant color difference (ΔE_1=3.4 ±1.4) was observed between the non-coated and TiO_2-coated silicone specimens when compared to the perceptibility threshold of ΔE of 1.1 (t(9)=5.208, *P*=.001). Nevertheless, this color difference after TiO_2 coating is not significantly higher (t(9)=0.945, *P*=.369) than the established acceptability threshold of ΔE=3.0. The non-coated specimens were found to undergo a significant color change (ΔE_2=2.5 ±0.7) after aging. This color change is significantly higher (t(7)=5.581, *P*=.001) than the perceptibility threshold (ΔE=1.1). However, TiO_2-coated silicone specimen group showed the smallest color change (ΔE_3=1.4 ±0.6) after aging compared to other specimen groups. This color change is not significant (t(7)=1.542, *P*=.167) compared to the perceptibility threshold, and is significantly lower (t(7)=-7.508, *P*<.001) than the acceptability threshold (ΔE=3.0). ALD coated specimens had statistically significantly (t (7) =3.294, *P*=.005) less color difference after aging (ΔE_3=1.4 ±0.6) compared to non-coated samples after aging (ΔE_2=2.5 ±0.7). In addition, when compared non-coated to coated and aged specimen groups, the color difference (ΔE_4=3.8 ±1.3) was significantly higher than the perceptibility threshold (t(7)=6.168, *P*<.001).

Figure 5 shows the XPS spectra of the non-coated and TiO_2-coated silicone specimens after experiencing artificial aging at 450kJ/m^2. It is observed that both the specimens have four distinct peaks. Those peaks are attributed to oxygen (O 1s: 532 eV), carbon (C 1s: 285 eV),

and silicon (Si 2s: 149.7 eV and Si 2p: 99.4 eV), which are the basic chemical components of silicone elastomers. In addition to O, C, and Si peaks, a distinct titanium peak (Ti 2p: 455 eV) was observed on the silicone specimens surface coated with a TiO_2 nano layer. This finding revealed that the protective TiO_2 nano coating can withstand artificial aging. Furthermore, it remains on the surface of the coated specimen even after the aging used.

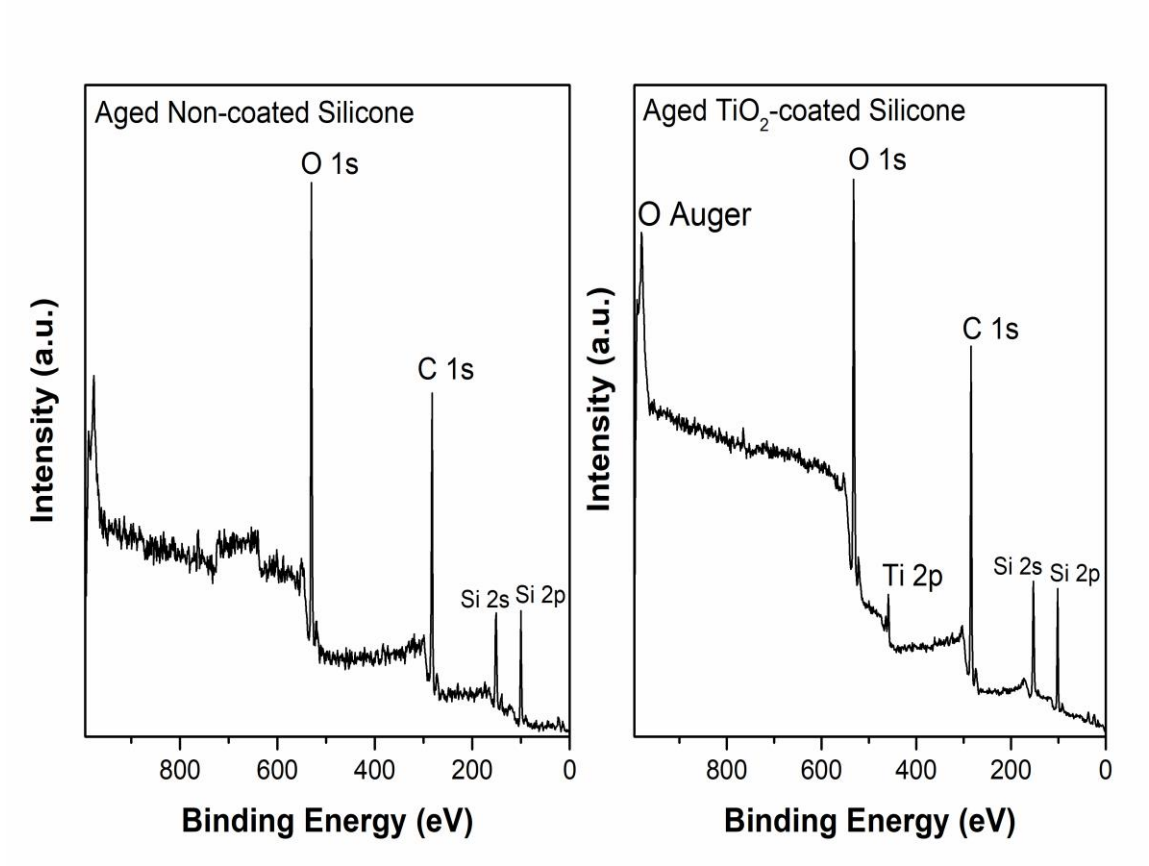

Figure 5: X-ray Photoelectron Spectroscopy (XPS) spectra showing surface chemical composition of non-coated and TiO_2-coated specimen after subjected to artificial aging.

2.1.4. Discussion

In this study, the color difference between ALD TiO_2 coated and non-coated silicone specimens was found to be significantly higher than perceptibility threshold of ΔE 1.1. In addition, there was significantly less color change after aging in coated silicone compared to non-coated aged specimens. Therefore, both null hypotheses were rejected.

According to the obtained results, a color change was also observed between the non-coated and TiO_2-coated groups. Although most of these color changes from TiO_2 coating (ΔE_1=3.4) were significantly higher than the perceptibility thresholds of 1.1, (54) this color change values were not significantly higher than the acceptability thresholds (3.0). (54) This implies that the color change of the coated silicone specimens in the present study is not considered clinically significant. A future study evaluating the effect of different coating thickness on color perceptibility threshold is warranted.

From this study, it is found that all specimen groups, irrespective of nano-oxide coating, showed color instability (ΔE>0) when exposed to artificial aging. Both the intrinsic (self-discoloration of the material) and extrinsic factors (adsorption or absorption of different substances) may cause this kind of color degradation.(65) Among the attributing environmental factors such as solar radiation, temperature and moisture, the UV radiation has a greater impact on color degradation of the facial prosthesis.(41) The obtained results indicate that a TiO_2 nano-coating is able to protect silicone elastomer from color degradation induced by artificial aging. Nano oxides are widely used as inorganic UV absorbers because of their better thermal and photo stability over decades unlike organic UV absorbers which are unstable for their migration in a polymeric matrix.(56) When an

electromagnetic wave like UV light interacts with the surface nano particles, part of this UV light is scattered and at the same time, some part of this light is absorbed by these nano particles and thus they create an UV shield protecting the surface.(41) Due to high refractive index and semiconductive properties, TiO_2 can offer similar kind of UV protection based on both scattering and absorption of UV rays.(58) These physical principles may contribute in interpreting the color stability of TiO_2-coated specimens presented in this study.

Additionally, TiO_2 coated specimens showed approximately 44% less color change as compared to the non-coated specimens upon exposure to artificial aging. Therefore, this TiO_2 nano coating appeared to be an efficient color protector for this kind of silicone elastomer. Previously, Han et al. studied the effect of TiO_2 nano oxide as opacifiers in the color stability of pigmented maxillofacial prosthetic silicone.(41) They reported that the color changes due to artificial aging was the least for the silicone prosthesis with 2-2.5% nano oxide of TiO_2 by weight as opacifier, though the color stability of their specimen containing TiO_2 nano oxide is approximately 29% better than their control. Also, these nano oxides are inorganic white powder added directly to bulk during specimen preparation. Additionally, it was also reported that 67 nm of ALD-TiO_2 coating (deposited at 80°C temperature, 1 mbar pressure) was able to almost completely protect biaxially oriented polypropylene polymer during 6 weeks of UV exposure, by preventing formation of UV induced photodegradation products in the film.(58)

Further, XPS was used to investigate the inorganic-organic bonding between TiO_2 nano coating and silicone elastomer. XPS results (Figure 5) confirmed the presence of Ti peak

for the TiO_2 coated silicone specimens after exposed to artificial aging test. This result indicated that the ALD process provided strong chemical bonding between silicone and TiO_2. The vapor phase surface chemical reactions of the ALD process attributed to such strong chemical bonding between coating material and the surface groups of the ALD substrate. (66)

There are limitations to this in vitro study. The color stability of the specimens in this study used artificial weathering or aging involving three factors: UV irradiation, temperature and moisture inside an artificial aging chamber. However, outdoor aging would be more appropriate for studying the color stability of this maxillofacial prosthetic silicone material accurately. The oxide nano-coating contributed positively in the color stability of silicone elastomers upon exposed to aging, although this coating itself changed the color of the specimens significantly when compared to perceptibility threshold. Additionally, the effect of only one oxide nano coating on color stability was examined on one type of silicone elastomer. Other limitation was that the color of the silicone was measured with a neutral backing. Ideally, it should be measured with black and white backing, and the true color should be determined by using the Kubelka Munk Theory (KM Theory). (67)

Therefore, further in-depth studies are important to investigate the influence of other oxide or inorganic nano coatings on the color stability of different types of pigmented silicone elastomers commonly used fabricating the maxillofacial prosthetic silicone in clinical practice. In addition, to test this intervention coating with actual patient's maxillofacial prosthetic silicone in a clinical setting to evaluate the range of clinical change occurs and the length required before clinically unacceptable color change occurs.

2.1.5. Conclusion

Within the limitation of the study, the following conclusions were drawn based on the results obtained:

1. All specimens underwent color changes when subjected to artificial aging at 450kJ/m^2.

2. Color changes (ΔE_1=3.4) of the TiO_2 nano coated silicone specimens were not significantly higher (*P*=.369) compared to the established clinical acceptability threshold (ΔE=3.0).

3. This nano-coating was stable after aging exposure as the chemical analysis confirmed the presence of the titanium oxide on surface after the aging was performed.

4. Upon expose to artificial aging, this nano coating of TiO_2 was able to reduce color degradation of the evaluated silicone elastomers, compared to the non-coated silicone specimens (44% more discoloration than TiO_2-coated specimens). This indicated that the silicon elastomer with a surface nano-coating of TiO_2 is a better color-stable novel material to be potentially used in the extraoral fabrication maxillofacial silicone prostheses.

2.2. Room temperature ALD of TiO_2 on collagen

This section was previously published as "Room temperature TiO_2 ALD on collagen membrane from a Titanium alkylamide precursor" in Journal of Vacuum Science & Technology A.

2.2.1. Introduction

Atomic Layer Deposition (ALD) is well known for its unique capabilities within chemical vapor deposition processes. It offers excellent composition tunability, and precise thickness control and uniformity in deposited very thin of metal oxides films (6; 68; 69). It can also facilitate conformal deposition across three dimensional substrates (70; 71). ALD of an oxide is a gas phase cyclic process and one cycle of ALD process typically consists of four main steps: precursor pulse, precursor purge, oxidizer pulse and oxidizer purge. Pulsing time, purging time and reaction temperature are important parameters for optimal growth during ALD processes(72). Different oxidizers and precursors play important roles in the thin film growth of a given metal oxide. For a typical ALD process the oxide film thickness generally increases linearly with increasing number of ALD cycles. The substrate also plays a significant role in the growth rate and oxide film quality(72).

ALD is typically carried out at relatively high temperature to obtain optimal film growth and quality. High temperature ALD is used in the semiconductor industry(6). However, low temperature or room temperature ALD is needed when the substrate is heat-sensitive. Precursors with high vapor pressure can facilitate this type of ALD process. This low temperature ALD enables deposition on heat-sensitive substrates like polymers, organics and biological materials. Knez et al reported different low temperature ALD processes in their review(73). In most of those ALD processes, water (H_2O) was used as the oxidizing

agent. In 1994, Gasser et al first published successful room temperature ALD of silicon dioxide (SiO_2) from tetraisocyanate silane ($Si(NCO)_4$) and H_2O(74). Room temperature ALD of cadmium sulfide (CdS) from dimethylcadmium ($Cd(Me)_2$) and hydrogen sulfide (H_2S) was also reported by Lou et al(75). ALD below 50°C was reported previously for boron trioxide (B_2O_3) (at 20°C from boron tribromide (BBr_3) and H_2O(76)), SiO_2 (at 27 and 30°C from silicon tetrachloride ($SiCl_4$) and H_2O(77; 78)), aluminium oxide (Al_2O_3) (at 33, 35 and 45°C using trimethylaluminum (TMA) and H_2O(27; 79; 80)), and TiO_2 (at 35°C from titanium isopropoxide ($Ti(OiPr)_4$) and H_2O(79)). These processes were used to deposit thin films on heat-fragile polymer substrates.

After low temperature ALD was reported, it became an increasingly used tool of nanotechnology to functionalize surfaces of different biomaterials. Such a type of attempt was first documented on tobacco mosaic virus (TMV) on which Al_2O_3 and TiO_2 were deposited at 35°C using TMA and TIP precursor, respectively, and water as oxidizer(79). Next, ALD was performed on some proteins such as ferritin(81) (deposition of Al_2O_3 and TiO_2) and S-layers(82) (deposition of HfO_2). ALD was also performed on peptides (83-85) and on DNA molecule (81; 86) to synthesize functionalized nanofibers or nanowires. Recently, applications of ALD were reported on other types of biomaterials such as collagen (28; 29), spider silk (32), cellulose fiber (from paper (87; 88) and cotton (59; 89)), bristles of sea mouse (90), butterfly wings (91; 92), fly eyes (93), legumes (94), legs of water strider (95), etc. Some of these materials had high aspect ratio structures where ALD might be the only possible way to obtain uniform conformal coating of an oxide layer.

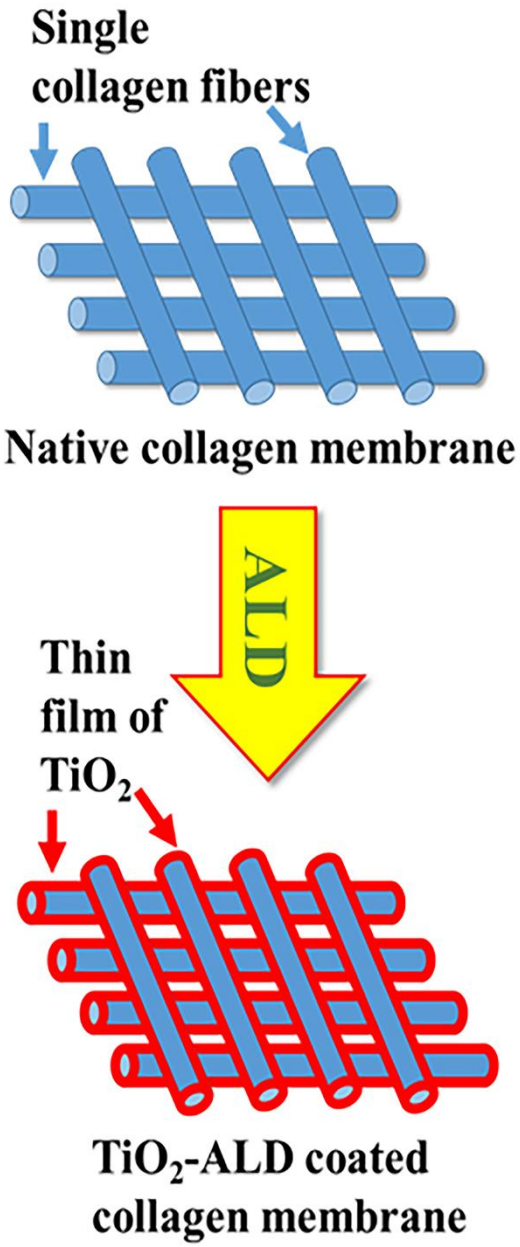

Figure 6. Schematic of collagen substrate before and after ALD is shown. A thin film of TiO_2 (illustrated by the shell or thicker lines) is deposited on collagen fibers (illustrated by the core or small cylindrical shapes).

Many of the above mentioned ALD were used for TiO_2 and Al_2O_3 thin oxide layers. Due to its attractive physicochemical properties, like large band gap(96), chemical stability(97), high dielectric constant(98; 99), highly photo-active surface(97), high refractive index(100; 101) and non-toxic environment-friendly nature(97), TiO_2 has a wide range of applications in modern technologies such as photocatalyst in solar cell(102), waste water purification(103), oxygen gas sensor(104; 105), memory devices and capacitors(106), food additives(107), pharmaceuticals(108), and in paint and cosmetics(106). Therefore, this oxide appears to have become a preferred coating material to functionalize biomaterials.

In this study we carried out ALD of TiO_2 at room temperature in a custom made ALD reactor, on a commercially available resorbable collagen membrane (Figure 6). Collagen is a naturally occurring fiber and one of the most abundant proteins found in the animal kingdom. ALD on fibrous materials has sparked a lot of interest as ALD can improve and functionalize these materials through successful infiltration into their complex structure. These ALD coated fibers have many applications such as in photovoltaic cells, chemical separations, barrier layers for medical, food packaging, organic electronics, surface engineering in textile, and biomedical and other industries (30; 61; 109). Previously, ALD was reported on different organic fibrous materials (TABLE II) like cellulosic fibers of cotton and paper (30; 31; 59; 88; 89; 109; 110), spider silk(32), inner egg shell membrane(28) and egg shell derived-collagen(29). Cellulose consists of polysaccharide (D-glucose units) and it has better resistance to heat treatment unlike protein-based biomaterials. Kemell et al first attempted TiO_2 ALD on natural cellulose fiber from paper at 150 and 250°C(88). In their study, TiO_2 replica of cellulose structure was obtained at 150°C and a photocatalytic crystalline TiO_2/cellulose composite was prepared at 250°C.

Cellulose fibers from cotton were also used as ALD substrates where the cellulose was highly crystallized. Hyde et al performed Al_2O_3 ALD on this type of cotton fiber at 100°C(59). They reported a uniform growth on convoluted fiber surface and this growth behavior was reported to be significantly different from that on planar surface processed at the same conditions. In their follow-up work, they also showed the tunability of wetting behavior of ALD-treated cotton fibers by varying the oxide film thickness, although the role of surface roughness changes with processing may need to be studied further (89).

ALD of a biocompatible TiN film was also reported on cotton fiber by Hyde et al(110). In their study, increased cellular adhesion was observed for the thin (<10 nm-thick) and most hydrophobic ALD coating, whereas the cell adhesion density decreased on the thicker (>100 nm-thick) ALD coating. Jur et al reported Al_2O_3 ALD at 60-90°C(109) and ZnO ALD at 115°C on cotton fiber(31). Uniform Al_2O_3 growth was reported after 100 ALD cycles. Also an effectively conductive cotton fiber was obtained with a ZnO ALD coating. Follow-up work by Lee et al showed transition of wetting behavior after performing ALD of Al_2O_3 and ZnO on cotton fibers(30). After an initial ALD, the cotton surface became hydrophobic, from hydrophilic, but with further ALD cycles the surface became hydrophilic again. Apart from cellulose, ALD was also reported on some other types of fibrous biomaterials such as spider silk and inner egg shell membrane. Lee et al reported increased toughness in dragline spider silk after deposition of ZnO, TiO_2 and Al_2O_3 at 70°C(32). A photocatalytic polycrystalline film was also obtained on eggshell membrane with ALD of TiO_2 and ZnO. ALD of all these natural fibrous biomaterials were performed mostly above 60°C. Recently, TiO_2 ALD on collagen extracted from eggshell matrix was

reported at 70°C using titanium(IV) isopropoxide [TIP] ($Ti(OiPr)_4$) precursor and water as oxidizer (29).

Substrate and oxide	Precursors	ALD parameters	Significant findings	References
TiO_2 on cellulose fiber of filter paper	$Ti(OMe)_4$ and H_2O	150 and 250°C, 10mbar	Accurate replication of cellulose structure	Kemell et al 2005(88)
Al_2O_3 on cellulose fiber of cotton	Trimethylalumi num (TMA) and deionized water	100°C, 5×10^{-7} Torr	Different film thickness in planar and complex structure, substrate became hydrophobic	Hyde et al 2007(59)
TiN on cellulose fiber of cotton	TDMAT and NH_3	100°C, 2 Torr	Surface showed increased biocompatibility	Hyde et al 2009(110)
TiO_2 and ZnO on inner egg shell membrane	Titanium(IV) isopropoxide ($Ti(OiPr)_4$,TIP), diethylzinc ($ZnEt_2$, DEZ) and water	70-300°C, 1×10^{-2} Torr	Photocatalytic polycrystalline film achieved at lower temperature	Lee et al 2009(28)
ZnO, TiO_2 and Al_2O_3 on spider dragline silks	DEZ, TIP and TMA, respectively, and water	70°C, 1×10^{-2} Torr	large enhancement of the mechanical properties of spider silks	Lee et al 2009(32)
Al_2O_3 on cellulose fiber of cotton	TMA and H_2O	120°C, 1-2 Torr	Wetting properties can be tuned by changing deposition temperature, number of ALD cycles	Hyde et al 2009(89)
Al_2O_3 on cellulose fiber of cotton	TMA and H_2O	60-90°C, 1×10^{-3} Torr	Oxide film showed abrupt interface with cellulose substrate	Jur et al 2010(109)
ZnO, TiO_2 and Al_2O_3 on collagen extracted from egg shell membrane	DEZ, TIP and TMA, respectively, and water	70°C, 1×10^{-2} Torr	Mechanical properties (toughness) improved	Lee et al 2010(29)

ZnO on cellulose of cotton and paper	DEZ and H_2O	115°C, 0.2 Torr	Conductive fiber was developed	Jur et al 2011(31)
Al_2O_3 and ZnO on cellulose fiber of cotton	TMA and DEZ, and deionized water	60-90°C, 2 Torr	Transition of wetting behavior back and forth	Lee et al 2012(30)

TABLE II. ALD of inorganic films on organic fibrous materials

In our study, it is the first-time room temperature TiO_2 ALD was performed on commercially available collagen membrane using a novel precursor for this process, TDMAT, and ozone as oxidizing agent. This can open up the tuning of the properties of commercial and other collagen.

2.2.2. Material and Methods

The deposition of TiO_2 was performed in a custom-made tubular, hot wall ALD reactor(62). The reactor can be heated up to 600°C and its base pressure is a few mTorr. This reactor has 4 precursor delivery lines and is capable of delivering four different types of oxidizers: ozone, oxygen, water vapor, and small molecular weight alcohols. During the deposition, the substrate and reactor were at room temperature while the precursor bubbler was kept at 50°C and the delivery line in between bubbler and reactor was kept 20-30°C higher than the bubbler temperature. The ALD chamber pressure was kept at 500 mTorr during deposition. TDMAT (Sigma Aldrich, 99.999%) and ozone (generated just upstream the ALD chamber with custom made UV lamp system) were used as precursor and oxidizer, respectively. The precursor and the oxidizer were introduced sequentially into the

reactor using computer controlled pneumatic valves. Argon (99.999%) was used as precursor carrier gas and purging gas. Geistlich Bio-Gide® (Geistlich Biomaterials, USA), commercially available collagen membrane was used as substrate and p-type Si(100) silicon wafer (University wafer Inc, USA) was used as reference substrate to measure deposited film thickness. The thickness of the deposited TiO_2 film on the reference silicon substrate was measured using spectral ellipsometry (Model M44, J.A. Woollam Co., Inc.). A custom made sample holder was used to hold the collagen sample and the reference silicon wafer inside the chamber during deposition (Figure 7). The surface chemical composition of the control collagen surface and ALD TiO_2-coated collagen substrates was studied using a high resolution x-ray photoelectron spectrometer (Kratos AXIS-165, Kratos Analytical Ltd., United Kingdom) equipped with a monochromatic Al Ka (1486.6 eV) x-ray source operating at 15 kV and 10 mA. Surface morphology of native collagen and TiO_2-coated collagen was analyzed using a high resolution Field Emission SEM (JEOL JSM-6320F, JEOL USA, Inc.). Prior to SEM, samples were gold-coated using a sputter coater to make them conductive. ImageJ software was used to measure the fiber diameters from the SEM images of samples. Glancing incidence X-ray diffraction (GIXRD) spectra of deposited TiO_2 film was obtained using a high resolution X-ray diffractometer (X'Pert, PANalytical, BV Co., Netherlands) configured with 0.1542 nm x-ray emission line of Cu. Diffraction spectra was collected at an incidence angle of 1° to enhance sensitivity for thin films and to reduce substrate interference.

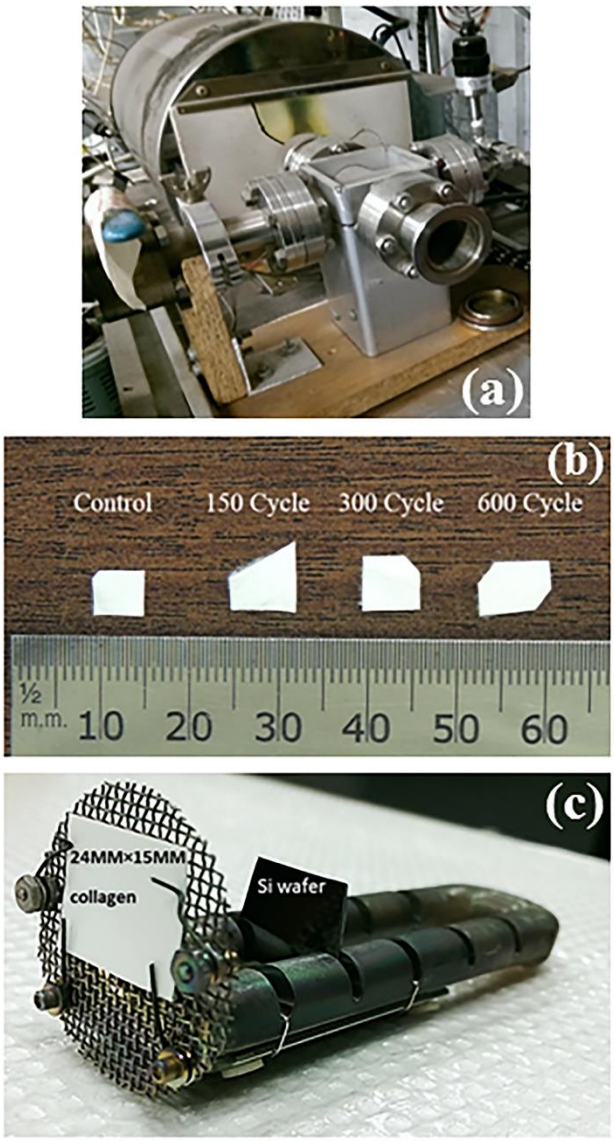

Figure 7: (a) The custom ALD reactor showing the loading port, (b) different collagen sample groups, (c) custom made ALD sample holder to hold collagen substrate and silicon wafer as reference sample.

2.2.3. Results and Discussion

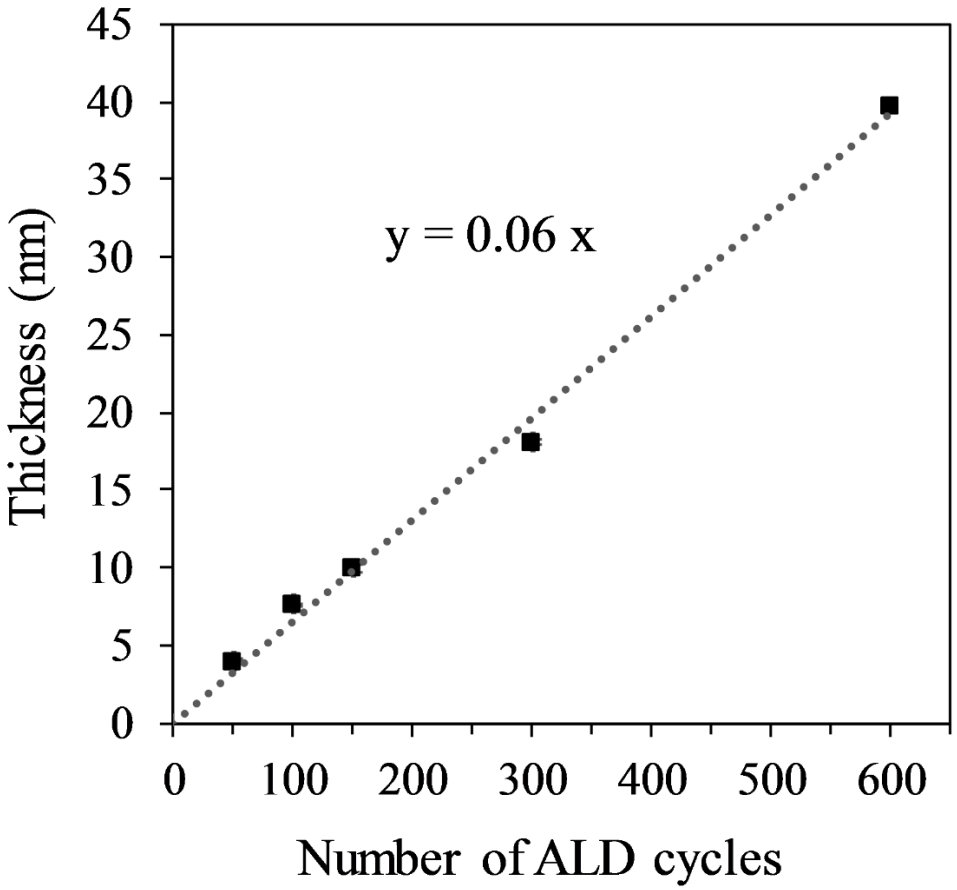

Figure 8: Thickness of deposited TiO_2 film on silicon reference substrate as a function of the number of ALD cycles. The deposition was carried out at room temperature and 500 mTorr using TDMAT as titanium precursor and ozone as oxidizer.

Room temperature growth behavior of TiO_2 deposited on our reference silicon substrate was investigated for 50-600 ALD cycles. Figure 8 shows the deposited TiO_2 film thickness on silicon substrate as a function of the corresponding number of TiO_2 ALD cycles. The standard deviation of the measurements at different positions across the substrate is indicated by the error bars in the graph. The film thickness was found to increase linearly with increasing number of ALD cycles without any apparent growth lag or rush. The growth rate is found to be 0.06 nm/cycle from the linear fit of the data. The apparent linear

growth behavior indicates that this ALD process offers a surface saturated growth and excellent tunability of film thickness. Additionally, the small error bars in Figure 8 are indicative of the uniformity of the room temperature ALD of TiO_2 films across the substrate surface. Deposition of TiO_2 from TDMAT and ozone was reported before for different substrates at higher temperatures, 60-300°C (58; 97; 106; 111-115). In 2008, Katamreddy et al first reported TiO_2 ALD using TDMAT and ozone with a growth rate of 0.065 nm/cycle at 225°C; they also reported an increase in the deposition rate at temperature higher than 225°C due to the decomposition of the TDMAT precursor (113). The deposition rate varies with the process temperature, and with gradually increasing temperature it first decreases, then reaches saturation and finally increases again. Specifically, with increasing substrate temperature from 75 to 150°C, the TiO_2 film growth rate first decreases from 0.052 nm/cycle to 0.045 nm/cycle; at temperature 150-250°C, a saturation phase of the growth rate at ~ 0.046 nm/cycle is found; further increase in the temperature results in strongly increasing growth rate again(106; 114). Rose et al also reported a growth rate of 0.04nm/cycle at 180°C(115). At lower temperatures, 60-65°C, the growth rate remained ~0.06 nm/cycle(111; 112) which is similar to the one obtained at room temperature (20-25°C), in our study.

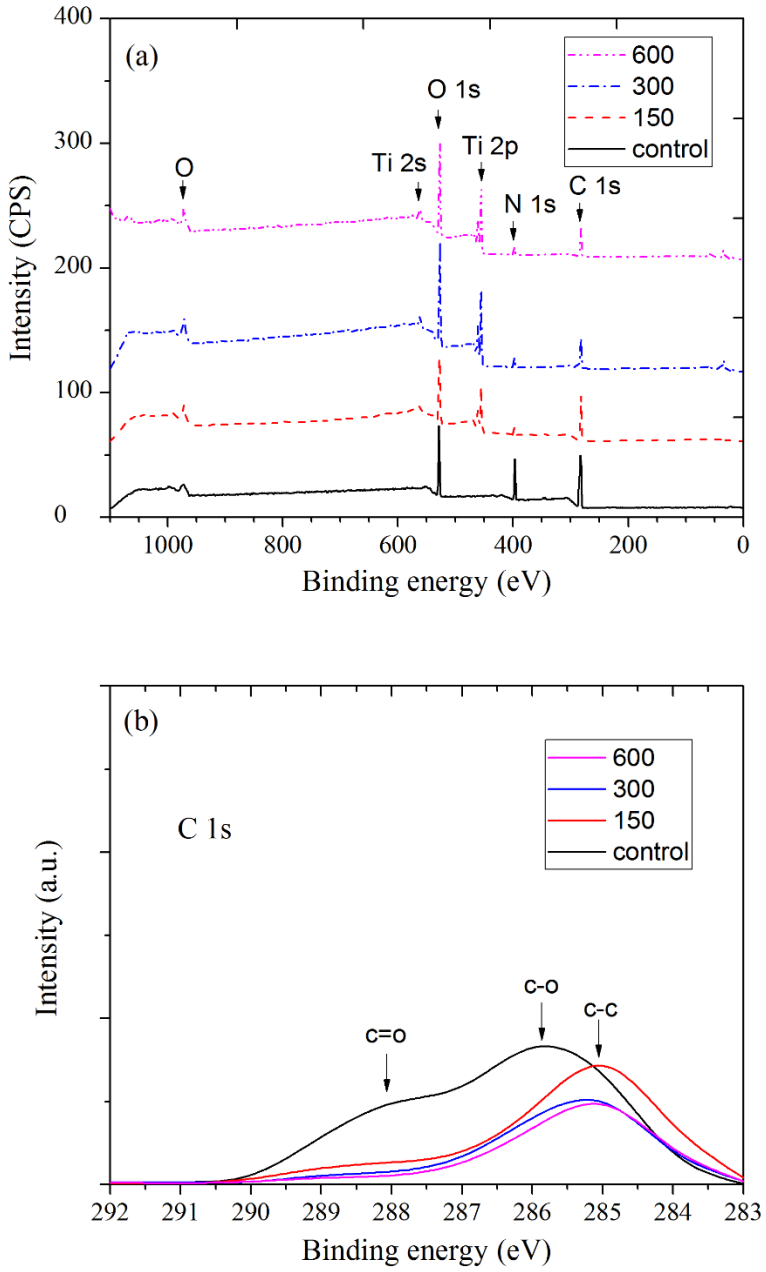

Figure 9: (a) XPS spectra of the collagen substrate after 0 (control), 150, 300 and 600 cycles of TiO_2 ALD, (b) detailed XPS spectra of C 1s (control, 150, 300, 600 cycles). Deposition conditions are the same as those in Figure 8.

Figure 9a shows the XPS spectra of native collagen substrate (i.e., control sample), collagen-150cycles, collagen-300cycles and collagen-600cycles. Three distinct peaks were

observed with the control collagen samples. Those peaks are attributed to oxygen (O 1s: 532eV), carbon (C 1s: 285eV) and nitrogen (N 1s: 398eV) which are the basic chemical components of collagen protein. In addition to O, C and N peaks, two other titanium peaks (Ti 2s: 560eV and Ti 2p: 455eV) were observed on the collagen samples with as-deposited

Sample analyzed	**O:Ti ratio**	**C contents (at %)**	**N contents (at %)**	**Ti contents (at %)**
Control collagen	-	63.5	15.7	-
Collagen-150cycles	3.46	53.9	3.82	9.47
Collagen-300cycles	2.71	37.6	5.98	14.5
Collagen-600cycles	2.77	39.2	5.91	15.2

TABLE III. Compositional quantitative analysis of the sample from XPS data

TiO_2 after 150, 300 and 600 ALD cycles. The highest levels of carbon (63.5 %) and nitrogen (15.7 %) were detected in the control collagen and these levels were found to decrease after the ALD of TiO_2 thin films on collagen (TABLE III). With increasing number of the TiO_2 ALD cycles, the Ti 2p peaks became more intense. These results on collagen are in qualitative agreement with our finding of increasing TiO_2 film thickness with increasing number of ALD cycles on the silicon reference substrate. The Ti peaks in the 454-468eV region are the Ti $2p_{3/2}$ and Ti $2p_{1/2}$ peaks and are mostly attributed to Ti^{4+} (106; 113). TABLE III shows the O:Ti ratio/stoichiometry estimated from quantitative

analysis of the XPS data. This data revealed the ratio of O:Ti of the first 6-10 nm of the TiO_2 film deposited on collagen substrate to be 2.7-3.4, indicating excess oxygen within the film, while the film mainly consists of TiO_2. Similar ratio of O:Ti was reported before for TiO_2 film grown from alkylamide-ozone system on inorganic substrates (113; 114). Yet, those depositions were carried out at significantly higher substrate temperatures (150-250°C); thus, the O:Ti ratio apparently seems to be minimally affected by the deposition temperature used(114).

Additionally, the C 1s peak at 285 eV is attributed to C-C bonding and this indicates the existence of mostly organic-bonded carbon on the film(114). The collagen protein structure itself contains several types of carbon bonds like C-C (285 eV), C-O (286 eV) and C=O bonds (288 eV)(29; 59). As a result, XPS detected larger amount of carbon on the control sample and also on the collagen-150cycles one. With further increase in the number of ALD cycles, the signal from collagen C-O and C=O could barely be detected. The collagen-300cycles and collagen-600cycles samples exhibited peaks attributed only to C-C bonds, indicating mostly the presence of adventitious carbon (Figure 9b). Considering the sensitivity of the biological substrate, the collagen samples were not sputtered with an Argon (Ar+) beam before XPS scans, and this might lead to the presence of adventitious carbon on the ALD-coated collagen in spite of having a thicker TiO_2 coating. To investigate this issue further, XPS scans were performed on the corresponding Si reference samples (after 150, 300 and 600 cycles) before and after sputter cleaning. The carbon content (atomic %) of Si-150cycles, -300cycles and -600cycles before sputtering was found to be 28.3, 34.0, 31.5 %, respectively, while after sputter cleaning the carbon content was 7.4, 5.7 and 5.6 %, respectively. This suggests that most of the carbon on the ALD-coated

collagen is indeed adventitious carbon present on top of the ALD TiO_2 thin film. Additionally, ~18% Ti and ~48% O was detected before sputtering for these three reference Si samples with ALD TiO_2, while after removing the adventitious carbon through sputtering the Ti and O content were determined to be ~30% and ~62%, respectively. This result also indicated the deposition of mostly pure (uniform) TiO_2 film.

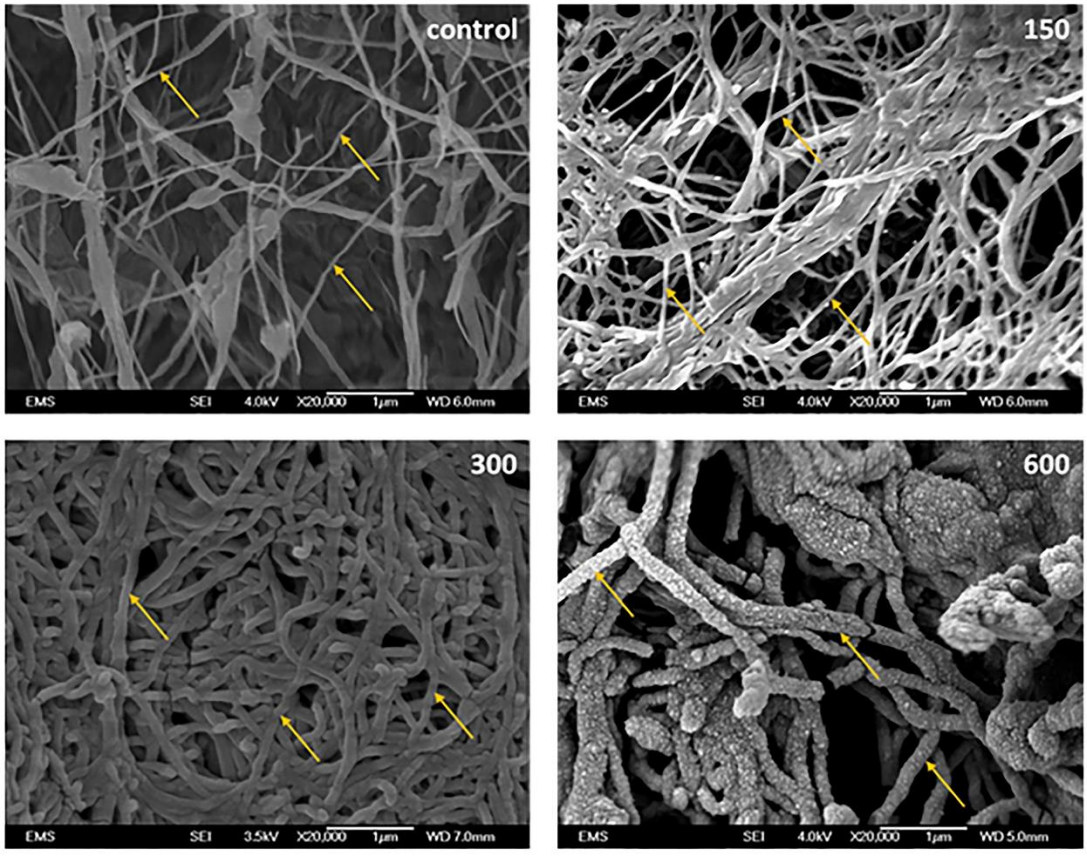

Figure 10. (Color online) SEM micrographs of control collagen (upper left), collagen-150cycles (upper right), collagen-300cycles (lower left) and collagen-600cycles (lower right). Deposition conditions are the same as those in Figure 8.

Surface morphology of the collagen samples was studied using scanning electron microscopy (SEM). Figure 10 shows the SEM images of all four sample groups. There is an apparent difference of fiber morphology among the samples. In the control sample the collagen fibers are seen to be thin. The fibers became increasingly thicker in the collagen samples with increasing number of TiO_2 ALD cycles.

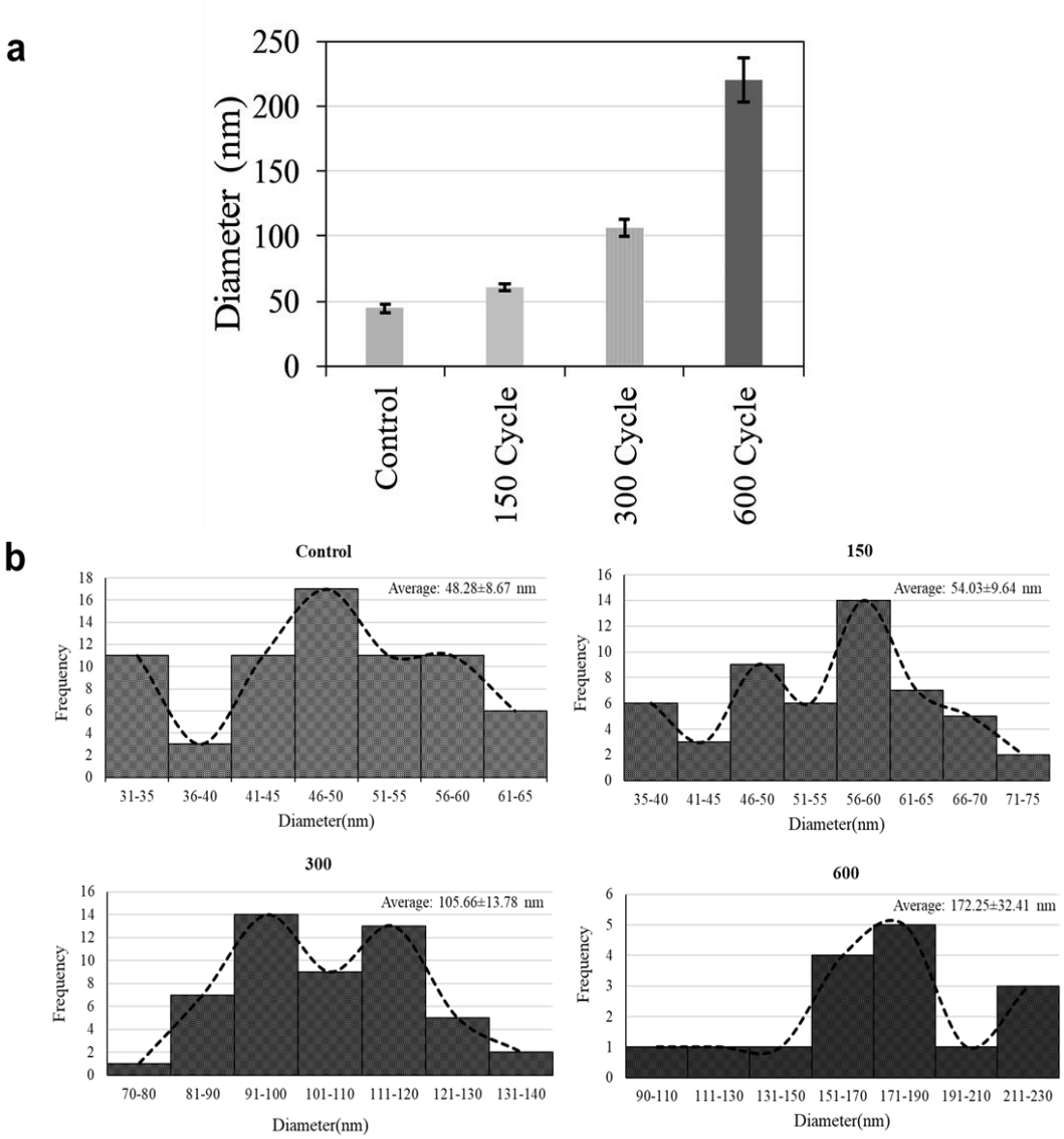

Figure 11. (a) Average single fiber outer diameter of control and as deposited collagen. (b) Histograms of fiber diameters measured from the SEM images of all the sample groups. Deposition conditions are the same as mentioned in Figure 8.

The average outer diameter of single fibers was measured from SEM images of each sample using the ImageJ software. For each sample group three fibers were primarily used for measurement and those fibers have been labelled with arrows in Figure 10. Both conjugated fibers and single fibers are present in the collagen membrane; only single fibers were chosen. The results of these measurements are presented in Figure 11. The single fiber diameter average of the control sample was 44.3±2.9 nm; after 150, 300 and 600 TiO_2 ALD cycles it was 60.3±2.2, 106.7±6.3 and 220.3±17.3 nm, respectively. A stronger than linear increase in fiber diameter is therefore observed for as-deposited TiO_2 coated collagen samples with increasing number of ALD cycles. This finding suggests the ability of TiO_2 ALD to uniformly coat 3-dimensional (3D) substrates at room temperature.

The significant difference of the growth rate per ALD cycle observed on the planar Si reference substrates from that on non-planar collagen substrates, even though they were processed at the same conditions, is discussed next. A linear growth at a constant rate of 0.06 nm/cycle was observed on the planar Si reference substrate while much higher growth rate per cycle was observed on non-planar collagen substrates, which was found to increase with further increasing number of TiO_2 ALD cycles. After 150 ALD cycles, the growth rate on collagen was about 0.05 nm/cycle, while after 300 and 600 cycles it reached 0.10 and 0.14 nm/cycle, respectively. These deposition rates on non-planar collagen samples were calculated based on the average outer diameter of single fibers measured from the corresponding surface SEM images. Cross-sectional interface study might be more effective to accurately measure the TiO_2 thickness and the growth rate for each of the coated collagen samples. Similar increased growth on non-planar three dimensional substrates was reported previously for Al_2O_3 and TiO_2 films. Hyde et al reported on planar

Si substrate that the Al_2O_3 growth rate was 0.2 nm/cycle which increased to 0.3-0.5 nm/cycle on a non-planar cotton fiber substrate(59). Although in their report, the growth rate on non-planar substrate was very high initially (0.5 nm/cycle for 50-100 ALD cycles) most likely due to the absorption of water oxidizer, the growth rate decreased (to 0.3 nm/cycle) as ALD proceed further. However, their growth rate was still higher on the non-planar substrate than that on planar substrate with further ALD cycles. Deposited TiO_2 amount on planar Si substrate was also reported to increase significantly on irregular non-planar multi-walled carbon nanotubes (MWCNTs) substrate(97).

There could be several reasons behind this increased growth on non-planar complex 3D substrates. One reason could be the higher surface area of 3D substrates compared to two-dimensional ones. This exposure of higher effective surface area could lead to larger amount of deposited oxide, although the deposition rate could be the same. Deng et al reported 183 times higher amount of TiO_2 deposited on irregular MWCNTs due to its 183 times higher surface area compared to the surface area of planar Si substrate(97). A possible reason *for higher growth rate* on non-planar substrates could be the complex 3D structure of such porous fiber networks. Due to this 3D pathway, it may take a longer diffusion time for reactant precursor molecules and vapor byproducts to diffuse out of these tortuous fiber networks. As a result, excess precursor may remain inside the fiber structure, even after the end of the precursor purging steps and this could cause higher film growth on 3D substrates(59). For optimal growth behavior, longer pulsing and purging of precursor might be an effective approach to avoid this kind of non-linear growth rate in the case of porous 3D fiber substrates allowing longer diffusion time for the reactant molecules and reaction byproducts to get in and out.

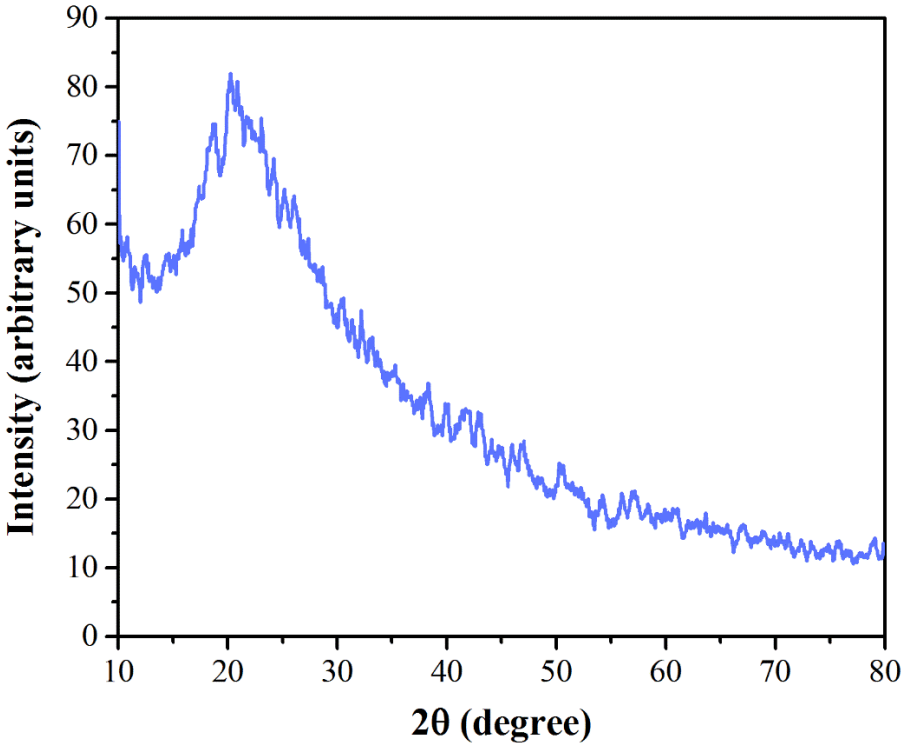

Figure 12. (Color online) GIXRD pattern of collagen-600cycles TiO_2 coating. Deposition conditions are the same as those in Figure 8.

GIXRD was performed to investigate the crystalline property of room temperature deposited TiO_2 film on collagen substrates. Samples with the thickest ALD TiO_2 film (i.e., after 600 cycles) were used. Figure 12 shows a GIXRD sample pattern. No distinct crystalline peak was observed, indicating the amorphous nature of the deposited oxide. This was not surprising, since the ALD of TiO_2 was carried out at room temperature, which is well below its crystalline temperature (>250°C)(106). The broad peak shown in Figure 12 is mostly from collagen. Lee et al also reported similar diffraction pattern from collagen substrate and their TiO_2 film deposited at 70°C was also reported to be amorphous(29).

2.2.4. Conclusion

TiO_2 thin film was deposited on commercially available collagen using TDMAT precursor and ozone oxidizer in a custom ALD system. The deposition was carried out at room temperature and this ALD process had linear growth behavior with a rate of 0.06 nm/cycle on the planar Si reference sample. XPS data showed the basic elemental composition of collagen protein and it confirmed the presence of TiO_2 on all collagen samples subjected to TiO_2 ALD. GIXRD data indicated that the deposited film was amorphous. SEM images showed a distinct morphological difference among the sample groups. The average fiber diameter of the control sample was found to increase ~ 36 % after 150 cycles of TiO_2 ALD, and this corresponded to 0.05 nm/cycle. The fiber diameter was found to increase more strongly than linearly with further increase of the number of TiO_2 ALD cycles to 300 and then to 600, with growth rates of 0.10 and 0.14 nm/cycle, respectively. The deposition rate on collagen coated with ALD TiO_2 was therefore higher by a factor of 2-3 than that on the corresponding silicon reference substrate, most likely due to its 3D fiber network and diffusion processes in it. This TiO_2 ALD-coated dense collagen could become a novel biomaterial, the mechanical and chemical properties of which could be tuned through ALD so that it could be used in a variety of biomedical applications like bone-grafting, wound-healing, etc. Further studies are under way to investigate the extent of ALD-driven versatile applicability of collagen in material science and biomedical engineering.

2.3. Bioactivity of ALD-TiO_2 functionalized collagen

2.3.1. Introduction

Bone tissue engineering strategy requires a special biomaterial scaffold with major attributes such as biocompatibility, osteoconductivity, biomineralization capability, biodegradability and proper biomechanical properties.(116) A biomaterial scaffold possessing all those properties can directly be implanted in-vivo for guided tissue regeneration.(117) Scaffolds, especially synthesized from natural polymeric resources, are frequently used due to their excellent biological performances and similarities with the extracellular matrix (ECM).(118) The usage of collagen-based biomaterials has been growing intensively in different biomedical applications particularly in the field of tissue engineering applications, due to its biocompatibility, biodegradability, role in tissue formation and other desired biological properties.(119-121) Collagen is the single most abundant protein found in the animal kingdom and one of the main elements for different parts of human body especially bone, cartilage, skin and tendon.(122) Collagen has a triple helical structure made of three polypeptide strands/chains which have a repetitive sequence of amino acids, particularly glycine, proline and hydroxyproline.(119) So far, 29 distinct types of collagen have been identified, but collagen type I, II, III and V are the most commonly found.(120) Type I collagen is the main organic component of bone.

Collagen can be prepared in various forms like sponges, films and matrices, although fibrillar collagen scaffold are the most popular in tissue regeneration as they can biomimic the ECM structure.(123) In bone implants, simple collagen scaffolds or constructs could be used; however, they have disadvantages such as poor mechanical properties, low fibrillar density, and insufficient and delayed osseointegration.(121; 124) To promote bone

regeneration in the scaffold, in bone tissue engineering it is important to establish favorable interaction between the cells and the scaffold surface.(125) Additionally, the ability to stimulate the nucleation of calcium phosphate from physiological solution is essential to enhance the strength of the bone-matrix interface.(126) The scaffold surface properties also play a significant role in its successful interaction with surrounding tissue and mineralization process. Therefore, several attempts were made to synthesize collagen composites or to modify the surface properties of collagen by incorporating bioactive components such as direct inclusion of Hydroxyapatite (HA),(127) incorporation of bioactive glass,(121) coating with inorganic materials (e.g., ceramic) and other nanomaterials (e.g., β-tricalcium phosphate (β-TCP) nanoparticle,(128) graphene oxide (GO)(129) and reduced graphene oxide (RGO)(130)). Ceramics, especially alumina and titania, were found to be biocompatible with favorable bone bonding properties.(131; 132) Titania was also reported to attract calcium and phosphorous in aqueous environment to nucleate calcium phosphate or HA.(132-134) Consequently, it is novel to functionalize collagen scaffold surface with ultrathin film of titania while retaining the original structural properties of the substrate, and thus this strategy combines the advantages of titania and minimization/elimination of the drawbacks of the intrinsic native substrate.

Recently we have successfully deposited ultrathin film of titania on commercially available collagen membranes for the first time at room temperature by using atomic layer deposition (ALD).(1) ALD is a powerful and unique approach of nanotechnology to deposit conformal, uniform, ultrathin film (e.g., a few Å or nanometers thick) of inorganic material on porous, high aspect ratio, complex nanostructured substrates. ALD is a cyclic process with sequential, self-limiting surface chemical reactions, and the thickness of the deposited

film typically increases linearly with the number of ALD cycles. Thus, ALD offers precise control over deposited film's thickness and stoichiometry. Low deposition temperature, pinhole free coating, low impurity content and independence of line of sight are other major advantages of the ALD process.(124) ALD of titania thin film was deposited previously on different organic substrates like cellulose fibers of paper,(88) porous poly(styrene-divinylbenzene) polymer,(124) inner egg shell membrane(28) and spider dragline silks(32) from titanium precursor-oxidizer combinations such as $Ti(OMe)_4$-H_2O, $TiCl_4$-H_2O_2 and TIP-H_2O, respectively. ALD of TiO_2 on natural collagen extracted from hen's egg shell membrane was reported.(29) However, for all these TiO_2-ALD processes the lowest deposition temperature was reported to be 70°C which could alter the intrinsic properties of heat sensitive biological substrates like collagen.(135) Therefore, we chose a room temperature TiO_2-ALD functionalization process from a novel precursor-oxidizer system (TDMAT-O_3) on commercial collagen membranes to enhance their biomedical functionality while maintaining the original structure and properties of the substrate.

The objective of our study is to demonstrate the feasibility of enhancing or improving the bioactivity of the collagen membrane by functionalizing the membrane surface with ultrathin titania film deposited using ALD (Figure 13a) at room temperature in a custom-designed and made ALD reactor.(62) As a proof of concept, a commercially available collagen membrane was used as ALD substrate. Different surface characterizations were performed to investigate the properties of the native and surface-coated collagen. The bioactivity of the samples was tested in-vitro by using different cell proliferation and differentiation assay, and calcium phosphate attachment assay. We hypothesized that our titania coated collagen would promote accelerated bone regeneration by supporting human

osteoblastic and mesenchymal stem cells growth and favor the nucleation process of calcium phosphate from body fluid solutions.

2.3.2. Material and Methods

Sample Preparation: A commercially available collagen membrane (Biomend®, Zimmer, USA) was used as substrate in this study. The as-received membranes were cut into small pieces (25mm×15mm) before oxide deposition. The detailed ALD process for room temperature deposition of TiO_2 on collagen membrane was described elsewhere.(1) Three different thicknesses of TiO_2 films i.e., after 150, 300 and 600 ALD cycles were used on collagen samples in a custom-built ALD reactor with a custom-made sample holder. This TiO_2 ALD was carried out at 500mTorr operating pressure, using Tetrakis(dimethylamino)titanium (TDAMT) and Ozone (O_3) as titanium precursor source and oxidizer source, respectively. The non-coated collagen served as "control" group, and "150", "300" and "600" groups are the collagen samples with 3 different TiO_2 thickness obtained after 150, 300 and 600 ALD cycles, respectively.

Sample Surface Characterization: Numerous surface characterization techniques were used to investigate the properties of the ALD-TiO_2 coated collagen surface compared to these of non-coated control collagen samples. Scanning Electron Microscopy (SEM) (JEOL JSM-6320F, JEOL, Inc.) was used to study the surface morphology of the samples. Prior to SEM, samples were gold-coated using a sputter coater to make them conductive. To better study the structure and interface of the thin film and the collagen fibers, a high-resolution Scanning Transmission Electron Microscope (STEM, Aberration Corrected Analytical Electron Microscope, JEM-ARM200CF, JEOL, Inc.) was used for imaging the cross-section of the samples. For this STEM experiment, the sample was first mounted on

Si using embedding epoxy (EPO-TEK® cold cure epoxy) and allowed to cure for 24 hours. It was then sliced with a low speed diamond saw, mounted on a tripod polisher with cyanoacrylate, and wedge-polished on diamond lapping film (South Bay Technologies) using isopropanol rather than water. The specimen was then mounted on a copper aperture grid and released from the tripod by soaking in acetone. Finally, it was ion-milled for ~2 hours at 6 kV, followed by 30 min at 1 kV. X-ray Photoelectron Spectroscopy (XPS) (Kratos AXIS-165, Kratos Analytical, Ltd., UK equipped with a monochromatic Al Ka (1486.6 eV) x-ray source operating at 15 kV and 10mA) was utilized to study the surface chemical composition of the sample groups. For Raman Spectroscopy, a 633nm/17.5mW red HeNe laser source was used in a Raman Spectrometer (inVia Reflex, Renishaw). The wetting behavior of the surface was examined using static water droplet contact angle (WCA) measurement method using a contact angle goniometer (Model 100-00, Ramé-Hart Instrument Co.). WCA measurements were performed immediately after taking the ALD-deposited sample out of the reactor, to minimize the effect of surface contamination from surrounding environment during storage in normal lab air conditions. To investigate the mechanical properties of the single collagen fibers before and after deposition of TiO_2 thin film, Atomic Force Microscopy (AFM) was used. For this AFM experiments, modified mica substrate was first prepared to immobilize the collagen fibers. Freshly cleaved mica was treated by 1% 3-aminopropyl-triethoxysilane (APTES, Sigma-Aldrich, Inc., St Louis, MO, U.S.A.) for 5 min, followed by washing with DI water and drying with airflow. The modified mica was further treated at 120°C for 2 h and cooled to room temperature for use. After that, 1 mm^2 piece of each collagen sample were cut and immersed in DI water for 2 hours, in order to loosen the tangles of collagen fibrils. Then the samples were placed on

APTES modified mica for 10 minutes to immobilize the fibrils on mica substrates. All AFM experiments were carried out with a Dimension ICON AFM system (Bruker, USA). Peak force Tapping mode was applied for all the nano-mechanical measurements and topography imaging. RTESPA silicon cantilevers (Bruker, USA) were used. The spring constant was calibrated using Sader's methods(136) before each experiment, and the calibrated values were in the range from 42 to 49 N/m.

Ca and P Attachment Assay: Bio-activity of the collagen samples were subsequently evaluated using a biomineralization study to assess their ability in nucleating calcium phosphate or hydroxyapatite (HAp) from aqueous solution. For this experiment, the control and coated collagen samples ("150" and "600") were immersed in simulated body fluid solution (SBF) for two different periods of time i.e. 1 day and 7 days. The SBF solution was prepared by dissolving reagent grade (all chemicals from Sigma Aldrich) NaCl (>99%), $NaHCO_3$(≥99.7%), KCl (99.7%), $K_2HPO_4 \cdot 3H_2O$ (≥99.0%), $MgCl_2 \cdot 6H_2O$ (99.0-102.0%), $CaCl_2$ (≥97%), and Na_2SO_4 (≥99.0%) in deionized water and buffering at a pH value of 7.4 with tris(hydroxymethyl)aminomethane ($(CH_2OH)_3CNH_2$) (≥99.8%) and hydrochloric acid (HCl) to attain ion concentrations nearly equal to those of human blood plasma.(137) Every 2-3 days the SBF solution was changed to avoid precipitation. The entire experiment was performed inside an incubator at 37°C and 5% CO_2 condition to biomimic human body environment. After incubation for defined periods of time, the collagen samples were removed from the SBF, rinsed gently with deionized water twice, and vacuum-dried overnight. Chemical characterization of mineralized collagens were performed by Attenuated Total Reflectance Fourier-transform Infrared Spectroscopy (ATR-FTIR) using Nicolet iS5 FT-IR Spectrometer (ThermoFisher Scientific). Surface

chemical composition of mineralized collagen samples was studied using XPS. Alizarin red staining was used to further detect the presence of calcium (Ca) in the mineralized collagen samples. The mineralized dry collagen samples were first cut and placed on top of a glass slide. After that they were stained using alizarin red solution and kept for 30 s. Right after that, the stained samples were washed gradually using acetone solution and left under hood for air drying. Finally, the images of the stained samples were captured using an optical microscope equipped with a digital camera (EVOS® XL Core Imaging System, ThermoFisher Scientific, USA). The histogram of red pixel count and the total number of red pixels are derived using a MATLAB program from the digital images of the sample groups.

Biological Assay: Osteogenic cell response of our sample groups was studied by culturing human osteoblast cell (MG63 cell lines). MG63 human osteoblasts cells were cultured in Dulbecco's Modified Eagle Medium (DMEM) (Gibco) with 10% fetal bovine serum (FBS) (Gibco) and 1% antibiotic (Gibco) until roughly 80% confluence in a cell culture incubator at 37°C and 5% CO_2 conditions. After reaching confluence (~80%), cells were then detached using trypsin-EDTA (Gibco, Life Technologies), centrifuged and re-suspended in culture medium for sub-culturing and seeding over the collagen samples. Cells were seeded on the three selected sample groups of collagen (Control, "150" and "600") for different cell experiments.

Fluorescence assay was used to observe cells attachment, spreading and morphology on different sample groups. This assay was performed after 1 and 7 days of seeding the cells on the sample surface. Fluorescent dye based reagent labelling (Molecular Probes™, ThermoFisher Scientific) and fluorescence microscopy were used for this experiment.

Cells were imaged with a fully automated inverted microscope (Leica DMI6000 B, Leica Microsystem, Germany) and post-processing of the images were performed using LAS AF software (Leica, Germany). Prior to imaging, cells were first fixed in 3.7% Formaldehyde, permeabilized with 0.1 % Triton X-100 and stained in phosphate-buffered saline (PBS). Actin and nuclei of the cells were stained with ActinGreen™ 488 ReadyProbes® Reagent (Molecular Probes™, ThermoFisher Scientific) and NucBlue® Fixed Cell ReadyProbes® Reagent (Molecular Probes™, ThermoFisher Scientific) respectively. Nucleus counts were performed from the obtained fluorescence images using ImageJ software.

MTT assay was used to evaluate osteoblast cell proliferation and cellular viability or metabolic activities. Cell proliferation was evaluated at two separate time points like fluorescence assay i.e. after 1 day of incubation, and after 7 days of incubation, to understand the effects of short-term and long-term attachment and proliferation on the treated surfaces. CellTiter 96® (Promega) assay was used for this analysis. After the aforementioned incubation periods, the pre-optimized dye solution (MTT, a yellow tetrazole dye) was added for the conversion of tetrazolium into formazan product (purple crystals), produced by the reduction of MTT salt by mitochondrial reductase enzyme in the functional mitochondria of viable cells. After an additional 4 hours of incubation at 37°C, the dimethyl sulfoxide (DMSO) (Sigma-Aldrich, USA) solution was added to the 24-well plates to solubilize the formazan product. Three aliquots of 100 µL of each sample from the 24-well plates were then transferred to a 96-well plate and analyzed for absorbance changes. Absorbance values were measured at 570nm using an Elisa microplate reader (VersaMax, Molecular Devices, Sunnyvale, CA, USA). The mean of the three reads of each 96-well plate was considered as a single value of the 24-well plate.

Furthermore, qRT-PCR was used to determine the mRNA expression levels of osteogenic genes of human stem cells. For this experiment, human Mesenchymal Stem Cells (hMSCs), derived from adult bone marrow (Tulane University), were cultured on the control and coated collagen surface. The hMSCs were cultured for two time points (7 and 14 days) in a previous mentioned culture medium, enriched with 0.05 mM L-ascorbic acid, 100 nM dexamethasone and 10mM ß-glycerophosphate disodium salt hydrate to allow osteoblastic cells differentiation. The RNeasy Plus Mini Kit (Qiagen, Qiagen Sciences) was used to extract the total RNA. The RNA concentration was detected by a spectrophotometer (Nanodrop 1000, Thermo Scientific), and cDNA was prepared using RT^2 First Strand Kit for RT-PCR (Qiagen, Qiagen Sciences). Quantitative real-time PCR was performed with Fast Start Universal SYBR Green Master (Roche, Roche Diagnostics GmbH) and human osteogenic primers by using Applied Biosystem® StepOnePlus™ instrument (ThermoFisher Scientific). The expression levels of alkaline phosphatase (ALP), osteocalcin (OC), runt-related transcription factor 2 (RUNX-2), Collagen-1 (Col-1), bone morphogenetic protein 2 (BMP-2), transforming growth factor beta 1 (TGF-β1) and glyceraldehyde 3-phosphate dehydrogenase (GAPDH) were analyzed. GAPDH was used as an internal reference. The relative gene expression level was estimated by transforming the logarithmic values into absolute values using $2^{-\Delta\Delta C_T}$method, where the average threshold cycle (C_T) values were used to quantify the gene expression in each sample: $-\Delta\Delta C_T = -(\Delta C_{T,\mathrm{Target}} - \Delta C_{T,\mathrm{GAPDH}})$.

2.3.3. Results and Discussion

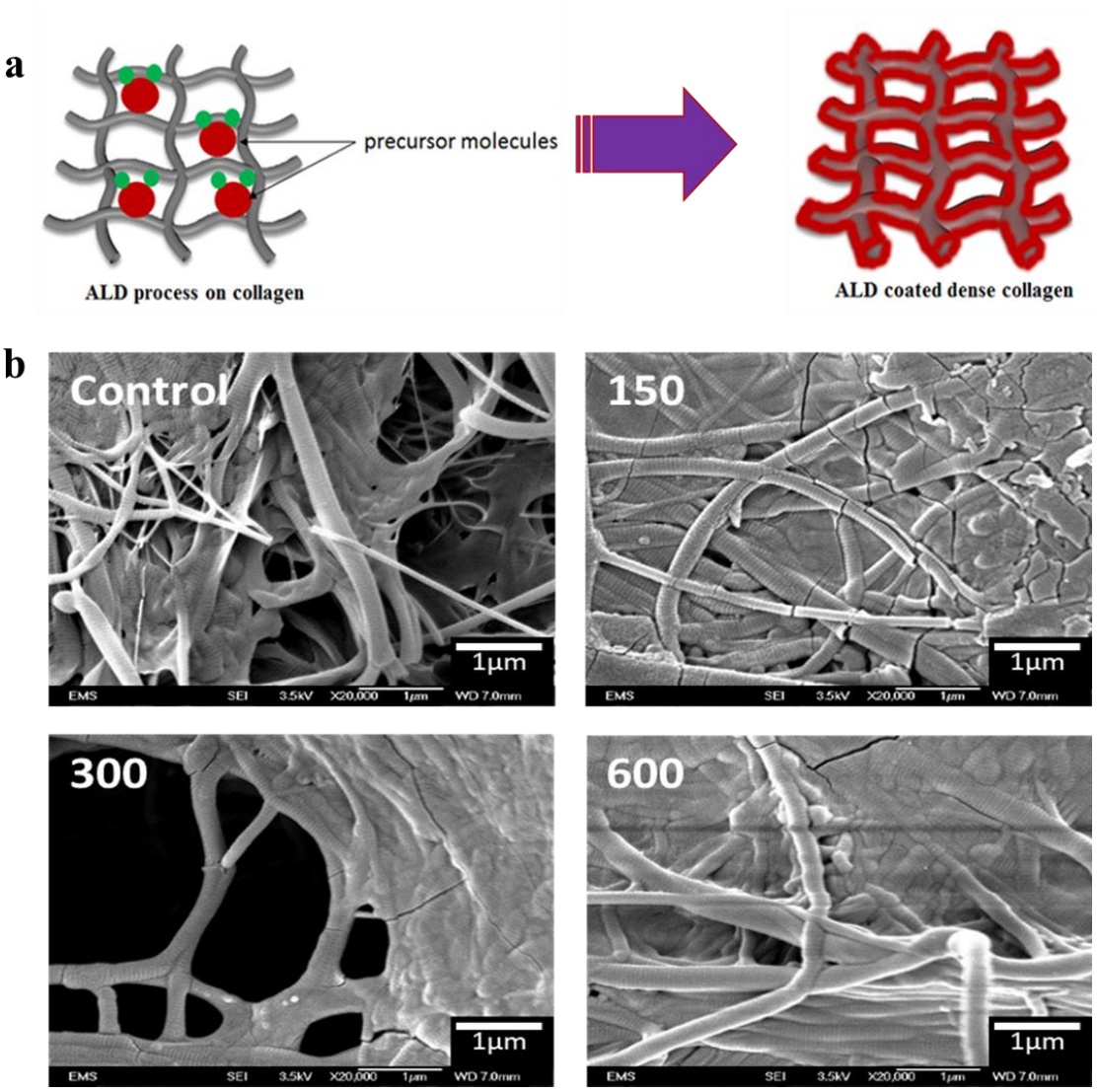

Figure 13**.** a) Schematic representation of the ALD process on the collagen fibrous substrate. Grey core represents the collagen fiber and red shell represents the thin ALD coating of TiO_2. b) Scanning Electron Microscopy (SEM) micrographs (each 1µm scale, X20000 magnification) of all sample groups. The non-coated collagen is the control; the collagen samples labelled as "150", "300" and "600" are the ones with 150, 300 and 600 cycles of ALD-TiO_2 at room temperature, respectively.

The non-coated collagen served as control group, and “150”, “300” and “600” groups are the collagen samples with 150, 300 and 600 cycles of ALD-TiO_2 at room temperature, respectively. To have an in-depth understanding of the surface morphology, SEM was performed on all sample surfaces and the corresponding micrographs are presented in Figure 13b. These SEM images revealed changes in surface morphology of the collagen samples after exposure to increasing number of ALD cycles. The fibers of the control collagen are seen to become thicker with increasing number of ALD cycles and as a result the membrane became denser with the increasing nano-fibrillar density. This was expected as ALD is a cyclic process, where the deposited oxide thickness increases with increasing number of cycles. Increasing the fibrillary density of collagen is important for bone tissue engineering applications.(121; 138; 139) Brown et al first reported a rapid and reproducible method to increase the fibrillar density of collagen matrix by plastic compression and this technique increased the fibrillar density more than 10% by weight.(140) However, our ALD process offered a uniform, conformal and high precision approach to augment the fibrillar density of collagen membrane by infiltrating a bioactive ultrathin film coating of TiO_2 which presumably induces an upsurge of the interfibrillar cross-linking density.

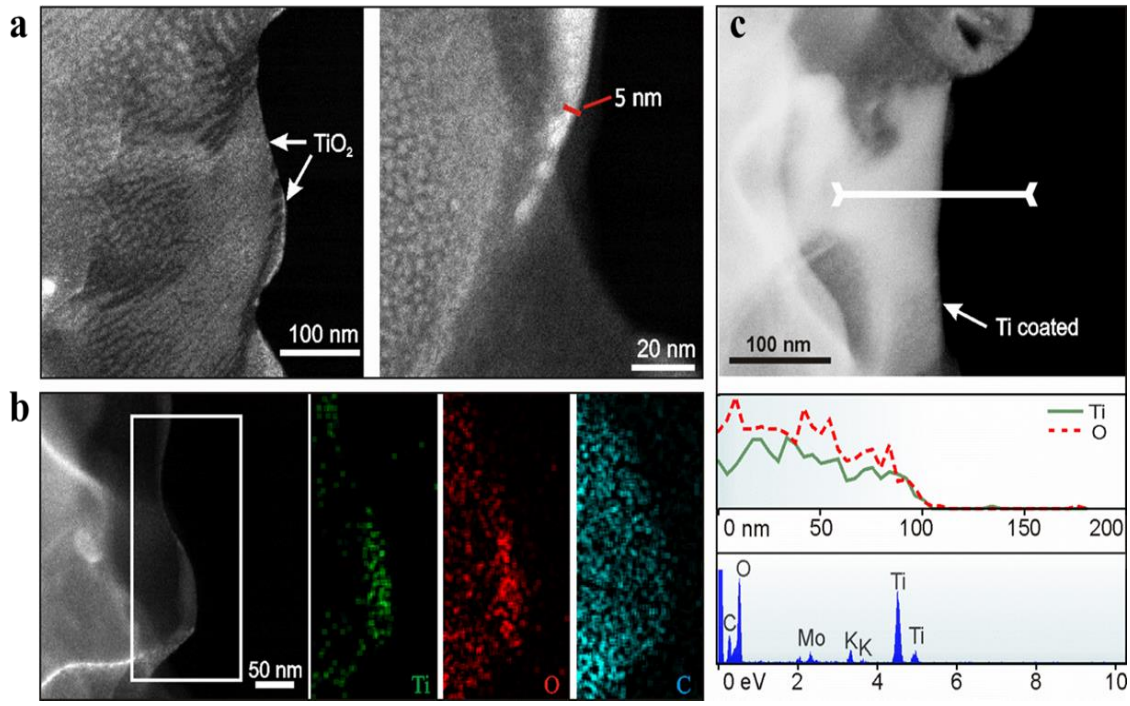

Figure 14**.** a) Scanning Transmission Electron Microscopy (STEM) results of cross-sectioned "600" group showing Z-contrast high angle annular dark field (HAADF) STEM images, b) Energy Dispersive X-ray Spectroscopy (EDS) mapping of Ti, O, and C elements, c) an EDS line scan showing the Ti and O signals at the edge of the cross section and the EDS sum spectrum.

From preliminary STEM analysis (Figure 14a) of the cross-sectioned TiO_2 coated collagen sample ("600" group), clear contrast was observed between the TiO_2 coating (bright phase), and the much lower atomic number collagen substrate (darker) in the HAADF images. The extra brightness at the edge of the specimen corresponds to a region where the film is seen edge-on, and therefore has greater apparent thickness and contrast. The coating thickness appears to vary between 5-20 nm, is conformal to the fiber surface, and shows considerable nanoscale roughness, on the order of ~5nm. EDS mapping in Figure 14b and an EDS linescan in Figure 14c confirmed the identity of the TiO2 shell form by the strong

Ti and O signals at the surface compared to the C signal from the bulk collagen core. This is most clear in areas where the cross section is thin, as in the area mapped in Figure 15b. Due to the surface roughness of the collagen fiber mat, edge-on views of the film were rare, and images of the specimen surface show it to be well-coated with TiO_2, as is shown in the line scan in Figure 14b. This STEM and EDS analysis also has revealed that the ALD TiO_2 coating was conformed to the shape of the collagen fibers, which was consistent with ALD conformal growth on three-dimensional substrates, with good infiltration into the rough surface of the fiber mat. Additionally, the nano-scale roughness similar to that seen in these films has previously been shown to aid osteoblast growth.(141)

STEM-EDS analysis of a cross-sectioned (prepared by focused ion beam) Ti infiltrated collagen has previously been reported for a natural dried collagen (extracted from hen's egg shell membrane) after infiltrated with ALD-TiO_2 at 70°C, using titanium isopropoxide (TIP, $Ti[OCH(CH_3)_2]_4$) as the precursor and water as oxidizer.(29) They also observed that the interface between the TiO_2 shell and the collagen was not sharp, but showed a gradient in the mass concentration of Ti well into the bulk. This is likely a result of infiltration of the precursor solution as noted by the authors, though aspects of sample preparation may play a role as the interface is not uniform in the z-direction in the relatively thick sample, and there is the possibility of redeposition of Ti after sputtering during FIB. In contrast, the interface between coating and substrate in our samples appears much sharper, as seen in Figure 14b, where the Ti seen away from the interface can be attributed to the specimen geometry.

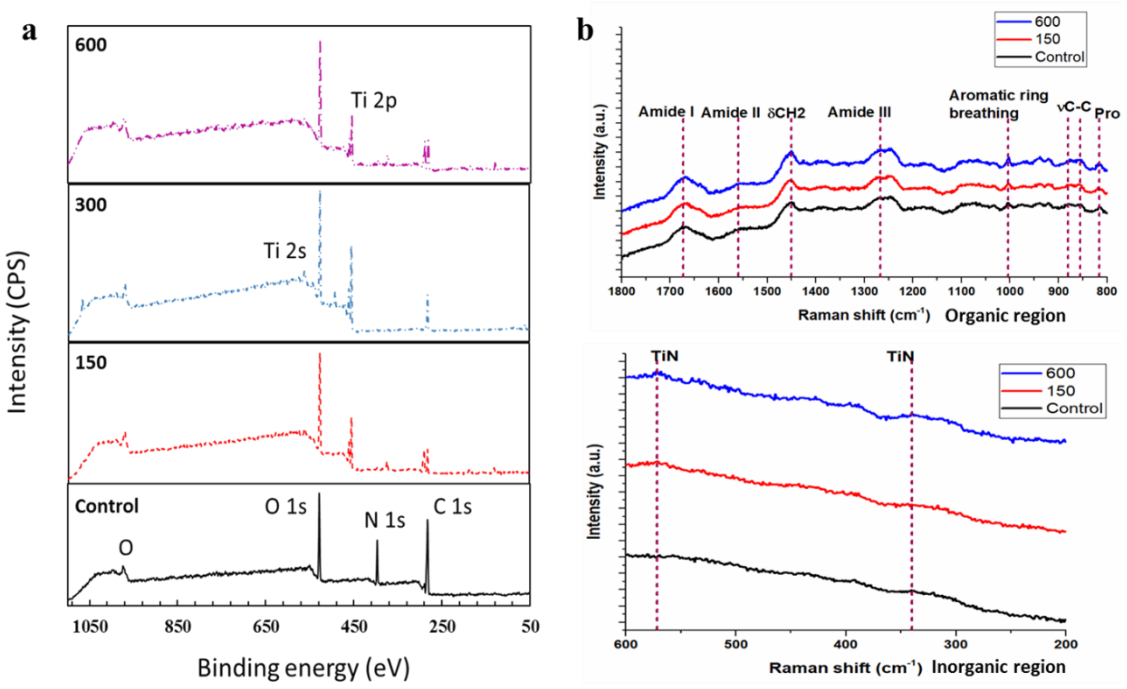

Figure 15**.** a) X-ray Photoelectron Spectroscopy (XPS) analysis of our sample groups showing surface chemical composition, b) Raman spectra showing organic (top right) and inorganic (bottom right) regions of the control and TiO_2 coated sample groups.

Figure 3a shows XPS results of our 4 sample groups. This analysis was performed to study the chemical composition of the sample surface before and after the room temperature ALD process. The control collagen sample had only three distinct peaks attributed to carbon (C 1s: 285eV), nitrogen (N 1s: 398eV) and oxygen (O 1s: 532eV) elements. This is expected as collagen is a protein and C, N and O are the basic elements of a protein. For all ALD-TiO_2 deposited sample groups (i.e., "150", "300" and "600") distinct peaks of titanium (Ti 2s: 560eV and Ti 2p: 455eV) are observed. These results confirmed the successful deposition of TiO_2 thin film on the collagen surface. Raman spectra of the control and TiO_2 coated collagen samples are presented in Figure 15b. In the organic region of the scan (e.g., 1800-800 cm^{-1}), signals from the Amide I, Amide II, Amide III, CH_2 bending (δCH_2), C-C stretching (νC-C) of Proline were observed in all sample groups, suggesting the presence of helical conformation of this collagen membrane. There might be a conformational change in the collagen structure due to the infiltration of TiO_2 through the ALD process used. In the inorganic region (e.g., 700-200 cm^{-1}) of the Raman scan, weak Ti-N spectral features were also observed and attributed to likely Ti mediated new bond formation between nitrogen and carbonyl groups, presumably substituting hydrogen (H) in the N-H•••O=C bond with Ti.(29) However, the nucleation of TiO_2 on collagen and/or the exact binding site of Ti to collagen needs further investigation. Though Raman is not very surface sensitive technique, from this data it also indicates there was no real change or damage of collagen sample from ALD treatment or exposure to ozone (1000 PPM), as no significant peak shifts was observed in the organic region of Raman scan. Similar observation was also presented from the ATR-FTIR scan later, in Figure 19b.

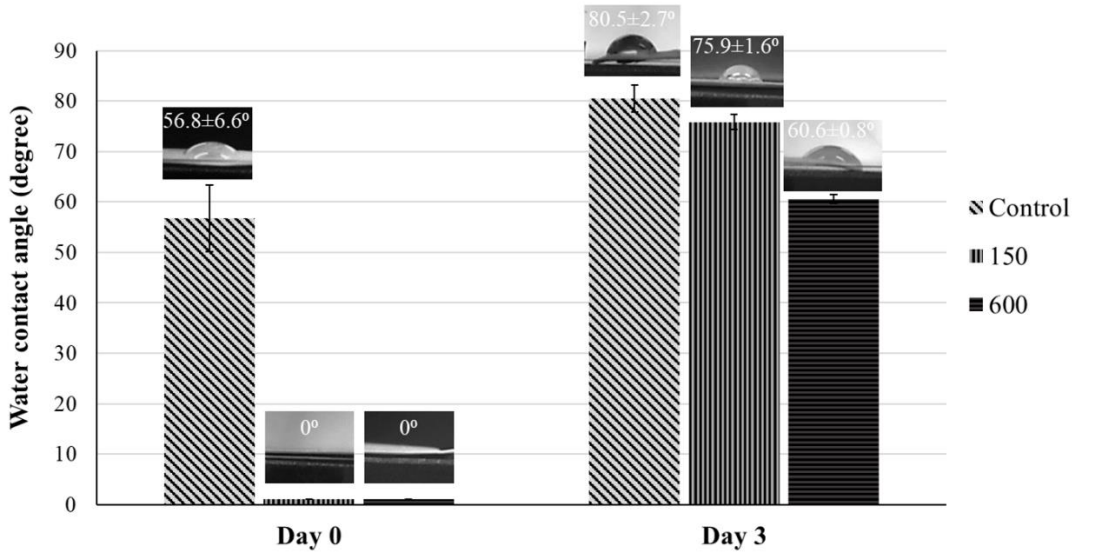

Figure 16**.** Wettability behavior of the samples studied from water drop contact angle measurements at day 0 and day 3 in lab ambient.

Wettability property of the samples surface were investigated using static water drop contact angle measurement (Figure 16). The samples became superhydrophilic (water contact angle (WCA) is almost 0°) right after ALD-TiO_2. The control sample is hydrophobic (WCA ~60°) compared to the TiO_2-coated samples. After 3 days of storing the samples in normal lab air environment, all samples became hydrophobic, while the TiO_2-coated samples remained less hydrophobic compared to the control sample. Storing conditions/environments can therefore have a large impact on wettability. This hydrophobicity was most likely just ambience effect (no real chemical alteration of samples), attributed to surface contamination from the lab air environment during storage. Measuring this hydrophilic/hydrophobic character of a biomaterial surface in terms of

relative wettability is essential, since the wetting behavior of a surface plays a significant role in the early stages of cell responses.(142)

Sample group	**Elastic Modulus [GPa][a)]**
Control	1.97±0.44
"150"	2.1±0.42
"600"	2.58±0.41

[a)]((Giga Pascal));

TABLE IV**.** Atomic Force Microscopy (AFM) results showing the corresponding elastic modulus of collagen fibers for our sample groups.

Mechanical properties of the single collagen fiber were tested using AFM technique and the results of elastic modulus is presented in TABLE IV. ALD TiO_2 coating was found to slightly increase the elastic modulus of the control collagen fiber. This indicated that the ALD-TiO_2 coating did not really alter the mechanical properties of the native collagen to a great extent, that is, the flexibility of the native collagen was retained. AFM was previously used to probe the elastic modulus of individual collagen fibrils, and the effective stiffness of a collagen thin film (prepared from denatured Type I collagen), using experimental and modelling approach.(143) The elastic modulus was reported to significantly change after dehydration; more specifically, the elastic modulus for small fibers, large fibrils and the natural collagen film was reported to be 22±4 kPa, 12-230 MPa and 40±9 kPa, respectively.(143) Recently, Lee et al reported the mechanical property of

natural collagen (inner shell membrane collected from hen's eggs) in a dried state, and the mechanical property of that native collagen after TiO_2-ALD metal oxide infiltration using titanium (IV) isopropoxide[TIP] ($Ti(OiPr)_4$) precursor and water oxidizer at 70°C substrate temperature.(29) Under uniaxial tension, they reported that the toughness and fracture strain of their native collagen were about 23MJ/m^3 and 6.1% respectively, while those values increased (almost 3 times) to 77MJ/m^3 and 10.2%, respectively, after the TiO_2-ALD process. They also reported that the native collagen had the fracture stress, yield stress and stiffness values of 6.2 MPa, 4.8 GPa and 1.5 MPa respectively; on the other hand, after performing TiO_2-ALD of the native collagen those values rose to 11.8 MPa, 7.6 GPa and 1.8 MPa respectively.(29) However, the elastic modulus of the collagen membrane used in this study was higher compared to natural collagen membranes, as the mechanical stability (tensile strength) of this barrier membrane was enhanced by cross-linking it with a chemical cross-linker, glutaraldehyde (GTA).(144)

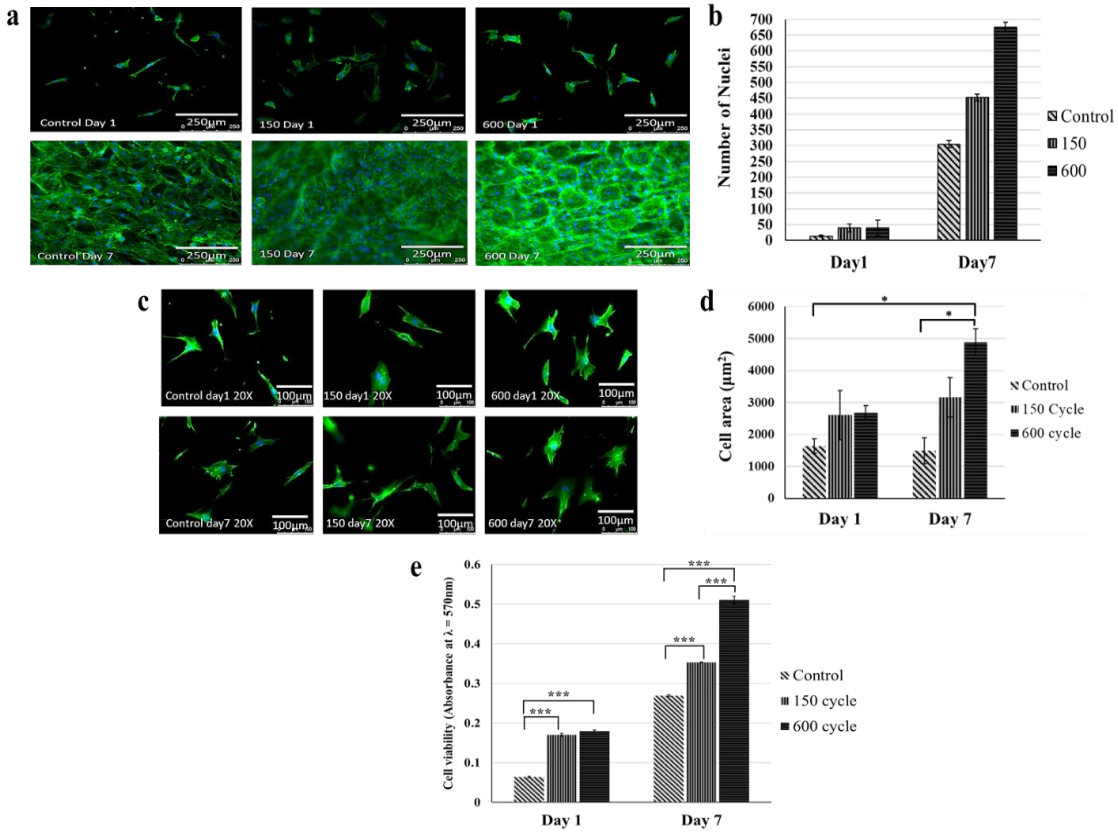

Figure 17**.** MG63 cell spreading and proliferation assay results. a) Fluorescence images of MG63 cells seeded on control, "150" and "600" for day 1 and day 7, b) nucleus counts results from fluorescence images, c) higher magnification (20X) of the fluorescence images focusing on single MG63 cells seeded on control, "150" and "600" for day 1 and day 7, d) area of the single cells measured from those 20X fluorescence images, e) MTT viability assay results showing absorbance expressed as a measure of cell viability of MG63 cells cultured on the sample groups for day 1 and day 7 ($p < 0.05$: * and $p < 0.001$: ***).

MG63 osteoblasts was used as a model cell line to assess the potential of the uncoated and TiO_2 coated collagen in promoting cell growth, spreading and attachment. Figure 17a showed the MG63 cell morphology cultured on control and TiO_2 coated collagen samples for both day 1 and day 7. After 1 day of cell seeding, the degree of cell growth and cell spreading was less for all the sample groups. However, it clearly indicated that all the TiO_2 coated collagen surface also supported the growth of MG63 cells like a biocompatible native collagen membrane. The cell morphology was more clearly observed after 7 days. At day 7, the cell density was much higher on both the TiO_2 coated collagen groups ("150" and "600") compared to that on the uncoated control. This finding indicated that the ALD TiO_2 coated surface was more bioactive in promoting osteoblast cellular growth. Additionally, nuclei counts were obtained from the captured fluorescence images for both day 1 and 7, to analyze the number of healthy cells present on each sample group (Figure 17b). Nuclei counts clearly showed that TiO_2 coated collagen surfaces ("150" and "600") had higher number of cells compared to the control surface. Cell spreading was quantitatively studied by measuring the area of single cells from the corresponding higher magnification fluorescence images presented in Figure 17c and the associated cell area measurements data were provided in Figure 17d. Cells appeared to be more widely spread on TiO_2 coated collagen surface compared to control in both day 1 and day 7 time points. Particularly, a significant increase in cell spreading was observed for "600" groups at day 7 as compared to the uncoated control. These results revealed that TiO_2 coated collagen surface can successfully promote osteoblast cell growth and spreading.

MTT assay was performed to further quantify the proliferation of the MG63 osteoblast cells cultured on the uncoated control and TiO_2-coated collagen samples. The viability percentage results were presented as absorbance value. These absorbance values for control and two TiO_2 coated collagen samples ("150" and "600") for day 1 and day 7 are presented in Figure 17e. Significant differences in the cell proliferation was observed among the sample groups. Both at day 1 and day 7, cells responses were significantly higher for the two TiO_2-coated collagen sample groups as compared to the control sample. For day 7, significantly high cell proliferation was observed for the "600" samples compared to the "150" ones. These MTT assay results also corroborate our finding from the fluorescence assay and clearly demonstrate that osteoblast cells had better growth characteristics, spreading and higher cell proliferation rate on the ALD TiO_2-coated collagen compared to control, and this higher cellular response appeared to increase with thicker TiO_2 film on the sample (i.e., "600").

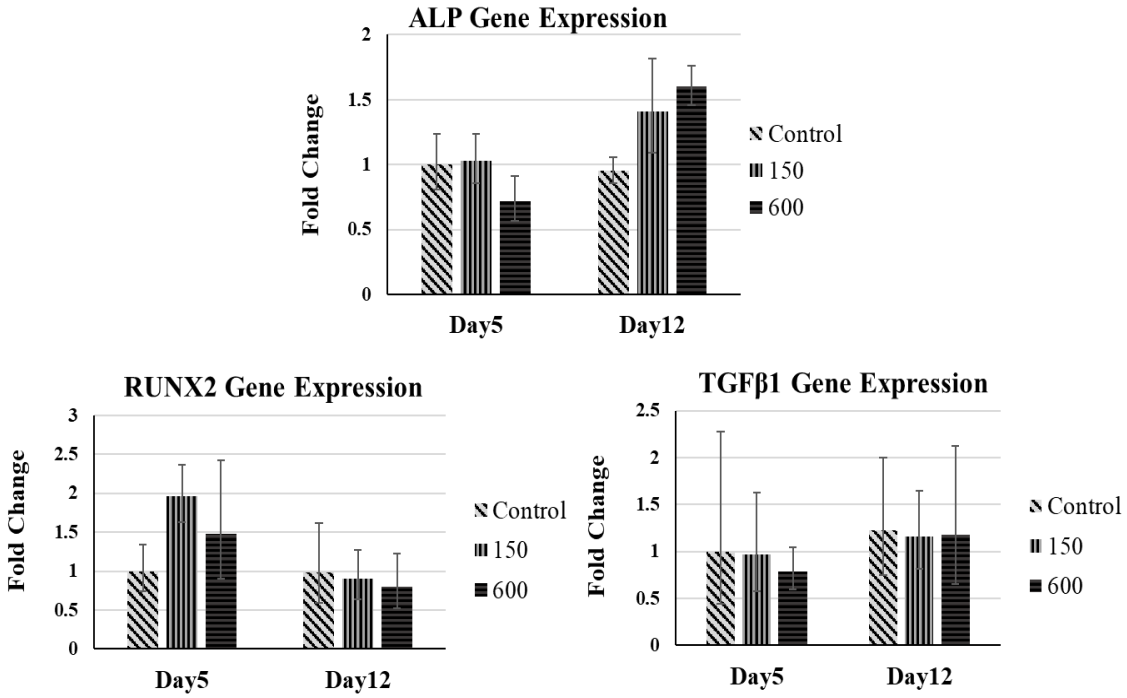

Figure 18**.** Quantitative polymerase chain reactions (qRT-PCR) results showing the osteogenic gene expression of ALP, RUNX2 and TGFβ1 genes for hMSCs cultured on control and ALD-TiO_2 coated collagen sample surface over 5 and 12 days.

Quantitative Real-Time Polymerase Chain Reaction (qRT-PCR) was performed to investigate the osteogenic differentiation of hMSCs cultured on control and TiO_2-coated collagen samples over 5 and 12 days. Expressions of ALP, RunX2 and TGFβ1 are presented in Figure 18. ALP activity is an important factor in evaluating the early stage of osteogenic differentiation, and it is also considered one of the earliest criteria of osteoblasts mineralization.(145; 146) On the other hand, RunX2 is another important transcription factor in osteogenic differentiation, the activity of which indicates the differentiation of MSCs to osteogenic linage.(147; 148) Overall it was observed, that ALP was upregulated for the MSCs cultured on TiO_2-coated collagen compared to control at day 12, despite showing downregulation at the initial phase of day 5. RunX2 was upregulated for the MSCs cultured on TiO_2 coated collagen compared to control at day 5, while at day 12 the expression level was almost same as control. These results were attributed to the effectiveness of TiO_2 coated collagen surface in inducing higher level of gene expression, and thus enhanced bone forming ability as compared to that of uncoated control collagen surface. Additionally, TGFβ1 gene plays important role in controlling the immune system signaling and thus serves as a marker of any kind of inflammations (149). No difference was observed in the expression of TGFβ1 for both control and TiO_2 coated collagen surface. This result may indicate that there was no inflammatory response detected for MSCs cultured even on the TiO_2 thin film mediated surface modified collagen, suggesting the biocompatibility of this modified membrane surface.

Osteogenic differentiation was previously reported to be induced on TiO_2 surface with different nanostructures (e.g., nano-pits, nanodot pattern, nanopillars).(150-152)

Upregulation of ALP gene was reported on nanostructured TiO_2 surface (nanopores embedded with TiO_2 nanoparticles).(153) Enhanced expression level of RunX2 gene was also reported on different titanium nanosurface with hydrophilic behavior, high surface energy and nanotopography (e.g., grooved, roughened surface, nanostructures with distinctive topographical features).(148; 154-156) Additionally, it was also reported that the expression level of ALP and RunX2 gene enhanced in similar cross-linked and noncross-linked commercial collagen membranes indicating their sufficient diffusibility to support osteoblast like cell differentiation.(145; 157; 158) Considering this osteogenic differentiation attributed to titanium nanosurface and collagen biomaterials, the obtained gene expression on this room temperature TiO_2-coated collagen membranes seemed to be consistent with reported data.

This improved biocompatibility in terms of higher bone cell proliferation, growth and spreading on TiO_2 deposited collagen samples, can be attributed to an individual or cumulative positive contributions of all possible enhanced surface properties such as surface morphology, increased fibrillar density, surface chemistry and especially the surface hydrophilicity. Surface wetting behavior, particularly a hydrophilic surface was reported to promote cell proliferation and spreading in numerous previous works.(148; 159-164) Desired cell adhesion and growth was achieved by using different hydrophilic coatings.(159; 160; 164) Higher cell spreading on a hydrophilic (WCA=18°) sputter-deposited Ti thin film was also reported.(148) Significantly higher cell attachment and spreading was also reported on superhydrophilic (WCA < 5°) titanium surfaces through activation of necessary cell signaling cascade.(161-163) Consequently, the hydrophilic

nature of this TiO_2-ALD coating can explain the observed cellular responses for MG63 cells. Furthermore, dense collagen with higher fibrillar density prepared using plastic compression demonstrated improved cellular responses.(138; 165-167) Nano-topographical features presents on the surface of a biomaterial also have a significant role in mediating cell responses, as those can increase overall surface areas, thereby increasing surface activities.(168) For example, nanograined or nanorough Ti surface, nanotubular Ti are well-known for enhancing osteoblast cell responses.(169-171) Furthermore, Denis et al also reported better osteoblast cell adhesion and spreading on 20nm crystalline ALD-TiO_2 thin film deposited on a chemically etched nanotitanium surface using TIP precursor at 250°C.(172) STEM analysis also revealed that this ALD-TiO_2 coated collagen had nanostructural features with nano-roughness on the surface which was previously reported to promote osteoblast growth.(141) Therefore, all these surface properties presumably played their role in enhancing the osteoblast cell response on this TiO_2 thin film coated collagen surfaces.

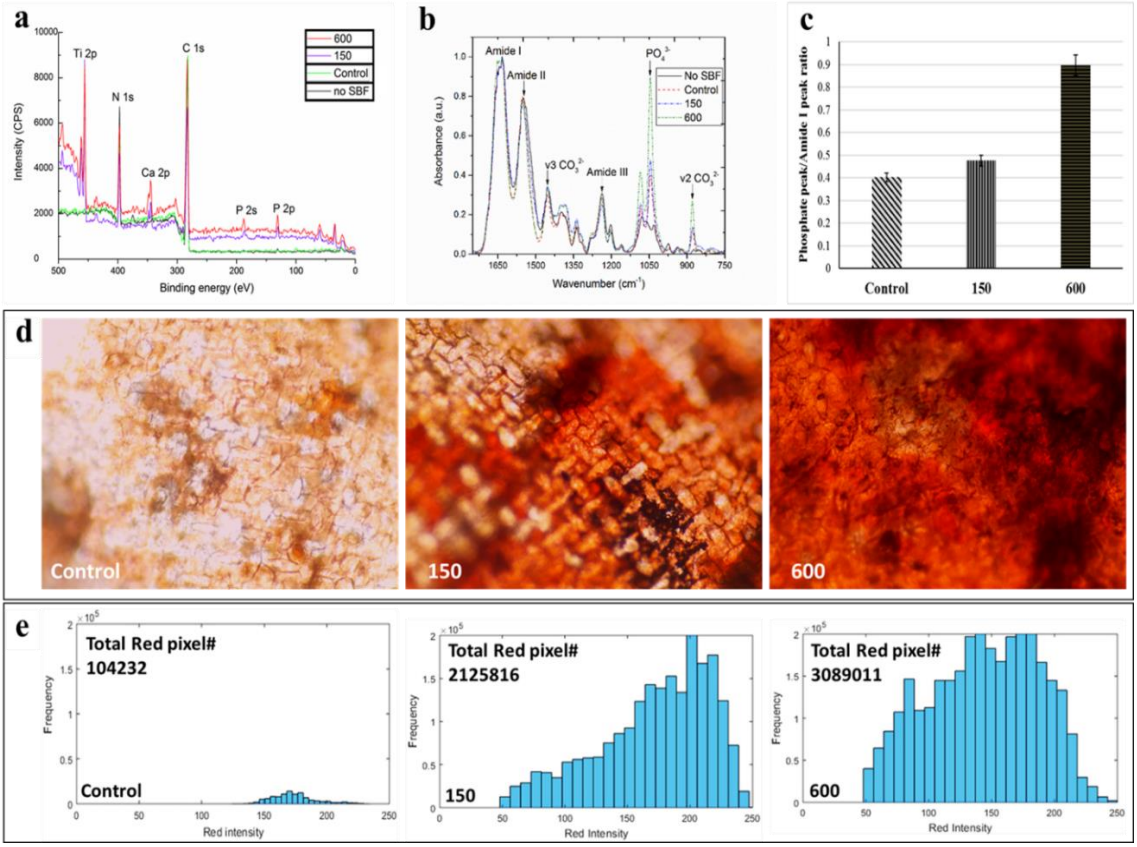

Figure 19**.** Calcium Phosphate attachment assay results. a) XPS analysis of collagen samples after incubation in SBF solution for 7 days at 37°C. The "no SBF" refers to an uncoated collagen sample without SBF incubation, b) Attenuated total reflectance Fourier transform infrared spectroscopy (ATR-FTIR) of the collagen samples incubated for 7 days in SBF solution at 37°C. The obtained spectra were baseline corrected and normalized to absorbance 1.0 of the Amide I peak for comparison purposes, c) A quantitative analysis (the ratio of phosphate peak to the Amide I peak) from the ATR-FTIR results, for the collagen samples incubated for 7 days in SBF at 37°C, d) Images of the mineralized collagen samples (i.e., Control, "150" and "600") in SBF for 7 days and stained in Alizarin red S stain, e) A quantitative analysis by red pixel counts and histogram of red intensity from the images of the stained samples.

The calcium-phosphorous attachment assay was performed using SBF to investigate the mineralization capability of the control and TiO_2-coated collagen samples. Several post chemical analysis were performed on the mineralized collagen samples to determine the existence and the level of calcium and phosphorus elements or the calcium phosphate compound, qualitatively and quantitatively. Firstly, XPS scan was performed to determine the surface chemical composition of the mineralized collagen samples (Figure 19a). The results clearly indicated that calcium and phosphorous elements were present on the surface of both TiO_2-coated collagen. For both coated collagen samples, clear distinct peaks of calcium (Ca 2p: 347 and 351 eV) and phosphorous (P 2s: 187 eV and P 2p: 133 eV) were observed indicating the attachment of those elements onto the surface of the TiO_2-coated collagen samples. On the other hand, those elements were absent on the surface of the non-coated control sample. This result suggests that TiO_2 coated collagen can facilitate Ca and P attachment compared to that of control collagen.

From the ATR-FTIR analysis, all the three amide characteristic peaks of a collagen protein, i.e., Amide I, II and III, were distinctly identified on all the collagen samples (Figure 19b). Phosphate (PO_4^{3-}) and carbonate (CO_3^{2-}) peaks were also observed on the collagen samples incubated in SBF solution for 7 days. From the presence and shape of these two absorbance peaks, a mineral phase of carbonated-apatite was likely present in those mineralized samples. The absorbance level of the PO_4^{3-} peak for control differed from that on "150" and "600" samples and the peak height was minimum, intermediate and maximum for control, "150" and "600", respectively. This increase in the absorbance of the PO_4^{3-} peak with thicker TiO_2 film coated collagen samples was corroborated by the quantitative

analysis of the FTIR results where the ratio of PO_4^{3-} to Amide I peak are presented in Figure 19c. These findings revealed the ability of the TiO_2-coated collagen samples to attract higher amount of P from SBF solution compared to the control; further the level of PO_4^{3-} increased with increasing TiO_2 nanofilm thickness.

To further detect the Ca level in the mineralized collagen samples, a rapid screening method using a calcium stain, Alizarin Red S, was employed. This staining clearly showed the difference in Ca levels among the studied sample groups. The staining was negative for the control collagen samples, whereas the staining was found to be positive for both the TiO_2-coated collagen samples (Figure 19d). For "150", the staining result was weakly positive, while "600" revealed strongly positive staining. From the histogram of the red intensity and the total number of red pixel counts of the images, a quantitative indirect correlation can be drawn for the level of Ca present in the mineralized collagen samples (Figure 19e). These results showed that the Ca level and the calcium phosphate quantity increased on TiO_2-coated collagen samples when compared to the control non-coated collagen. Additionally, the Ca level increased with increasing thickness of the TiO_2 coating and, consequently, the "600" samples had the highest red pixel count or intensity. This result also corroborates our finding through our ATR-FTIR and XPS analyses of the mineralized samples. Overall, the chemical analysis of the mineralized samples revealed that the TiO_2 coated collagen sample can attract higher amounts of Ca and P from SBF solution compared to control non-coated collagen sample and thus TiO_2 coated collagen samples can better facilitate the nucleation of calcium phosphate or apatite formation in physiological environment. Moreover, this mineralization capability was found to increase

with TiO_2 coating thickness of the ALD-coated sample groups, within the film thicknesses studied.

Nucleation of calcium phosphate or HA is a well-studied topic. Among the different contributing surface properties, the topography, surface energy, surface hydrophilicity and especially surface charge distribution were reported to promote the nucleation and growth of calcium phosphate.(124; 133; 134; 173) Moreover, it was also reported that TiO_2 coating provided favorable features to mineralize calcium phosphate in physiological solution, due to its special "negatively charged surface".(124) TiO_2 surface is capable of forming Ti-OH groups by absorbing water on its surface which helps as a nucleation site for calcium phosphate. A model was also proposed on the nucleation kinetics of calcium phosphate, where H_2O/H_3O^+ was described to provide the source of counterion protons for growing phosphate groups, and a Ca^{2+} cation bridge was suggested to form at the interface between the phosphate and the TiO_2 surface.(133) Järn et al reported that the Ti-OH groups mediated hydrophilicity of TiO_2 surface that favors the initiation of forming calcium phosphate.(134) Additionally, the increased fibrillar density of collagen also predominantly regulates better mineralization as dense collagen was reported to mineralize higher amount of calcium phosphate.(121; 138; 139) Therefore, our hydrophilic TiO_2-coated collagen surface with dense fibers mineralized high level of calcium phosphate from SBF solution as compared to control collagen. The control non-coated collagen also showed a low level of calcium phosphate nucleation that is probably due to the presence of negatively charge carboxyl groups present in the amino acid residue of this molecule.(173)

2.3.4. Conclusion

The surface of a commercially available collagen membrane was modified with an ultrathin film of TiO_2 deposited using ALD at room temperature in a custom-designed and built ALD reactor. Surface characterizations revealed the successful deposition of a uniform TiO_2 thin film on collagen fibrous surface. SEM results showed that the collagen fibers got thicker with increasing number of ALD cycles and, as a result, the collagen membrane became denser. From the biocompatibility assay, human osteoblast cells were found to grow and proliferate at a significantly higher rate on the TiO_2-coated collagen surface when compared to those on the control one. The TiO_2 coated collagen samples were also found to be bioactive with the ability to nucleate higher amount of calcium phosphate or apatite by better attaching higher levels of Ca and P elements from SBF solution compared to non-coated control collagen samples. Our findings suggest that the collagen material, the surface of which was prepared and modified through this room temperature ALD of TiO_2 thin film, shows enhanced biocompatibility and bioactivity. This novel biomaterial was found to be osteophilic and can be used for accelerated bone healing and/or regeneration in bone tissue engineering applications. Further, this novel process of surface modification can also be employed to improve or enhance the functionality of other similar biomaterials with a complex fibrous nanostructure.

2.4. Low temperature ALD of Pt on Collagen

2.4.1. Introduction

Conductive and flexible materials that are biocompatible, have the potential for a wide range of biomedical applications including tissue engineering, (174-176) implantable neurological electrodes, (177-181) controlled drug delivery (182-186) and electrochemical actuators. (187-189) This class of materials belongs to ecofriendly or "green electronics" (190) materials which are benign to our surrounding environment. "Green" and "Transient" technology refers to, electronic devices and system which, after stable operation, are capable of being disappeared completely within a defined period of time with minimal or non-traceable remains or byproducts. (191; 192) While durability is a factor for electronic devices for its stable performance for a given period, in the concept of modern electronics transient or biodegradable materials as well as biocompatible system are gaining much attention. (191) Indeed, in this 21st century electronic hazards or waste is one of the biggest problems for environment. (192) This environmental challenge can be resolved using these biodegradable transient electronics as they can disintegrate into the surroundings without leaving any harmful impact. On the other hand, these transient electronics can also be used as biomedical diagnostic device implanted into human body, and thus eliminating the need of expensive secondary surgery to extract those devices from body. (191; 192).

Following the concept of developing this kind of system, the choice of green and transient material is becoming attractive in modern biomaterial based electronics. (190; 193) Selection of the suitable material is the key behind success of green and transient technology. This kind of materials require to have some unique properties such as

biodegradability, bioresorbability, biocompatibility and environmentally safe. (190; 193; 194) The advantages behind using these materials are: low cost, energy efficient production due to their natural origin, no long term adverse effects, no need of retrieval as they can resorb by themselves and above all they can minimize hazardous waste for our environment. (193) Previously, efforts have been made to develop this kind of electronics from transient materials mostly based on some polymer or metal or semiconductor materials. (192) Partially transient or soluble electronics were developed based on organic substrates such as cotton and silk, where the device remained insoluble in spite of the substrates are soluble. (191) Recently, attempts have been made to develop completely soluble electronics. In those system, silicon (Si) substrate based fabrication was used due to the high solubility of silicon in body-fluids and even in water. (193) In silicon based transient electronics, silicon dioxide (SiO_2), magnesium (Mg) and magnesium oxide (MgO) were used as gate dielectric, conductors and inter-layer dielectric respectively. (193) Although these electronics are soluble, they are mostly inorganic substrate based device, as a result biocompatibility could be an issue for those devices used for implantable diagnostic devices where biocompatibility is a significant factor behind the success of any such device. Additionally, silicon based electronics materials or their byproducts may still leave some impact on our environment. Considering these aspects, potential usage of collagen as a substrate material was proposed in our study. Collagen is an important biomaterial which is used in several biomedical applications. It has a triple helix structure made of polypeptide chains. (119; 194) Glycine, proline are the most abundant amino acids found in its structure. Collagen is a flexible biomaterial which is also

biodegradable/bioresorbable, (144) biocompatible (144) and piezoelectric. (194) For these unique properties of collagen biomaterial, it might be an ideal choice for this kind application in implantable electronics. On top of that, collagen is a natural origin material and thus collagen based electronics would be able to minimize environmental hazards. Flexible, biocompatible material is always desired in bioelectronics. Collagen is being used popularly in different biomedical applications due to its excellent biocompatibility and bioresorbability. However, it is not electrically conductive due to its high resistivity and as a result deposition of a conductive metal film is required to turn collagen into an electrically conductive biomaterial facilitating the fabrication of collagen based flexible biocompatible electronics. On the other hand, transient electronics also required very thin layer of material film for its early dissolution into surrounding environment.

Compared to different available thin film deposition techniques, Atomic Layer Deposition (ALD) offers a unique approach to conformally deposit a very thin film (few Å or nanometers) of metal or metal oxide on high aspect ratio structural substrates, and the stoichiometry as well as the thickness of this deposited thin film can precisely be tuned. (73; 195) Low temperature (room or near room temperature) ALD process is also necessary to functionalize heat-sensitive biomaterials organic substrates avoiding denaturation from higher temperature. Several attempts have been reported to coat biomaterials using ALD thin films after recognizing the possibility of some low temperature ALD reactions. (19) Previously, low temperature ALD of Pt was reported on different organic substrates including Nylon-6, polyethylene naphthalate (PEN) and polyethylene terephthalate (PET) polymer, cotton, paper, and human hair. (196-198) In this work, we report for the first time

a low temperature Pt-ALD process on collagen substrate and thus this enables ultrathin conductive Pt film conformally coated on collagen fibers, producing a flexible and conductive biomaterial which can potentially be used in wide range of applications such as implantable biosensor fabrication and electrogenic tissue regeneration.

Platinum is bioinert and has a wide operating range -260 °C to 1400 °C with minimum corrosion. (194) Given the wide operating temperature range, platinum is an attractive metal for the fabrication of resistive temperature detectors (RTD). RTD is a thermometer that monitors temperature based on the resistive change of platinum metal. Many RTD elements consist of thin films of platinum metal with two or four leadwires which are connected to a multimeter to monitor resistance at various temperatures. Temperature and resistance have a linear relationship, and is explained through this equation $R = R_0(1+\alpha\Delta T)$, where α is known as temperature coefficient of resistance, and describes how much resistance changes per one Celsius increment. (194) A bulk platinum metal has a TCR=0.00385 $°C^{-1}$ between 0 °C and 100 °C, and exhibits excellent accuracy and precision. (199)

The resistive temperature detector is becoming more versatile for thermal characterization in the healthcare applications. While current research is focusing on the fabrication of flexibles electronics to monitor skin temperature in thin polymeric film surfaces, such as polyethylene terephthalate (PET), and polydimethylsiloxane (PDMS), we developed an intuitive technique to deposit platinum metals onto nanofibrous collagen (natural polymer) substrate. The structure of collagen substrate is a triple helix with two large ∝ chain, one $\propto_1$ chain and one $\propto_2$ chain. Collagen thus have enough compliance to withstand skin

deformation, and exhibits an elastic modulus $E_{collagen}$ = 2.04±0.26 GPa compared to that of PET E_{PET} = 2.43 GPa. (200) Platinum metals deposited in collagen substrate holds significance biocompatibility and mechanical properties in developing biointegrated RTD sensor.

2.4.2. Material and Methods

Sample Preparation: All ALD process was carried out in a custom built, horizontal hot wall tubular ALD reactor modified for low temperature ALD with a new mass flow controlled inert gas flow line and fast filling line (Figure 20A). The reactor chamber consists of a 48 cm long quartz tube with an internal diameter of 38 mm. This reactor is heated using a tube furnace (1000 Series Marshall™ Tubular Furnace) connected with a proportional-integral-derivative temperature controller (OMEGA® CN9000A Series Miniature Autotune Microprocessor Controllers). The delivery lines consists of ¼-in stainless steel tubing and several pneumatic and manual valves. Reactor chamber is continuously evacuated using a vacuum pump (Fisherbrand™ Maxima™ C Plus Vacuum Pump, Model M8C) and the chamber pressure is monitored downstream of the reactor.

During the deposition, the substrate and reactor were at 150°C while the precursor bubbler was kept at 50°C and the delivery line in between bubbler and reactor was kept 20-30°C higher than the bubbler temperature. The ALD chamber pressure was kept at 500 mTorr during deposition. (Trimethyl)methylcyclopentadienylplatinum(IV) [$MeCpPtMe_3$] (99.999%-Pt PURATREM, Strem Chemicals Inc.) and ozone (1000 ppm generated from 99.99% Oxygen just upstream the ALD chamber with custom made UV lamp system) were used as precursor and oxidizer, respectively for the Pt-ALD process. For TiO_2 deposition

TDMAT (Sigma Aldrich, 99.999%) was used as precursor and ozone was used as precursor and oxidizer. The precursor and the oxidizer were introduced sequentially into the reactor using computer controlled pneumatic valves. Argon (99.999%) was used as both precursor carrier gas and purging gas. Immediately following TiO_2 seed layer deposition, Pt-ALD film were deposited on collagen without vacuum break. A commercially available collagen barrier membrane (Biomend®, Zimmer, USA) was used as substrate in this study and p-type Si(100) silicon wafer (University wafer Inc, USA) was used as reference substrate to measure deposited film thickness. The thickness of the deposited film on the reference silicon substrate was measured using spectral ellipsometry (Model M44, J.A. Woollam Co., Inc.). The ALD process on collagen samples are schematically represented in Figure 21A. Non-coated collagen served as control group, while collagen coated with 400 ALD cycles of Pt refers to Coll-Pt400, Coll-TiO_2-Pt200 and Coll-TiO_2-Pt400 stands for 200 and 400 ALD cycles of Pt respectively on collagen samples with a ~9nm seed layer of TiO_2 deposited at room temperature.

Surface Characterization: Surface morphology of native collagen and Pt-coated collagen was analyzed using a high-resolution Field Emission SEM (JEOL JSM-6320F, JEOL USA, Inc.). Prior to SEM, samples were gold-coated using a sputter coater to make them conductive. The surface chemical composition of the control collagen surface and ALD TiO_2-coated collagen substrates was studied using a high-resolution x-ray photoelectron spectrometer (Kratos AXIS-165, Kratos Analytical Ltd., United Kingdom) equipped with a monochromatic Al Ka (1486.6 eV) x-ray source operating at 15 kV and 10 mA. In addition to SEM, the surface of the native collagen and Pt-coated collagen was imaged

using a Keyence VHX6000 optical microscope at 500x magnification using Keyence's depth scanning mode.

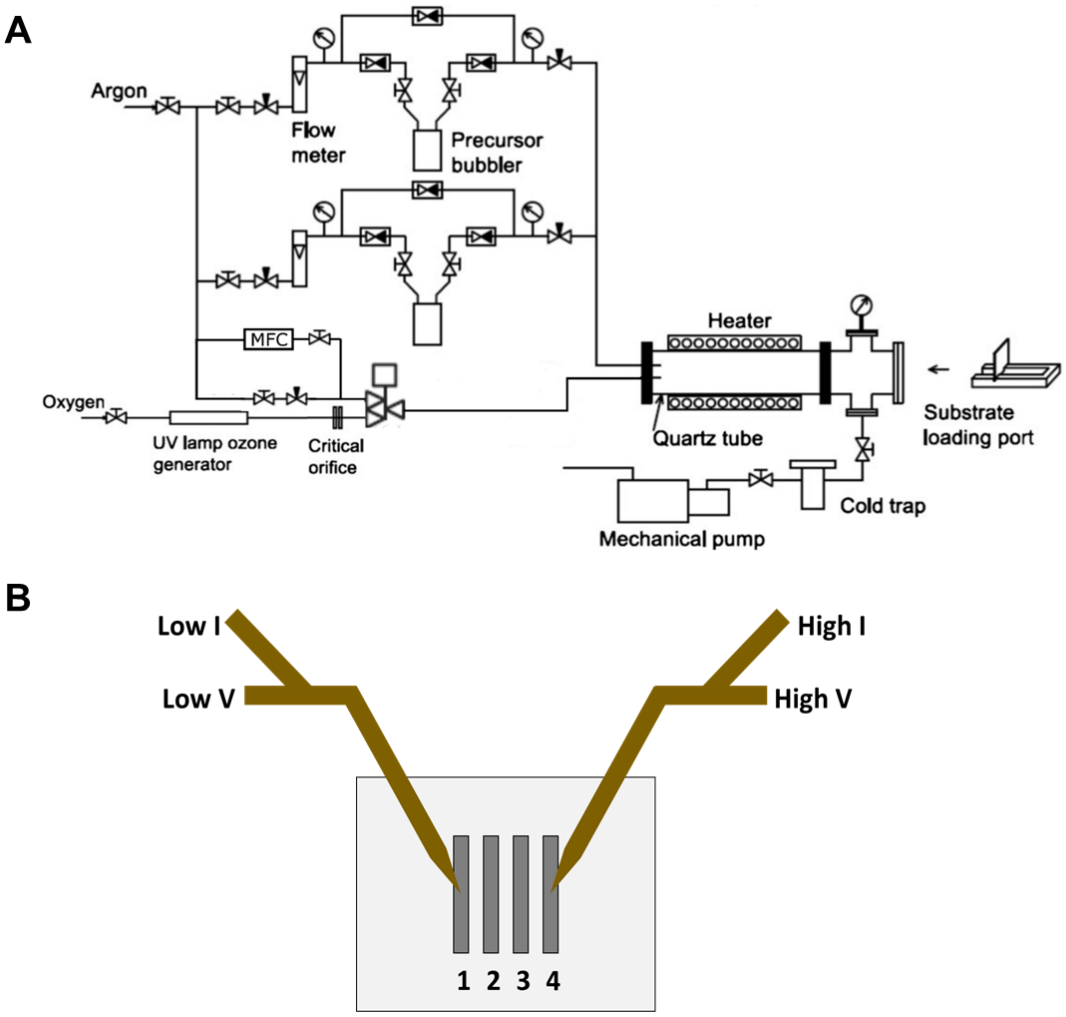

Figure 20: (A) Schematic of the custom built ALD reactor used in this study, (B) Diagram of electrical measurements. 1, 2, 3, and 4 indicate the contact numbers for the screen printed silver ink contacts. Low V and High V indicate the low and high potential connections to the LCR meter and Low I and High I indicate the low and high current connections to the LCR meter.

Electrical Characterization: Ag-530 conductive silver ink from Applied Ink Solutions was manually screen printed onto the thin films to provide consistent probe locations, reduce contact resistance and protect the films from damage during electrical measurements. Screen printing was done using a Gold Print SPR-25 screen printer, a 70 durometer (Shore A) squeegee blade, and a printing offset of 3 mm. The screen used had wire diameters of 228.6 um, with 325 wires per inch set at a mesh angle of 45°. The line pattern used had four lines with line widths of 0.5 mm, line spacings of 1 mm and line lengths of 5 mm. After printing, the silver ink was dried in a laboratory oven at 100°C for two hours with 15.6 L/min filtered air flow.

Two-probe resistance measurements were performed with a Keysight E4980AL precision LCR meter and a Micromanipulator probe station with tungsten probes in Micromanipulator 210 probe holders (Figure 20B). Measurements were done using a 10 mV, 20 Hz signal with a 1.5V DC bias. Probe resistance and contact resistances were measured and subtracted to determine resistance of the platinum films. Probe resistance was measured as 0.4Ω by directly connecting the tips of the probes. Contact resistance was calculated using Equation 1 below, where R_{14}, is the resistance between contacts one and four, R_{12} is the resistance between contacts one and two, R_{23} is the resistance between contacts two and three and R_{34} is the resistance between contacts three and four.

$$\text{Contact Resistance} = \frac{R_{14} - (R_{12} + R_{23} + R_{34})}{2} \quad (1)$$

Volume resistivity was calculated using Equation 2 below, where R is the average of R_{12}, R_{23}, and R_{34} minus the probe resistance and contact resistance, w is the width of the sample, t is the film thickness, and l is the spacing between the contacts.

$$\text{Volume Resistivity} = R\frac{wt}{l} \quad (2)$$

Strain was applied by bending samples over various curved surfaces ranging from 10.5 cm to 1.7 cm and the resistance was measured before and after strain. Strain from the curvature was calculated using Equation 3 where γ is the distance of the film from the neutral axis, ρ is the radius of curvature, t is the film thickness, and r is the radius of the curved surface.

$$\text{Strain from Curvature } (\epsilon) = \frac{\gamma}{\rho} = \frac{\frac{t}{2}}{r + \frac{t}{2}} \quad (3)$$

The collagen samples were also connected to a light-emitting diode (LED) circuit involving 3 Volt battery to test the presence of a stable conductive coating on the collagen surface and to study the flexibility of the existing conductive coating.

Resistance-Temperature Study: Temperature resistance changes of the platinum coated collagen sample was determined using a multimeter. The platinum metal coated on nanofibrous layer was cut into 0.5 x 0.2 x 0.023 cm in length, width, and thickness. The thermal resistive response was monitoring by placing two wires from the multimeter onto the sample. Moreover, this was evaluated on the hot plate's surface by comparing their resistance readings from a standard thermometer. The resistance was recorded in

increments of 5 °C from 25 °C to 100 °C with two wire setup where each wire was placed along the length of the sample.

2.4.3. Results and Discussion

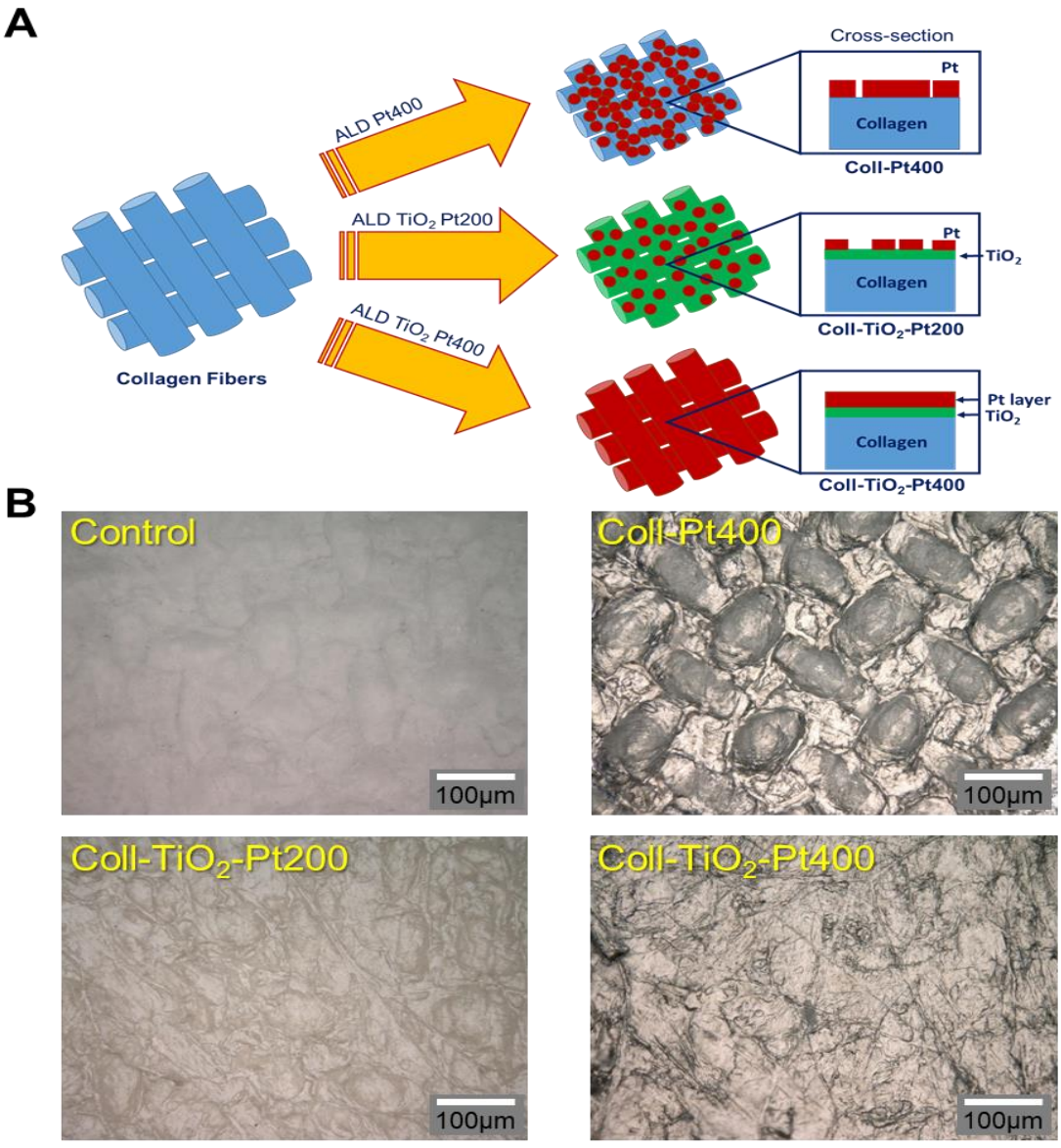

Figure 21: ALD on collagen membrane. (A) Schematic representation of ALD process for preparing different collagen sample groups. (B) Optical microscopic images of collagen sample groups showing the different surface features of non-coated and ALD-Pt coated collagen samples.

Surface features of the collagen samples were investigated using optical microscope before and after the Pt ALD process was carried out. ALD Pt coated collagen surfaces exhibited a very different surface characteristic under microscope compared to non-coated collagen surface (Figure 21B). Non-coated control surface did not show much distinguishable surface features while significant surface morphology with three-dimensional characteristics was observed for Coll-Pt400 group. In this Coll-Pt400 group, a woven fiber type structural features were observed including some ups and downs of different depths. In contrast, a near flat surface was found for both Coll-TiO_2-Pt200 and Coll-TiO_2-Pt400 groups. These two groups have a seed layer of TiO_2 thin film on their surfaces and Pt ALD was performed on top of this TiO_2 layer. This could fill the gaps of the surfaces and as a result flat surface was obtained after this process.

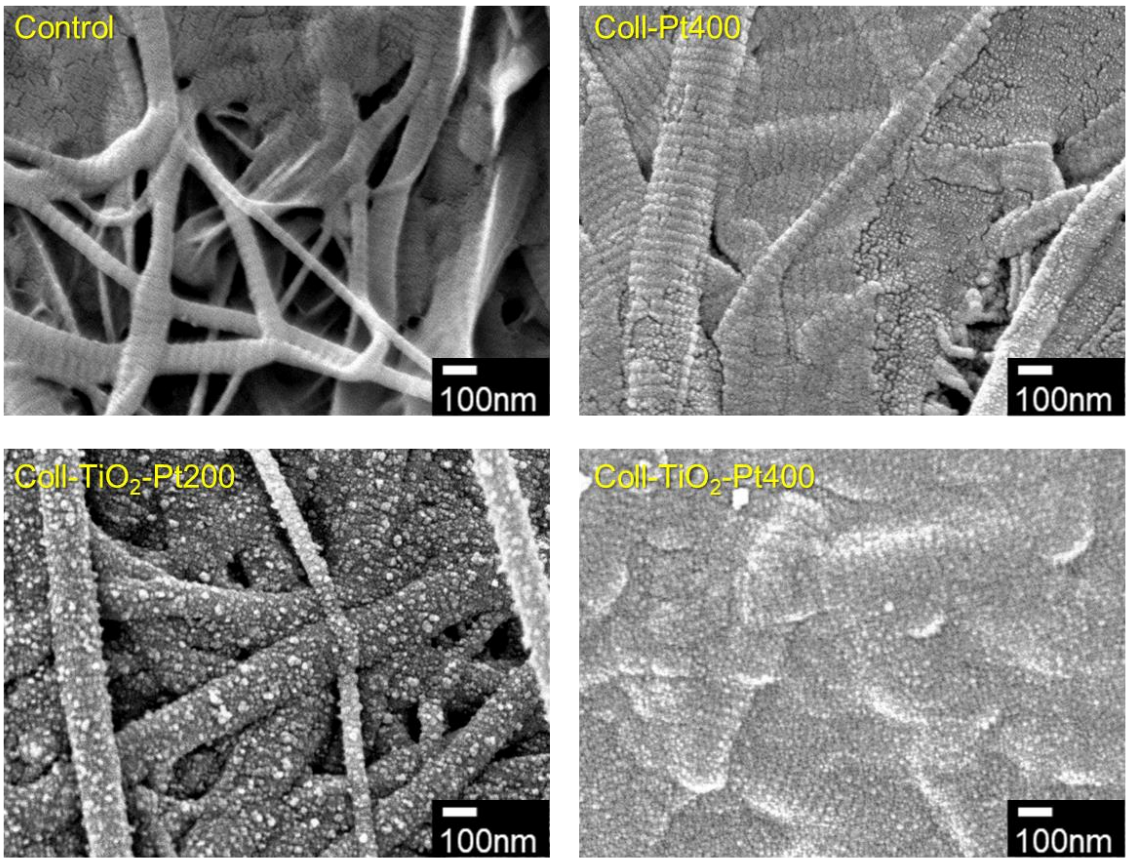

Figure 22: Scanning electron micrograph of collagen sample groups at 50,000X magnification showing surface morphology at nanoscale for pristine collagen sample and ALD-Pt coated collagen samples.

SEM was performed to have in-depth understanding of surface morphology at nanoscale and the corresponding SEM micrographs for all the collagen sample groups were displayed in Figure 22. For non-coated control the surface structures were fibrous and the characteristic "banding" pattern of individual collagen fibrils, the make up the larger anatomic fibers, was clearly visible. This collagen based membrane is manufactured from type I collagen fibers purified from bovine tendon source. (201) Similar characteristic

striping of collagen fibrils was reported before from the electron micrograph of untreated bovine tendon collagen tissue. (202) ALD Pt coated collagen samples exhibited significantly different surface morphology as compared to non-coated control. A conformal and uniform ALD coating with different Pt nucleation and different surface coverage were observed among the coated samples. In Coll-Pt400 the characteristic bands were still noticeable and conformal Pt film was observed though the surface coverage is not 100%. For Coll-TiO_2-Pt200 group, the island growth behavior of Pt was observed on collagen fibers coated with seed layer of TiO_2 thin film and the Pt nuclei are not connected at all. On the other hand, a continuous, conformal Pt film was obtained for Coll-TiO_2-Pt400 group with 100% surface coverage. This result supported our observation from optical microscope where the Coll-TiO_2-Pt400 was very flat and smooth due to continuous uniform Pt coating filled the gaps and thus turning the collagen membrane denser.

The SEM results indicated that the TiO_2 seed layer acted as a buffer layer to promote the nucleation of Pt on collagen surface. Additionally, it is also revealed that 400 ALD cycles of Pt is required to obtain a continuous fully covered Pt film on collagen surface coated with Titania nano-film. Collagen molecule consists of amide functional groups. Reactivity of $MeCpPtMe_3$ precursor towards organic amide groups is not well-studied. However, it was previously reported that a thin layer of alumina (Al_2O_3) promote the nucleation of Pt on organic substrate like Nylon-6 consists of amide backbone. (196) Though the Al_2O_3 layer deposited only at higher temperature, i.e. at 200°C through ALD was reported to promote Pt nucleation on Nylon-6. (196) A 3 nm of Al_2O_3 film deposited using plasma assisted ALD also showed to facilitate Pt growth on organic substrates like PEN, PET,

paper and cotton. (197) On the other hand, ALD TiO_2 thin film was also reported to promote Pt nucleation due to the hydrophilicity of TiO_2 film. (203) Xu et al also showed that hydrophilic -OH terminated silicon surface had much higher surface coverage compared to -H terminated hydrophobic surface. (204) Therefore surface hydrophilicity is one of the significant factor in nucleation of Pt as hydrophilic surfaces offer higher number of nucleation sites to facilitate the ALD process. (204; 205) Recently we developed a room temperature ALD process to deposit amorphous TiO_2 thin film on collagen surface. (1) Amorphous TiO_2 film was reported to be very hydrophilic due the abundant hydroxyl or -OH group present on this film surface. (206) Consequently, our amorphous TiO_2 seed layer helped in better nucleation of Pt on the collagen surface. Furthermore, previous reports also showed that at least 400 cycles of Pt ALD was needed to obtain 100% surface coverage. (198; 204; 207) Therefore our finding is in agreement with the other previously published reports.

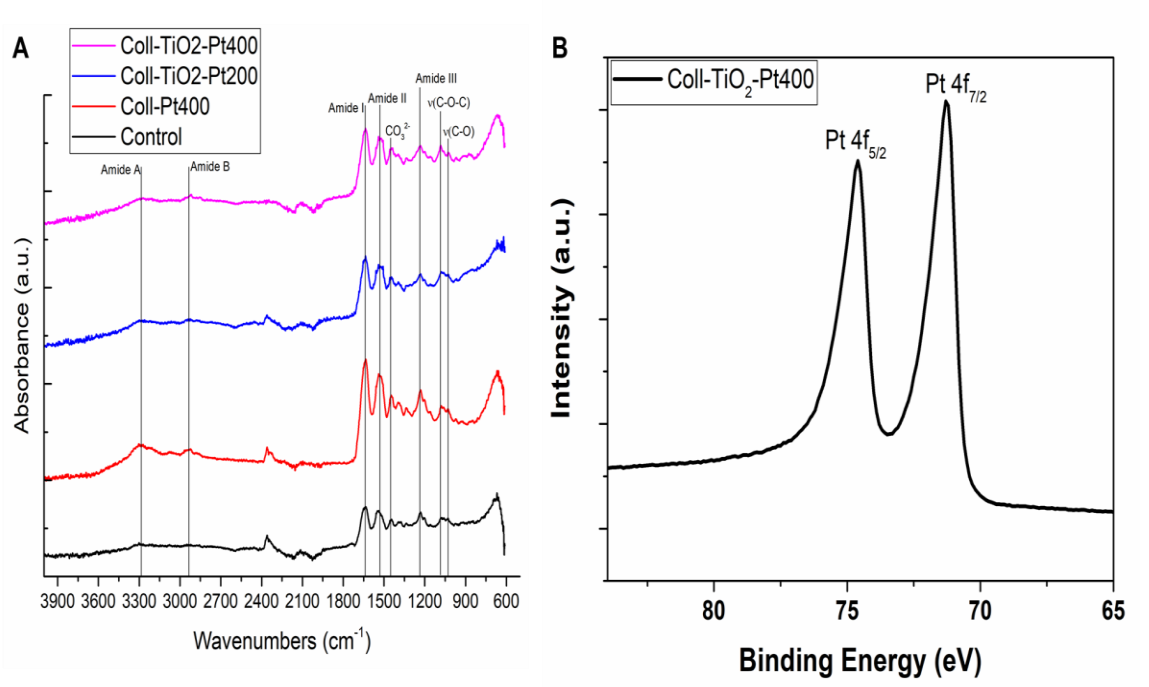

Figure 23: Chemical analysis of collagen sample. (A) ATR-FTIR spectrum of collagen sample groups. (B) X-ray photoelectron spectroscopy of Coll-TiO_2-Pt400 group showing Pt core level energy region.

ATR-FTIR was employed in absorbance mode to study the chemical composition of the collagen samples (Figure 23A). The principle behind FTIR technique is the different absorption intensities of incident IR by the covalent bonds of different biomolecules present in specimen, and depending on the molecular bonds and structure, the chemical information can be obtained from the resultant IR absorption intensity and wavenumber positions. (208) As shown in Figure 23A, all the collagen sample groups exhibited absorption of IR for scan region performed from 3900-600 cm^{-1} interval. Predominant amide peaks were identified for all the groups and these amide groups are functional groups for collagen type I. Amide peaks observed at wavenumbers 1700-1650 cm^{-1}, 1600-1500

cm^{-1}, 1300-1200 cm^{-1} are corresponding to Amide I, Amide II and Amide III respectively while 3330-3300 cm^{-1}, 3080-2900 cm^{-1} are related to Amide A and Amide B. (208; 209) Peaks observed at 1035 cm^{-1} and 1079 cm^{-1} attributed from ν(C-O) and ν(C-O-C). (208) No major peak shift or significantly different peak was observed for our ALD-Pt coated groups compared to non-coated control. This finding suggests that our ALD process is capable of functionalizing the collagen substrate without significantly altering the intrinsic properties or biomolecular structures of collagen.

X-ray photo electron spectroscopy was used in surface characterization, specifically with the aim of evaluating the quality of the Pt thin film deposited on collagen surface using ALD process at 150°C. The XPS spectra of Coll-TiO_2-Pt sample group was displayed in Figure 23B. Figure 23B showed the two major peaks in the Pt core-level energy region of XPS spectra. The peaks at 74.2 eV and 71 eV attributed from the metallic $Pt_{5/2}$ and $Pt_{7/2}$, respectively. Deconvolution of peaks were reported to observe typically at 72.3 eV and 73.8 eV owning to the formation of PtO_x. (198; 207) Therefore our XPS result indicates that our ALD Pt film is high purity metallic film despite being deposited at lower temperature at 150°C on an organic substrate i.e. collagen.

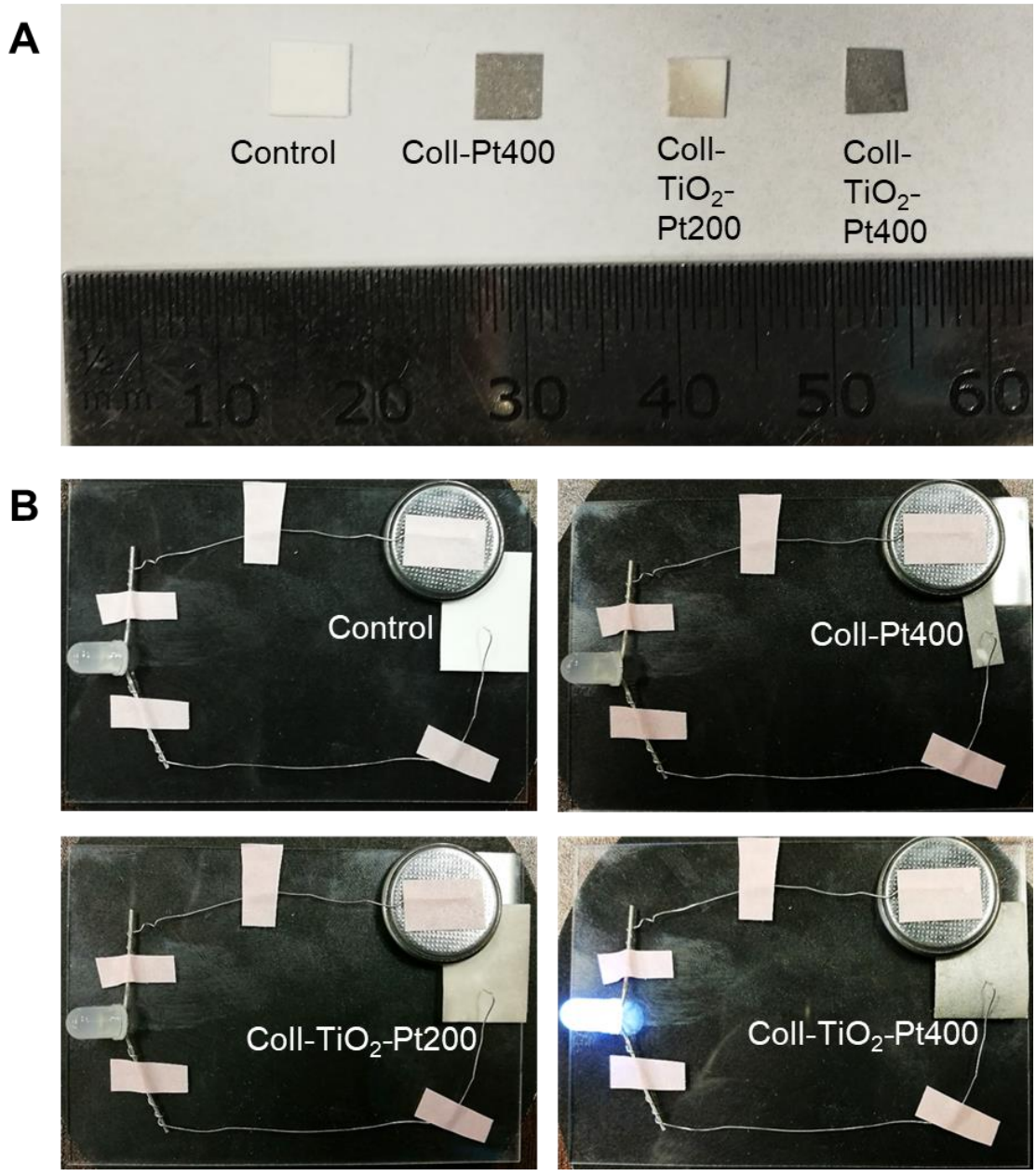

Figure 24: (A) Photograph of all the collagen sample groups showing color difference due to Pt nucleation on collagen surfaces. (B) Photograph of electrical conductivity test using LED light showing only Coll-TiO_2-Pt400 lightened on LED, but LED is not on by usimg other sample groups.

Pt growth initiation and nucleation behavior could also be visually observed as depicted in Figure 24A. The control collagen membrane is white while darkening of sample was observed after performing different ALD treatment on the collagen surfaces. After 400 cycles of ALD Pt (i.e. Coll-Pt400), white collagen became darker suggesting some nucleation of Pt on the collagen surface. For Coll-TiO_2-Pt200, the sample is slightly darker compared to control but not as dark as Coll-Pt400. This was expected because ALD is a cyclic process and consequently 200 ALD cycles had much less film thickness as compared to 400 ALD cycles. Finally, for Coll-TiO_2-Pt400 group a uniformly coated dark sample surface was observed indicating 100% surface coverage with higher level of Pt nucleation. These observations from our visual inspection supported our finding through optical and electron microscopy. Darkening of the sample due to Pt film growth was also reported previously for Nylon-6 substrate after performing Pt ALD on the surface. (196)

A simple test was performed involving LED to qualitatively prove the presence of a conductive metal thin film on the collagen surface (Figure 24B). Collagen itself is a non-conductive organic biomaterial and as a result it could not complete the circuit to flow current through it and lit up the LED thereby. For Coll-Pt400 and Coll-TiO_2-Pt200, growth of Pt was observed but Pt film was not continuous on the collagen surface for those two sample groups and consequently these groups also are not conductive enough to light up the LED light. On the other hand, LED lit up for the Coll-TiO_2-Pt400 sample group. This indicated that a continuous conductive Pt film was present on the surface of Coll-TiO_2-Pt400 turning it into a conductive material.

Sample	Pt film thickness on monitor Si (nm)	Average Volume Resistivity [Ω•cm]	Standard Deviation of Volume Resistivity [Ω•cm]
Control	-	$>10^{12}$	-
Coll-TiO_2-Pt200	11.2±0.9	$>10^{12}$	-
Coll-Pt400	26.7±0.4	$6.65x10^{-3}$	$2.85x10^{-3}$
Coll-TiO_2-Pt400	27.8±1.4	$2.95x10^{-3}$	$3.06x10^{-5}$

TABLE V: Electrical resistivity of Pt coated collagen sample groups

After determining that some of the platinum coatings on the collagen surfaces were conductive, two-probe resistance measurements were performed on the native collagen and Pt coated collagen samples to measure the resistivity quantitatively. The resistance of the native collagen, and Coll-TiO_2-Pt200 were beyond 10^{18} Ω, the upper range of our LCR meter; however, the resistances of the Coll-Pt400 and Coll-TiO_2-Pt400 were well within the range of our LCR meter. The average volume resistivity and standard deviation of the volume resistivity of three measurements from three different points on these samples is shown in TABLE V. The volume resistivity was calculated using the thickness of Pt measured from silicon substrates. The larger standard deviation of the volume resistivity for the Coll-Pt400 as compared to Coll-TiO_2-Pt400 is due to larger variation in resistance between three points on the sample and is indicative of a less uniform Pt coating. In addition to the Pt on collagen, the resistivity of 400 cycles of Pt were also measured on silicon. This sample had an average volume resistivity of 31.8 μΩ•cm, approximately 10

times lower than the Coll-TiO_2-Pt400 sample, with a standard deviation of 15.1 μΩ•cm. The lower volume resistivity on silicon is likely due to the smooth, non-porous surface which allows for more interconnection between the Pt coating; therefore, it is important to compare the resistivity with platinum deposited on similar substrates. The volume resistivity of 12 nm of Pt on Nylon-6 is reported as 175 μΩ•cm. (196) This resistivity is significantly lower than Pt on collagen likely due to the more ordered, less porous structure of Nylon-6 compared to collagen.

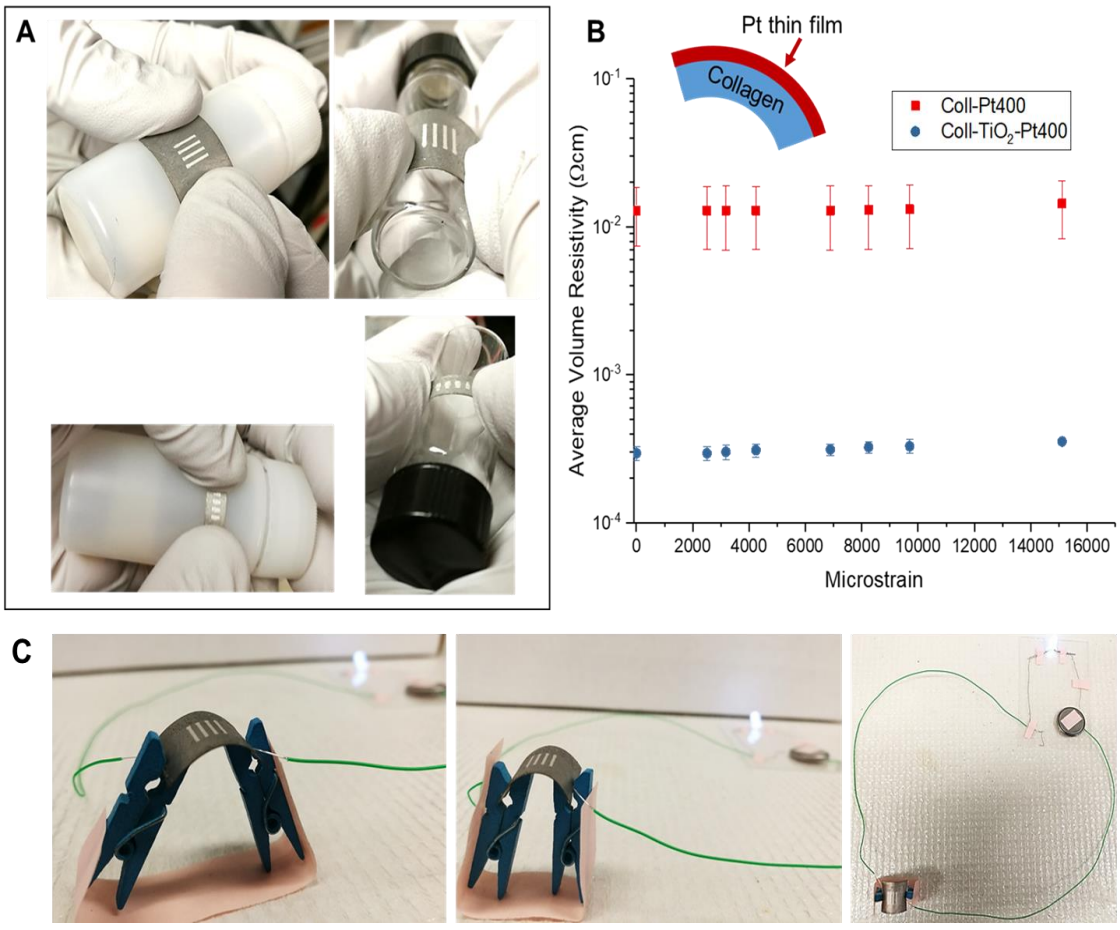

Figure 25: Flexibility of conductive collagen. (A) Photograph showing the bending of ALD-Pt coated collagen samples. (B) Average volume resisitvity versus microstrain for the Coll-Pt400 and Coll-TiO_2-Pt400 samples. Error bars indicate the standard deviation of the volume resistivity from three measurements on each sample. (C) Photograph of flexible Coll-TiO_2-Pt400 sample that lightened on the LED lamp while the sample is in bended state.

To characterize the flexibility of the platinum coatings, their resistances were measured before and after bending at different radii of curvature (Figure 25A). The radii of curvature ranged from 10.5 to 1.7 cm and induced strains as high as 1.5%. The results of these resistivity measurements after bending, are shown in Figure 25B. Less than one percent change in volume resistivity was measured after straining up to approximately 8200 microstrain for the Coll-Pt400 sample; however, a 1.3% increase and 11.1% increase were measured after straining at 9700 and 15100 microstrain, respectively. For the Coll-TiO_2-Pt400 sample, 5%, 10%, and 20% increases were measured after straining at approximately 4200, 8200, and 15100 microstrain. The larger increases in resistivity with microstrain for the Coll-TiO_2-Pt400 sample is due to the 9-nm thick TiO_2 coating. This TiO_2 coating increases the film thickness by approximately 37%, and may affect the adhesion of the coating. Both thicker films and lower adhesion strengths have been shown to cause cracking or failure of thin films at lower strains. (210) In comparison to the work by Mundy et al, which showed only a 7% decrease in conductivity for a radius of curvature of 6.0 mm or ~7.7% strain, our results show similar decreases below 1% strain. (196) The larger change for our samples could be due to a number of different factors including the different seed layer used for the platinum deposition, the larger thickness of our seed layer, the less ordered structure of the collagen compared to Nylon-6, and the different deposition conditions used. Additionally, the work by Lee et al showed only a 2% change in resistance after 1000 cycles of bending at a radius of 3 mm or ~8.4% strain for Pt deposited on cotton fibers. (198) Our Coll-TiO_2-Pt400 sample also showed a pretty stable conductivity and flexibility, as it lightened on the LED while remained at bending state (Figure 25C).

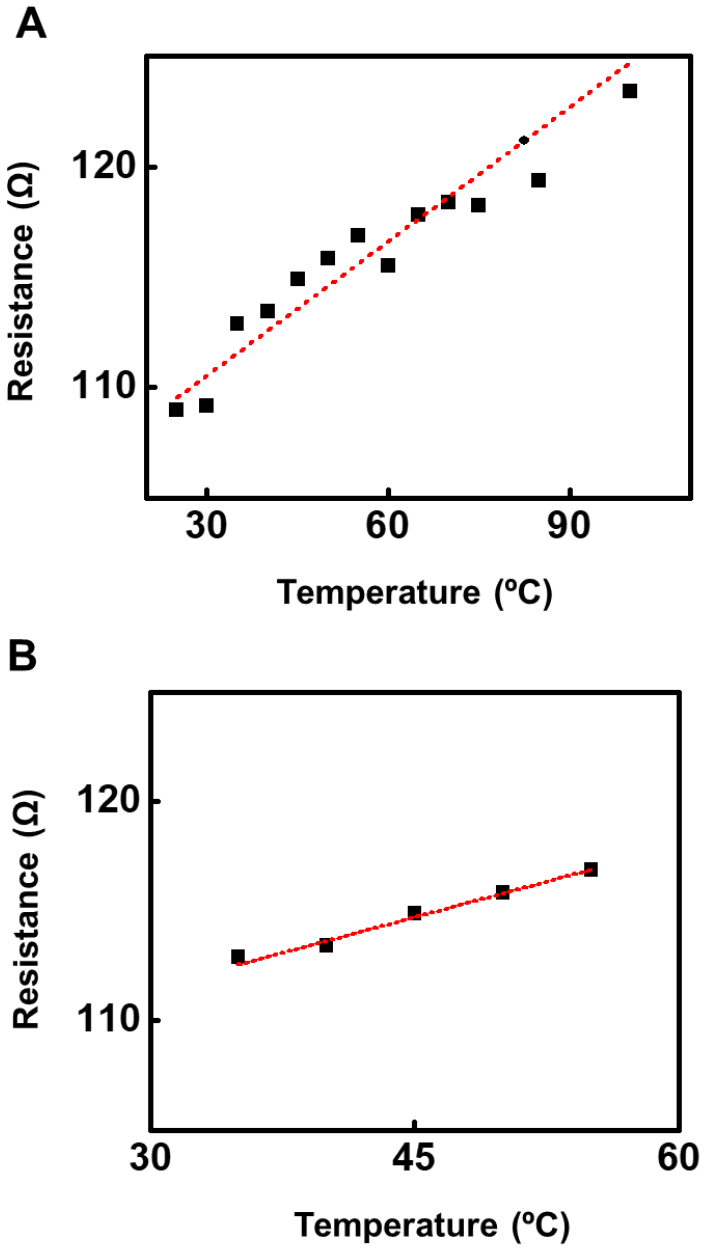

Figure 26: Temperature resistive change of platinum coated collagen sample monitored between (A) 25 ºC to 100 ºC and (B) 35 ºC to 55 ºC.

The sample rely on thin platinum layer coated on nanofibrous collagen structure. The platinum coated collagen showed an electrical resistance of 108.97 Ω at 25 °C and 123.43 Ω at 100 °C, and its dynamic range is 14.46 Ω. Figure 26A, shows the change in resistance of the Pt/collagen sample (ΔR) is directly proportional to the change of temperature, illustrating a positive trend between resistance and temperature. The Pt/collagen exhibits a positive temperature coefficient resistance (TCR), and its TCR value was 0.001770 $°C^{-1}$, based on the calibration against a commercial RTD sensor from 25 °C to 100 °C (R^2 = 0.90). The linearity was challenged by the collagen nanofibrous structure due to the overwhelming temperatures causing heat denaturation and thus leading to change in morphology. The structure of collagen became stiffer at higher temperatures compared to at room temperature. Indeed, at temperatures above 38°C, collagen fibers became thinner, while fibers aggregate at temperatures below 32 °C. (211) The thermal resistive response was highly linear (R^2 = 0.98) within biologically relevant temperature range, 35 °C to 55 °C as shown in Figure 26B. TCR in this temperature range was 0.0017714 $°C^{-1}$, with an excellent accuracy ±0.094 ºC. Despite this, bulk platinum metal is about twice as much compared to the Pt/collagen sample. Several factors could have affected the TCR of platinum coated collagen such as surface area, thickness, and nanofibrous structure of collagen.

2.4.4. Conclusion

Successful ALD of Pt thin film was achieved at 150°C on collagen biomaterial for the first time. It was found that at least 400 ALD cycles of Pt is required to obtain surface coverage of 100% on collagen. A 9 nm seed layer of amorphous TiO_2 layer, deposited using room

temperature ALD prior to Pt ALD, showed to promote higher nucleation and surface coverage to achieve continuous Pt thin film. Surface chemical analysis confirmed the presence of a pure metallic Pt film on collagen surface. A simple LED test qualitatively confirmed the existence of a conductive thin film on collagen surface. Furthermore, electrical measurements showed that the resistivity of 295 μΩ•cm was achieved for Pt coated collagen sample with TiO_2 seed layer while control non-coated collagen is highly resistive (resistance > 10^{12} Ω•cm). Therefore, our low temperature ALD-Pt process is suitable to functionalize heat sensitive biomaterial by successful deposition of a conductive metal thin film. This novel flexible and conductive biomaterial can potentially be used in wide range of applications. Consequently, future work will focus on its application as electrodes in tissue engineering, bioimplants, and as basis for biosensor devices.

3. CONCLUSION AND FUTURE WORK

3.1. Conclusion

Low temperature ALD processes were developed and optimized to improve functionalities of different biomaterials by depositing thin film of metal/metal oxides at low (room or near room) temperature. Functionalized biomaterials with ALD thin film were studied using different surface characterization techniques to investigate the physico-chemical surface properties of those materials. The functionality of those ALD-coated biomaterials was tested as proof of concept to study the enhancement and/or improvements of surface properties.

Pigmented silicone elastomer was surface coated with TiO_2 nano-film using low temperature ALD and the color stability was studied before and after exposure to artificial aging. This nano-coating was stable after aging, since chemical analyses confirmed the presence of titanium oxide on the surface after the aging used. Also, upon exposure to artificial aging, this nano-coating of TiO_2 was able to reduce color degradation of the evaluated silicone elastomers, compared to that of the non-coated silicone specimens (i.e., ~ 44% more discoloration than TiO_2-coated specimens). This indicated that the silicon elastomer with a surface nano-coating of TiO_2 was a better color-stable novel material to be potentially used in extraoral fabrication maxillofacial silicone prostheses.

A room temperature ALD process was developed to surface functionalize heat sensitive collagen biomaterial with a conformal nanometer length scale thin film of TiO_2. Chemical analysis confirmed the presence of amorphous, pure TiO_2 thin film on collagen surfaces. The average fiber diameter of the collagen sample was found to increase more strongly than linearly with increasing number of TiO_2 ALD cycles, thereby resulting in a dense collagen biomaterial.

In-vitro bioactivity of this ALD TiO_2 coated collagen was also investigated. From the biocompatibility assay, human osteoblast cells were found to grow and proliferate at a significantly higher rate on the TiO_2-coated collagen surface when compared to those on the control one. The TiO_2-coated collagen samples were also found to be bioactive with the ability to nucleate higher amount of calcium phosphate or apatite by more effectively attaching higher levels of Ca and P elements from SBF solution than those of non-coated control collagen samples. These findings suggest that the collagen material, the surface prepared and modified through this room temperature ALD of TiO_2 thin film, showed significantly enhanced biocompatibility and bioactivity.

A low temperature ALD process was developed to deposit a thin film of Pt metal on collagen surfaces. Chemical analysis confirmed the presence of pure metallic Pt film on collagen surface and LED tests indicated facilitated presence of a continuous and conductive Pt thin film on collagen surface when an ultrathin buffer layer of TiO_2 was used prior to the ALD of Pt. Electrical measurements involving bending tests showed that the ALD Pt-coated collagen remained highly conductive and very flexible since its conductivity did not degrade significantly when subjected to mechanical stresses applied through bending over different radii of curvature.

3.2. Future Work

3.2.1. Animal Studies of ALD-TiO_2 coated collagen

Ultimate success of biomaterials is achieved when they are implanted inside the human body to perform desirable functions, without any toxic effects or any unprecedented side

effects. Surface modification is one way to improve and/or enhance the surface properties as well as to incorporate new functionalities to cater to the specific clinical or other needs and requirements. After thorough surface characterizations to investigate new physico-chemical surface properties of ALD modified surfaces, extensive studies on the bio-activity of newly modified biomaterial surfaces is crucial. In this Thesis, the biocompatibility and biomineralization capability of ALD-TiO_2 collagen was investigated in-vitro by exposing this ALD coated surface to cell lines and simulated body fluid solution, respectively. The results of these in-vitro bioactivity assays indicated that our TiO_2 coated collagen is biocompatible and able to nucleate higher amount of calcium phosphate compared to non-coated collagen membranes. This suggests that the ALD-TiO_2 coated collagen has the potential to be used a osteophilic or osteogenic biomaterial. However, in-vivo bioactivity involving animal models need to be studied in-depth to assess accelerated bone healing and bone regeneration capability of the resulting nano-functionalized biomaterials.

3.2.2. ALD of transient metals on collagen

In the concept of modern electronics, transient or biodegradable materials as well as biocompatible systems are gaining increasing interest in. Being biodegradable, this class of material is green or eco-friendly thus minimizing environmental-hazards related issues. In biomedical implants, the biocompatibility of such a material plays an important role; at the same time, the transient nature of this material eliminates the need of expensive secondary surgery to retrieve it, after its desired functionalities have been accomplished. In this Thesis, low temperature ALD of Pt metal was achieved in order to deposit conductive, ultra-thin film of Pt on bio-resorbable collagen biomaterial. This ALD Pt

resulted in a highly conductive and flexible bio-resorbable material to be used in transient electronics or bio-sensors. However, other metals, for example magnesium and molybdenum are highly biodegradable and perhaps better studied for this kind of applications. Therefore, ALD of these degradable metals need to be studied on collagen and other biomaterials, with the goal of developing completely transient electronic biomaterials. Furthermore, selective ALD of metals on organic biomaterials can also be studied to deposit nano-patterns of metals for fabricating different kind of biosensors or for applications in electrogenic tissue regenerations.

CITED LITERATURE

1. Bishal, A.K., Sukotjo, C. and Takoudis, C.G.: Room temperature TiO2 atomic layer deposition on collagen membrane from a titanium alkylamide precursor. Journal of Vacuum Science & Technology A: Vacuum, Surfaces, and Films, 35(1): 01B134, 2017.

2. Bishal, A.K., Grotberg, J., Sukotjo, C., Mathew, M.T. and Takoudis, C.G.: Human Osteoblast Cell-Ti6Al4V Metal Alloy Interactions Under Varying Cathodic Potentials: A Pilot Study. Journal of Bio-and Tribo-Corrosion, 3(3): 40, 2017.

3. Liu, X., Chu, P.K. and Ding, C.: Surface nano-functionalization of biomaterials. Materials Science and Engineering: R: Reports, 70(3): 275-302, 2010.

4. Wu, G., Li, P., Feng, H., Zhang, X. and Chu, P.K.: Engineering and functionalization of biomaterials via surface modification. Journal of Materials Chemistry B, 3(10): 2024-2042, 2015.

5. Li, P.H. and Chu, P.K.: 1 - Thin film deposition technologies and processing of biomaterials A2 - Griesser, Hans J. in Thin Film Coatings for Biomaterials and Biomedical Applications. Woodhead Publishing. 3-28, 2016.

6. George, S.M.: Atomic layer deposition: an overview. Chemical Reviews, 110(1): 111-131, 2009.

7. Puurunen, R.L.: A short history of atomic layer deposition: Tuomo Suntola's atomic layer epitaxy. Chemical Vapor Deposition, 20(10-11-12): 332-344, 2014.

8. Sveshnikova, G., Kol'tsov, S. and Aleskovskii, V.: Overview of early publications on Atomic Layer Deposition. J. Appl. Chem. USSR, 40: 2644-2646, 1967.

9. Suntola, T.: Atomic layer epitaxy. Materials Science Reports, 4(5): 261-312, 1989.

10. Suntola, T. and Antson, J.: Method for producing compound thin films. U.S. Patent 4,058,430, 1977.

11. Suntola, T.S., Pakkala, A.J. and Lindfors, S.G.: Apparatus for performing growth of compound thin films. U.S. Patents 4,389,973, 1983.

12. Leskelä, M. and Ritala, M.: Atomic layer deposition chemistry: recent developments and future challenges. Angewandte Chemie International Edition, 42(45): 5548-5554, 2003.

13. Ritala, M. and Niinistö, J.: Industrial applications of atomic layer deposition. ECS transactions, 25(8): 641-652, 2009.

14. Pinna, N. and Knez, M.: Atomic layer deposition of nanostructured materials. John Wiley & Sons, 2012.

15. Nicolet, M.-A.: Diffusion barriers in thin films. Thin Solid Films, 52(3): 415-443, 1978.

16. Alcock, C.B.: Thermochemical processes: principles and models. Butterworth-Heinemann, 2000.

17. Pierson, H.O.: Handbook of chemical vapor deposition: principles, technology and applications. William Andrew, 1999.

18. Yan, X.-T. and Xu, Y.: Chemical vapour deposition: an integrated engineering design for advanced materials. Springer Science & Business Media, 2010.

19. Knez, M.: Application of ALD to Biomaterials and Biocompatible Coatings. Atomic Layer Deposition of Nanostructured Materials: 301-325, 2012.

20. Dubois, L.H.: Model studies of low temperature titanium nitride thin film growth. Polyhedron, 13(8): 1329-1336, 1994.

21. Kim, I.-W., Kim, S.-J., Kim, D.-H., Woo, H., Park, M.-Y. and Rhee, S.-W.: Fourier transform infrared spectroscopy studies on thermal decomposition of tetrakis-dimethyl-amido zirconium for chemical vapor deposition of ZrN. Korean Journal of Chemical Engineering, 21(6): 1256-1259, 2004.

22. Rie, K.-T. and Gebauer, A.: Plasma-assisted chemical vapour deposition of hard coatings with metallo-organic compounds. Materials Science and Engineering: A, 139: 61-66, 1991.

23. Hausmann, D.M. and Gordon, R.G.: Surface morphology and crystallinity control in the atomic layer deposition (ALD) of hafnium and zirconium oxide thin films. Journal of Crystal Growth, 249(1-2): 251-261, 2003.

24. Ritala, M. and Leskela, M.: Handbook of thin film materials. Deposition and processing of thin films, 1: 103, 2001.

25. Puurunen, R.L.: Surface chemistry of atomic layer deposition: A case study for the trimethylaluminum/water process. Journal of Applied Physics, 97(12): 9, 2005.

26. Cardin, D.J., Lappert, M.F. and Raston, C.L.: Chemistry of Organo-zirconium and-hafnium Compounds. 1986.

27. Groner, M.D., Fabreguette, F.H., Elam, J.W. and George, S.M.: Low-Temperature Al2O3 Atomic Layer Deposition. Chemistry of Materials, 16(4): 639-645, 2004.

28. Lee, S.-M., Grass, G., Kim, G.-M., Dresbach, C., Zhang, L., Gosele, U. and Knez, M.: Low-temperature ZnO atomic layer deposition on biotemplates: flexible photocatalytic ZnO structures from eggshell membranes. Physical Chemistry Chemical Physics, 11(19): 3608-3614, 2009.

29. Lee, S.-M., Pippel, E., Moutanabbir, O., Gunkel, I., Thurn-Albrecht, T. and Knez, M.: Improved Mechanical Stability of Dried Collagen Membrane after Metal Infiltration. ACS Applied Materials & Interfaces, 2(8): 2436-2441, 2010.

30. Lee, K., Jur, J.S. and Parsons, G.N.: Mechanisms for hydrophilic/hydrophobic wetting transitions on cellulose cotton fibers coated using Al2O3 atomic layer deposition. Journal of Vacuum Science & Technology A, 30(1): 01A163, 2012.

31. Jur, J., Sweet, W.J., Oldham, C.J. and Parsons, G.N.: Atomic layer deposition of conductive coatings on cotton, paper, and synthetic fibers: conductivity analysis and functional chemical sensing using “all-fiber” capacitors. Advanced Functional Materials, 21(11): 1993-2002, 2011.

32. Lee, S.-M., Pippel, E., Gösele, U., Dresbach, C., Qin, Y., Chandran, C.V., Bräuniger, T., Hause, G. and Knez, M.: Greatly increased toughness of infiltrated spider silk. Science, 324(5926): 488-492, 2009.

33. Curtis, J. and Colas, A.: Chapter II.5.18 - Medical Applications of Silicones A2 - Ratner, Buddy D. in Biomaterials Science (Third Edition), A.S. Hoffman, F.J. Schoen, and J.E. Lemons, Editors. Academic Press. 1106-1116, 2013.

34. Hoftyzer, P. and Van Krevelen, D.: Properties of polymers. Butterworth, London, 152, 1976.

35. Clarson, S.J. and Semlyen, J.A.: Siloxane polymers. Prentice Hall, 1993.

36. Lötters, J., Olthuis, W., Veltink, P. and Bergveld, P.: The mechanical properties of the rubber elastic polymer polydimethylsiloxane for sensor applications. Journal of Micromechanics and Microengineering, 7(3): 145, 1997.

37. Ariani, N., Visser, A., van Oort, R.P., Kusdhany, L., Rahardjo, T., Krom, B.P., van der Mei, H.C. and Vissink, A.: Current state of craniofacial prosthetic rehabilitation. Int J Prosthodont, 26(1): 57-67, 2013.

38. Brandão, T.B., Vechiato Filho, A.J., de Souza Batista, V.E., Ribeiro, A.C.P., Nary Filho, H., Chilvarquer, I., Nunn, M.E., Santos-Silva, A.R., Barão, V.A.R. and Wee, A.G.: Assessment of treatment outcomes for facial prostheses in patients with craniofacial defects: A pilot retrospective study. The Journal of prosthetic dentistry, 2017.

39. Chang, T.-L., Garrett, N., Roumanas, E. and Beumer, J.: Treatment satisfaction with facial prostheses. The Journal of prosthetic dentistry, 94(3): 275-280, 2005.

40. Nemli, S.K., Aydin, C., Yilmaz, H., Bal, B.T. and Arici, Y.K.: Quality of life of patients with implant-retained maxillofacial prostheses: a prospective and retrospective study. The Journal of prosthetic dentistry, 109(1): 44-52, 2013.

41. Han, Y., Zhao, Y., Xie, C., Powers, J.M. and Kiat-amnuay, S.: Color stability of pigmented maxillofacial silicone elastomer: effects of nano-oxides as opacifiers. Journal of dentistry, 38: e100-e105, 2010.

42. Jani, R. and Schaaf, N.: An evaluation of facial prostheses. The Journal of prosthetic dentistry, 39(5): 546-550, 1978.

43. Karakoca, S., Aydin, C., Yilmaz, H. and Bal, B.T.: Retrospective study of treatment outcomes with implant-retained extraoral prostheses: survival rates and prosthetic complications. The Journal of prosthetic dentistry, 103(2): 118-126, 2010.

44. Visser, A., Raghoebar, G.M., van Oort, R.P. and Vissink, A.: Fate of implant-retained craniofacial prostheses: life span and aftercare. International Journal of Oral & Maxillofacial Implants, 23(1), 2008.

45. Watson, R.M., Coward, T.J. and Forman, G.H.: Results of treatment of 20 patients with implant-retained auricular prostheses. International Journal of Oral & Maxillofacial Implants, 10(4), 1995.

46. Al-Harbi, F.A., Ayad, N.M., Saber, M.A., ArRejaie, A.S. and Morgano, S.M.: Mechanical behavior and color change of facial prosthetic elastomers after outdoor weathering in a hot and humid climate. The Journal of prosthetic dentistry, 113(2): 146-151, 2015.

47. Eleni, P.N., Krokida, M.K., Polyzois, G.L. and Gettleman, L.: Effect of different disinfecting procedures on the hardness and color stability of two maxillofacial elastomers over time. Journal of Applied Oral Science, 21(3): 278-283, 2013.

48. Hatamleh, M.M. and Watts, D.C.: Porosity and color of maxillofacial silicone elastomer. Journal of Prosthodontics, 20(1): 60-66, 2011.

49. Andres, C.J., Haug, S.P., Munoz, C.A. and Bernal, G.: Effects of environmental factors on maxillofacial elastomers: part I—literature review. The Journal of prosthetic dentistry, 68(2): 327-330, 1992.

50. Polyzois, G.L.: Color stability of facial silicone prosthetic polymers after outdoor weathering. The Journal of prosthetic dentistry, 82(4): 447-450, 1999.

51. Haug, S.P., Andres, C.J. and Moore, B.K.: Color stability and colorant effect on maxillofacial elastomers. Part III: weathering effect on color. The Journal of prosthetic dentistry, 81(4): 431-438, 1999.

52. Hulterström, A.K. and Eystein Ruyter, I.: Changes in appearance of silicone elastomers for maxillofacial prostheses as a result of aging. International Journal of Prosthodontics, 12(6), 1999.

53. Kulkarni, R. and Nagda, S.: Colour stability of maxillofacial silicone elastomers: a review of the literature. The European journal of prosthodontics and restorative dentistry, 22(3): 108-115, 2014.

54. Paravina, R.D., Majkic, G., Del Mar Perez, M. and Kiat-amnuay, S.: Color difference thresholds of maxillofacial skin replications. Journal of Prosthodontics, 18(7): 618-625, 2009.

55. Paravina, R.D. and Powers, J.M.: Esthetic Color Training in Dentistry. Elsevier Mosby, 2004.

56. Tran, N.H., Scarbecz, M. and Gary, J.J.: In vitro evaluation of color change in maxillofacial elastomer through the use of an ultraviolet light absorber and a hindered amine light stabilizer. The Journal of prosthetic dentistry, 91(5): 483-490, 2004.

57. Kiat-amnuay, S., Mekayarajjananonth, T., Powers, J.M., Chambers, M.S. and Lemon, J.C.: Interactions of pigments and opacifiers on color stability of MDX4-4210/type A maxillofacial elastomers subjected to artificial aging. The Journal of prosthetic dentistry, 95(3): 249-257, 2006.

58. Lahtinen, K., Maydannik, P., Seppänen, T., Cameron, D.C., Johansson, P., Kotkamo, S. and Kuusipalo, J.: Protecting BOPP film from UV degradation with an atomic layer deposited titanium oxide surface coating. Applied Surface Science, 282: 506-511, 2013.

59. Hyde, G.K., Park, K.J., Stewart, S.M., Hinestroza, J.P. and Parsons, G.N.: Atomic layer deposition of conformal inorganic nanoscale coatings on three-dimensional natural fiber systems: effect of surface topology on film growth characteristics. Langmuir, 23(19): 9844-9849, 2007.

60. Kemell, M., Ritala, M., Leskelä, M., Groenen, R. and Lindfors, S.: Coating of highly porous fiber matrices by atomic layer deposition. Chemical Vapor Deposition, 14(11-12): 347-352, 2008.

61. Spagnola, J.C., Gong, B., Arvidson, S.A., Jur, J.S., Khan, S.A. and Parsons, G.N.: Surface and sub-surface reactions during low temperature aluminium oxide atomic layer deposition on fiber-forming polymers. Journal of Materials Chemistry, 20(20): 4213-4222, 2010.

62. Xu, R., Tao, Q., Yang, Y. and Takoudis, C.G.: Atomic layer deposition and characterization of stoichiometric erbium oxide thin dielectrics on Si (100) using (CpMe) 3 Er precursor and ozone. Applied Surface Science, 258(22): 8514-8520, 2012.

63. Gozalo-Diaz, D.J., Lindsey, D.T., Johnston, W.M. and Wee, A.G.: Measurement of color for craniofacial structures using a 45/0-degree optical configuration. The Journal of prosthetic dentistry, 97(1): 45-53, 2007.

64. 12a, A.G.: Standard Practice for Operating Fluorescent Ultraviolet (UV) Lamp Apparatus for Exposure of Nonmetallic Materials. 2012.

65. Mancuso, D.N., Goiato, M.C. and Santos, D.M.d.: Color stability after accelerated aging of two silicones, pigmented or not, for use in facial prostheses. Brazilian oral research, 23(2): 144-148, 2009.

66. Rai, V.R. and Agarwal, S.: Surface reaction mechanisms during ozone-based atomic layer deposition of titanium dioxide. The Journal of Physical Chemistry C, 112(26): 9552-9554, 2008.

67. Johnston, W., Hesse, N., Davis, B. and Seghi, R.: Analysis of edge-losses in reflectance measurements of pigmented maxillofacial elastomer. Journal of dental research, 75(2): 752-760, 1996.

68. Fabreguette, F.H., Wind, R.A. and George, S.M.: Ultrahigh x-ray reflectivity from W/Al2O3 multilayers fabricated using atomic layer deposition. Applied Physics Letters, 88(1): 013116, 2006.

69. George, S.M., Ott, A.W. and Klaus, J.W.: Surface Chemistry for Atomic Layer Growth. The Journal of Physical Chemistry, 100(31): 13121-13131, 1996.

70. Detavernier, C., Dendooven, J., Pulinthanathu Sree, S., Ludwig, K.F. and Martens, J.A.: Tailoring nanoporous materials by atomic layer deposition. Chemical Society Reviews, 40(11): 5242-5253, 2011.

71. Kim, S.K., Kim, K.-M., Kwon, O.S., Lee, S.W., Jeon, C.B., Park, W.Y., Hwang, C.S. and Jeong, J.: Structurally and Electrically Uniform Deposition of High-k TiO2 Thin Films on a Ru Electrode in Three-Dimensional Contact Holes Using Atomic Layer Deposition. Electrochemical and Solid-State Letters, 8(12): F59-F62, 2005.

72. Chiappim, W., Testoni, G.E., de Lima, J.S.B., Medeiros, H.S., Pessoa, R.S., Grigorov, K.G., Vieira, L. and Maciel, H.S.: Effect of Process Temperature and Reaction Cycle Number on Atomic Layer Deposition of TiO2 Thin Films Using TiCl4 and H2O Precursors: Correlation Between Material Properties and Process Environment. Brazilian Journal of Physics, 46(1): 56-69, 2016.

73. Knez, M., Nielsch, K. and Niinistö, L.: Synthesis and surface engineering of complex nanostructures by atomic layer deposition. Advanced Materials, 19(21): 3425-3438, 2007.

74. Gasser, W., Uchida, Y. and Matsumura, M.: Quasi-monolayer deposition of silicon dioxide. Thin Solid Films, 250(1): 213-218, 1994.

75. Luo, Y., Slater, D., Han, M., Moryl, J. and Osgood, R.M.: Low-temperature, chemically driven atomic-layer epitaxy: In situ monitored growth of CdS/ZnSe(100). Applied Physics Letters, 71(26): 3799-3801, 1997.

76. Putkonen, M. and Niinistö, L.: Atomic layer deposition of B2O3 thin films at room temperature. Thin Solid Films, 514(1–2): 145-149, 2006.

77. Klaus, J.W. and George, S.M.: Atomic layer deposition of SiO2 at room temperature using NH3-catalyzed sequential surface reactions. Surface Science, 447(1–3): 81-90, 2000.

78. Klaus, J.W., Sneh, O. and George, S.M.: Growth of SiO2 at Room Temperature with the Use of Catalyzed Sequential Half-Reactions. Science, 278(5345): 1934-1936, 1997.

79. Knez, M., Kadri, A., Wege, C., Gösele, U., Jeske, H. and Nielsch, K.: Atomic Layer Deposition on Biological Macromolecules: Metal Oxide Coating of Tobacco Mosaic Virus and Ferritin. Nano Letters, 6(6): 1172-1177, 2006.

80. Peng, Q., Sun, X.-Y., Spagnola, J.C., Hyde, G.K., Spontak, R.J. and Parsons, G.N.: Atomic Layer Deposition on Electrospun Polymer Fibers as a Direct Route to Al2O3 Microtubes with Precise Wall Thickness Control. Nano Letters, 7(3): 719-722, 2007.

81. Knez, M., Nielsch, K., Patil, A.J., Mann, S. and Gösele, U.: Atomic Layer Deposition on Biological Macromolecules. ECS transactions, 3(15): 219-225, 2007.

82. Liu, J., Mao, Y., Lan, E., Banatao, D.R., Forse, G.J., Lu, J., Blom, H.-O., Yeates, T.O., Dunn, B. and Chang, J.P.: Generation of Oxide Nanopatterns by Combining Self-Assembly of S-Layer Proteins and Area-Selective Atomic Layer Deposition. Journal of the American Chemical Society, 130(50): 16908-16913, 2008.

83. Han, T.H., Oh, J.K., Park, J.S., Kwon, S.-H., Kim, S.-W. and Kim, S.O.: Highly entangled hollow TiO2nanoribbons templating diphenylalanine assembly. Journal of Materials Chemistry, 19(21): 3512-3516, 2009.

84. Kim, S.-W., Han, T.H., Kim, J., Gwon, H., Moon, H.-S., Kang, S.-W., Kim, S.O. and Kang, K.: Fabrication and Electrochemical Characterization of TiO2 Three-Dimensional Nanonetwork Based on Peptide Assembly. ACS Nano, 3(5): 1085-1090, 2009.

85. Tae Hee, H., Hyoung-Seok, M., Jin Ok, H., Sang Il, S., Sang Hyuk, I. and Sang Ouk, K.: Peptide-templating dye-sensitized solar cells. Nanotechnology, 21(18): 185601, 2010.

86. Lu, Y., Bangsaruntip, S., Wang, X., Zhang, L., Nishi, Y. and Dai, H.: DNA Functionalization of Carbon Nanotubes for Ultrathin Atomic Layer Deposition of High κ Dielectrics for Nanotube Transistors with 60 mV/Decade Switching. Journal of the American Chemical Society, 128(11): 3518-3519, 2006.

87. Kemell, M., Pore, V., Ritala, M. and Leskelä, M.: Ir/Oxide/Cellulose Composites for Catalytic Purposes Prepared by Atomic Layer Deposition. Chemical Vapor Deposition, 12(7): 419-422, 2006.

88. Kemell, M., Pore, V., Ritala, M., Leskelä, M. and Lindén, M.: Atomic layer deposition in nanometer-level replication of cellulosic substances and preparation of photocatalytic TiO2/cellulose composites. Journal of the American Chemical Society, 127(41): 14178-14179, 2005.

89. Hyde, G.K., Scarel, G., Spagnola, J.C., Peng, Q., Lee, K., Gong, B., Roberts, K.G., Roth, K.M., Hanson, C.A. and Devine, C.K.: Atomic layer deposition and abrupt wetting transitions on nonwoven polypropylene and woven cotton fabrics. Langmuir, 26(4): 2550-2558, 2009.

90. Mumm, F., Kemell, M., Leskelä, M. and Sikorski, P.: A bio-originated porous template for the fabrication of very long, inorganic nanotubes and nanowires. Bioinspiration & biomimetics, 5(2): 026005, 2010.

91. Gaillot, D.P., Deparis, O., Welch, V., Wagner, B.K., Vigneron, J.P. and Summers, C.J.: Composite organic-inorganic butterfly scales: Production of photonic structures with atomic layer deposition. Physical review E, 78(3): 031922, 2008.

92. Huang, J., Wang, X. and Wang, Z.L.: Controlled replication of butterfly wings for achieving tunable photonic properties. Nano Letters, 6(10): 2325-2331, 2006.

93. Huang, J., Wang, X. and Wang, Z.L.: Bio-inspired fabrication of antireflection nanostructures by replicating fly eyes. Nanotechnology, 19(2): 025602, 2007.

94. Zhao, Y., Wei, M., Lu, J., Wang, Z.L. and Duan, X.: Biotemplated hierarchical nanostructure of layered double hydroxides with improved photocatalysis performance. Acs Nano, 3(12): 4009-4016, 2009.

95. Ding, Y., Xu, S., Zhang, Y., Wang, A.C., Wang, M.H., Xiu, Y., Wong, C.P. and Wang, Z.L.: Modifying the anti-wetting property of butterfly wings and water strider legs by atomic layer deposition coating: surface materials versus geometry. Nanotechnology, 19(35): 355708, 2008.

96. Tang, H., Prasad, K., Sanjines, R., Schmid, P. and Levy, F.: Electrical and optical properties of TiO2 anatase thin films. Journal of Applied Physics, 75(4): 2042-2047, 1994.

97. Deng, S., Verbruggen, S.W., He, Z., Cott, D.J., Vereecken, P.M., Martens, J.A., Bals, S., Lenaerts, S. and Detavernier, C.: Atomic layer deposition-based synthesis of photoactive TiO2 nanoparticle chains by using carbon nanotubes as sacrificial templates. RSC Advances, 4(23): 11648-11653, 2014.

98. Campbell, S.A., Gilmer, D.C., Wang, X.-C., Hsieh, M.-T., Kim, H.-S., Gladfelter, W.L. and Yan, J.: MOSFET transistors fabricated with high permitivity TiO 2 dielectrics. IEEE Transactions on Electron Devices, 44(1): 104-109, 1997.

99. Fukuda, H., Namioka, S., Miura, M., Ishikawa, Y., Yoshino, M. and Nomura, S.: Structural and electrical properties of crystalline TiO2 thin films formed by metalorganic decomposition. Japanese Journal of Applied Physics, 38(10R): 6034, 1999.

100. Chao, S., Wang, W.-H. and Lee, C.-C.: Low-loss dielectric mirror with ion-beam-sputtered TiO 2–SiO 2 mixed films. Applied Optics, 40(13): 2177-2182, 2001.

101. Yokogawa, T., Yoshii, S., Tsujimura, A., Sasai, Y. and Merz, J.: Electrically pumped CdZnSe/ZnSe blue-green vertical-cavity surface-emitting lasers. Japanese Journal of Applied Physics, 34(6B): L751, 1995.

102. O'regan, B. and Grfitzeli, M.: A low-cost, high-efficiency solar cell based on dye-sensitized. nature, 353(6346): 737-740, 1991.

103. Mills, A., Davies, R.H. and Worsley, D.: Water purification by semiconductor photocatalysis. Chemical Society Reviews, 22(6): 417-425, 1993.

104. Dutta, P.K., Ginwalla, A., Hogg, B., Patton, B.R., Chwieroth, B., Liang, Z., Gouma, P., Mills, M. and Akbar, S.: Interaction of carbon monoxide with anatase surfaces at high temperatures: optimization of a carbon monoxide sensor. The Journal of Physical Chemistry B, 103(21): 4412-4422, 1999.

105. Xu, Y., Yao, K., Zhou, X. and Cao, Q.: Platinum-titania oxygen sensors and their sensing mechanisms. Sensors and Actuators B: Chemical, 14(1): 492-494, 1993.

106. Jin, C., Liu, B., Lei, Z. and Sun, J.: Structure and photoluminescence of the TiO2 films grown by atomic layer deposition using tetrakis-dimethylamino titanium and ozone. Nanoscale research letters, 10(1): 1-9, 2015.

107. Phillips, L.G. and Barbano, D.M.: The influence of fat substitutes based on protein and titanium dioxide on the sensory properties of lowfat milks. Journal of Dairy Science, 80(11): 2726-2731, 1997.

108. Tryk, D., Fujishima, A. and Honda, K.: Recent topics in photoelectrochemistry: achievements and future prospects. Electrochimica Acta, 45(15): 2363-2376, 2000.

109. Jur, J.S., Spagnola, J.C., Lee, K., Gong, B., Peng, Q. and Parsons, G.N.: Temperature-dependent subsurface growth during atomic layer deposition on polypropylene and cellulose fibers. Langmuir, 26(11): 8239-8244, 2010.

110. Hyde, G., McCullen, S., Jeon, S., Stewart, S., Jeon, H., Loboa, E. and Parsons, G.: Atomic layer deposition and biocompatibility of titanium nitride nano-coatings on cellulose fiber substrates. Biomedical materials, 4(2): 025001, 2009.

111. Kääriäinen, T.O., Cameron, D.C. and Tanttari, M.: Adhesion of Ti and TiC coatings on PMMA subject to plasma treatment: effect of intermediate layers of Al2O3 and TiO2 deposited by atomic layer deposition. Plasma Processes and Polymers, 6(10): 631-641, 2009.

112. Kääriäinen, T.O., Kelly, P.J., Cameron, D.C., Beake, B., Li, H., Barker, P.M. and Struller, C.F.: Nanoscratch testing of atomic layer deposition and magnetron sputtered TiO2 and Al2O3 coatings on polymeric substrates. Journal of Vacuum Science & Technology A, 30(1): 01A132, 2012.

113. Katamreddy, R., Omarjee, V., Feist, B. and Dussarrat, C.: Ti source precursors for atomic layer deposition of TiO2, STO and BST. ECS transactions, 16(4): 113-122, 2008.

114. Kim, Y.-W. and Kim, D.-H.: Atomic layer deposition of TiO2 from tetrakis-dimethylamido-titanium and ozone. Korean Journal of Chemical Engineering, 29(7): 969-973, 2012.

115. Rose, M. and Bartha, J.: Method to determine the sticking coefficient of precursor molecules in atomic layer deposition. Applied Surface Science, 255(13): 6620-6623, 2009.

116. Yunos, D.M., Bretcanu, O. and Boccaccini, A.R.: Polymer-bioceramic composites for tissue engineering scaffolds. Journal of Materials Science, 43(13): 4433, 2008.

117. Zdrahala, R.J. and Zdrahala, I.J.: In vivo tissue engineering: Part I. Concept genesis and guidelines for its realization. Journal of Biomaterials Applications, 14(2): 192-209, 1999.

118. Mano, J., Silva, G., Azevedo, H.S., Malafaya, P., Sousa, R., Silva, S., Boesel, L., Oliveira, J.M., Santos, T. and Marques, A.: Natural origin biodegradable systems in tissue engineering and regenerative medicine: present status and some moving trends. Journal of the Royal Society Interface, 4(17): 999-1030, 2007.

119. Khan, R. and Khan, M.H.: Use of collagen as a biomaterial: An update. Journal of Indian Society of Periodontology, 17(4): 539, 2013.

120. Cen, L., Liu, W., Cui, L., Zhang, W. and Cao, Y.: Collagen tissue engineering: development of novel biomaterials and applications. Pediatric research, 63(5): 492-496, 2008.

121. Marelli, B., Ghezzi, C.E., Barralet, J.E., Boccaccini, A.R. and Nazhat, S.N.: Three-Dimensional Mineralization of Dense Nanofibrillar Collagen− Bioglass Hybrid Scaffolds. Biomacromolecules, 11(6): 1470-1479, 2010.

122. Tomoaia, G. and Pasca, R.-D.: On the collagen mineralization. A review. Clujul Medical, 88(1): 15, 2015.

123. Lee, C.H., Singla, A. and Lee, Y.: Biomedical applications of collagen. International Journal of Pharmaceutics, 221(1): 1-22, 2001.

124. Liang, X., Lynn, A.D., King, D.M., Bryant, S.J. and Weimer, A.W.: Biocompatible interface films deposited within porous polymers by atomic layer deposition (ALD). ACS applied materials & interfaces, 1(9): 1988-1995, 2009.

125. Morra, M., Cassinelli, C., Cascardo, G., Mazzucco, L., Borzini, P., Fini, M., Giavaresi, G. and Giardino, R.: Collagen I-coated titanium surfaces: Mesenchymal cell adhesion and in vivo evaluation in trabecular bone implants. Journal of Biomedical Materials Research Part A, 78(3): 449-458, 2006.

126. Khan, Y., Yaszemski, M.J., Mikos, A.G. and Laurencin, C.T.: Tissue engineering of bone: material and matrix considerations. The Journal of Bone & Joint Surgery, 90(Supplement 1): 36-42, 2008.

127. Wahl, D. and Czernuszka, J.: Collagen-hydroxyapatite composites for hard tissue repair. Eur Cell Mater, 11: 43-56, 2006.

128. Ibara, A., Miyaji, H., Fugetsu, B., Nishida, E., Takita, H., Tanaka, S., Sugaya, T. and Kawanami, M.: Osteoconductivity and biodegradability of collagen scaffold coated with nano-β-TCP and fibroblast growth factor 2. Journal of Nanomaterials, 2013: 46, 2013.

129. Kanayama, I., Miyaji, H., Takita, H., Nishida, E., Tsuji, M., Fugetsu, B., Sun, L., Inoue, K., Ibara, A. and Akasaka, T.: Comparative study of bioactivity of collagen scaffolds coated with graphene oxide and reduced graphene oxide. International journal of nanomedicine, 9: 3363, 2014.

130. Vladkova, T.G., Ivanova, I.A., Staneva, A.D., Albu, M.G., Shalaby, A.S., Topousova, T.I. and Kostadinova, A.S.: Preparation and Biological Activity of New Collagen Composites Part II: Collagen/Reduced Graphene Oxide Composites. Journal of Archives in Military Medicine, 5(1), 2017.

131. Warashina, H., Sakano, S., Kitamura, S., Yamauchi, K.-I., Yamaguchi, J., Ishiguro, N. and Hasegawa, Y.: Biological reaction to alumina, zirconia, titanium and polyethylene particles implanted onto murine calvaria. Biomaterials, 24(21): 3655-3661, 2003.

132. Rezwan, K., Chen, Q., Blaker, J. and Boccaccini, A.R.: Biodegradable and bioactive porous polymer/inorganic composite scaffolds for bone tissue engineering. Biomaterials, 27(18): 3413-3431, 2006.

133. Chusuei, C.C., Goodman, D., Van Stipdonk, M., Justes, D., Loh, K. and Schweikert, E.: Solid− Liquid Adsorption of Calcium Phosphate on TiO2. Langmuir, 15(21): 7355-7360, 1999.

134. Järn, M., Areva, S., Pore, V., Peltonen, J. and Linden, M.: Topography and Surface Energy Dependent Calcium Phosphate Formation on Sol− Gel Derived TiO2 Coatings. Langmuir, 22(19): 8209-8213, 2006.

135. Gevorkian, S., Allahverdyan, A., Gevorgyan, D. and Simonian, A.: Thermal (in) stability of type I collagen fibrils. Physical Review Letters, 102(4): 048101, 2009.

136. Sader, J.E., Sanelli, J.A., Adamson, B.D., Monty, J.P., Wei, X., Crawford, S.A., Friend, J.R., Marusic, I., Mulvaney, P. and Bieske, E.J.: Spring constant calibration of atomic force microscope cantilevers of arbitrary shape. Review of Scientific Instruments, 83(10): 103705, 2012.

137. Kokubo, T. and Takadama, H.: How useful is SBF in predicting in vivo bone bioactivity? Biomaterials, 27(15): 2907-2915, 2006.

138. Marelli, B., Ghezzi, C.E., Mohn, D., Stark, W.J., Barralet, J.E., Boccaccini, A.R. and Nazhat, S.N.: Accelerated mineralization of dense collagen-nano bioactive glass hybrid gels increases scaffold stiffness and regulates osteoblastic function. Biomaterials, 32(34): 8915-8926, 2011.

139. Coyac, B., Chicatun, F., Hoac, B., Nelea, V., Chaussain, C., Nazhat, S. and McKee, M.: Mineralization of dense collagen hydrogel scaffolds by human pulp cells. Journal of dental research, 92(7): 648-654, 2013.

140. Brown, R.A., Wiseman, M., Chuo, C.B., Cheema, U. and Nazhat, S.N.: Ultrarapid engineering of biomimetic materials and tissues: Fabrication of nano-and microstructures by plastic compression. Advanced Functional Materials, 15(11): 1762-1770, 2005.

141. Gittens I, R.A., McLachlan, T., Cai, Y., Berner, S., Tannenbaum, R., Schwartz, Z., Sandhage, K.H. and Boyan, B.D.: The effects of combined micron-/submicron-scale surface roughness and nanoscale features on cell proliferation and differentiation. Biomaterials, 32(13): 3395-3403, 2011.

142. Mager, M.D., LaPointe, V. and Stevens, M.M.: Exploring and exploiting chemistry at the cell surface. Nature Chemistry, 3(8): 582-589, 2011.

143. Chung, K.-H., Bhadriraju, K., Spurlin, T.A., Cook, R.F. and Plant, A.L.: Nanomechanical properties of thin films of type I collagen fibrils. Langmuir, 26(5): 3629-3636, 2010.

144. Wang, J., Wang, L., Zhou, Z., Lai, H., Xu, P., Liao, L. and Wei, J.: Biodegradable polymer membranes applied in guided bone/tissue regeneration: a review. Polymers, 8(4): 115, 2016.

145. Friedmann, A., Dehnhardt, J., Kleber, B.M. and Bernimoulin, J.P.: Cytobiocompatibility of collagen and ePTFE membranes on osteoblast-like cells in vitro. Journal of Biomedical Materials Research Part A, 86(4): 935-941, 2008.

146. Kudelska-Mazur, D., Lewandowska-Szumieł, M., Mazur, M. and Komender, J.: Osteogenic cell contact with biomaterials influences phenotype expression. Cell and tissue banking, 6(1): 55-64, 2005.

147. Shui, C., Spelsberg, T.C., Riggs, B.L. and Khosla, S.: Changes in Runx2/Cbfa1 expression and activity during osteoblastic differentiation of human bone marrow stromal cells. Journal of Bone and Mineral Research, 18(2): 213-221, 2003.

148. McCafferty, M.M., Burke, G.A. and Meenan, B.J.: Mesenchymal stem cell response to conformal sputter deposited calcium phosphate thin films on nanostructured titanium surfaces. Journal of Biomedical Materials Research Part A, 102(10): 3585-3597, 2014.

149. Braga Gomes, K., Fontana Rodrigues, K. and Fernandes, A.P.: The role of transforming growth factor-beta in diabetic nephropathy. International Journal of Medical Genetics, 2014, 2014.

150. Yang, J., McNamara, L.E., Gadegaard, N., Alakpa, E.V., Burgess, K.V., Meek, R.D. and Dalby, M.J.: Nanotopographical induction of osteogenesis through adhesion, bone morphogenic protein cosignaling, and regulation of microRNAs. ACS nano, 8(10): 9941-9953, 2014.

151. Sjöström, T., McNamara, L.E., Meek, R., Dalby, M.J. and Su, B.: 2D and 3D nanopatterning of titanium for enhancing osteoinduction of stem cells at implant surfaces. Advanced healthcare materials, 2(9): 1285-1293, 2013.

152. McNamara, L.E., Sjöström, T., Burgess, K.E., Kim, J.J., Liu, E., Gordonov, S., Moghe, P.V., Meek, R.D., Oreffo, R.O. and Su, B.: Skeletal stem cell physiology on functionally distinct titania nanotopographies. Biomaterials, 32(30): 7403-7410, 2011.

153. Lu, T., Liu, X., Qian, S., Cao, H., Qiao, Y., Mei, Y., Chu, P.K. and Ding, C.: Multilevel surface engineering of nanostructured TiO 2 on carbon-fiber-reinforced polyetheretherketone. Biomaterials, 35(22): 5731-5740, 2014.

154. Moradian-Oldak, J., Wen, H.B., Schneider, G.B. and Stanford, C.M.: Tissue engineering strategies for the future generation of dental implants. Periodontology 2000, 41(1): 157-176, 2006.

155. Schneider, G.B., Zaharias, R., Seabold, D., Keller, J. and Stanford, C.: Differentiation of preosteoblasts is affected by implant surface microtopographies. Journal of Biomedical Materials Research Part A, 69(3): 462-468, 2004.

156. Stigter, M., De Groot, K. and Layrolle, P.: Incorporation of tobramycin into biomimetic hydroxyapatite coating on titanium. Biomaterials, 23(20): 4143-4153, 2002.

157. Fujioka-Kobayashi, M., Caballé-Serrano, J., Bosshardt, D.D., Gruber, R., Buser, D. and Miron, R.J.: Bone conditioned media (BCM) improves osteoblast adhesion and differentiation on collagen barrier membranes. BMC oral health, 17(1): 7, 2016.

158. Miron, R.J., Saulacic, N., Buser, D., Iizuka, T. and Sculean, A.: Osteoblast proliferation and differentiation on a barrier membrane in combination with BMP2 and TGFβ1. Clinical oral investigations, 17(3): 981-988, 2013.

159. Altankov, G., Grinnell, F. and Groth, T.: Studies on the biocompatibility of materials: Fibroblast reorganization of substratum-bound fibronectin on surfaces varying in wettability. Journal of Biomedical Materials Research Part A, 30(3): 385-391, 1996.

160. Finch, D.S., Oreskovic, T., Ramadurai, K., Herrmann, C.F., George, S.M. and Mahajan, R.L.: Biocompatibility of atomic layer-deposited alumina thin films. Journal of Biomedical Materials Research Part A, 87(1): 100-106, 2008.

161. Iwasa, F., Baba, K. and Ogawa, T.: Enhanced intracellular signaling pathway in osteoblasts on ultraviolet lighttreated hydrophilic titanium. Biomedical Research, 37(1): 1-11, 2016.

162. Saita, M., Ikeda, T., Yamada, M., Kimoto, K., Lee, M.C.-I. and Ogawa, T.: UV photofunctionalization promotes nano-biomimetic apatite deposition on titanium. International journal of nanomedicine, 11: 223, 2016.

163. Tabuchi, M., Ikeda, T., Hirota, M., Nakagawa, K., Park, W., Miyazawa, K., Goto, S. and Ogawa, T.: Effect of UV Photofunctionalization on Biologic and Anchoring Capability of Orthodontic Miniscrews. International Journal of Oral & Maxillofacial Implants, 30(4), 2015.

164. Webb, K., Hlady, V. and Tresco, P.A.: Relative importance of surface wettability and charged functional groups on NIH 3T3 fibroblast attachment, spreading, and cytoskeletal organization. Journal of biomedical materials research, 41(3): 422, 1998.

165. Neel, E.A.A., Cheema, U., Knowles, J.C., Brown, R.A. and Nazhat, S.N.: Use of multiple unconfined compression for control of collagen gel scaffold density and mechanical properties. Soft Matter, 2(11): 986-992, 2006.

166. Pedraza, C.E., Marelli, B., Chicatun, F., McKee, M.D. and Nazhat, S.N.: An In Vitro assessment of a cell-containing collagenous extracellular matrix–like scaffold for bone tissue engineering. Tissue engineering Part A, 16(3): 781-793, 2009.

167. Ghezzi, C.E., Marelli, B., Muja, N., Hirota, N., Martin, J.G., Barralet, J.E., Alessandrino, A., Freddi, G. and Nazhat, S.N.: Mesenchymal stem cell-seeded multilayered dense collagen-silk fibroin hybrid for tissue engineering applications. Biotechnology journal, 6(10): 1198-1207, 2011.

168. Yang, L., Liu, H. and Lin, Y.: Biomaterial nanotopography-mediated cell responses: experiment and modeling. International Journal of Smart and Nano Materials, 5(4): 227-256, 2014.

169. Webster, T.J., Ergun, C., Doremus, R.H., Siegel, R.W. and Bizios, R.: Enhanced functions of osteoblasts on nanophase ceramics. Biomaterials, 21(17): 1803-1810, 2000.

170. Huang, H.-H., Pan, S.-J., Lai, Y.-L., Lee, T.-H., Chen, C.-C. and Lu, F.-H.: Osteoblast-like cell initial adhesion onto a network-structured titanium oxide layer. Scripta Materialia, 51(11): 1017-1021, 2004.

171. Das, K., Bose, S. and Bandyopadhyay, A.: Surface modifications and cell–materials interactions with anodized Ti. Acta biomaterialia, 3(4): 573-585, 2007.

172. Nazarov, D.V., Zemtsova, E.G., Valiev, R.Z. and Smirnov, V.M.: Formation of micro- and nanostructures on the nanotitanium surface by chemical etching and deposition of titania films by atomic layer deposition (ALD). Materials, 8(12): 8366-8377, 2015.

173. Iafisco, M., Foltran, I., Sabbatini, S., Tosi, G. and Roveri, N.: Electrospun nanostructured fibers of collagen-biomimetic apatite on titanium alloy. Bioinorganic chemistry and applications, 2012, 2012.

174. Ghasemi-Mobarakeh, L., Prabhakaran, M.P., Morshed, M., Nasr-Esfahani, M.H., Baharvand, H., Kiani, S., Al-Deyab, S.S. and Ramakrishna, S.: Application of conductive

polymers, scaffolds and electrical stimulation for nerve tissue engineering. Journal of tissue engineering and regenerative medicine, 5(4), 2011.

175. Otero, T., Martinez, J. and Arias-Pardilla, J.: Biomimetic electrochemistry from conducting polymers. A review: artificial muscles, smart membranes, smart drug delivery and computer/neuron interfaces. Electrochimica Acta, 84: 112-128, 2012.

176. Wong, J.Y., Langer, R. and Ingber, D.E.: Electrically conducting polymers can noninvasively control the shape and growth of mammalian cells. Proceedings of the National Academy of Sciences, 91(8): 3201-3204, 1994.

177. Abidian, M.R. and Martin, D.C.: Experimental and theoretical characterization of implantable neural microelectrodes modified with conducting polymer nanotubes. Biomaterials, 29(9): 1273-1283, 2008.

178. Asplund, M., Nyberg, T. and Inganäs, O.: Electroactive polymers for neural interfaces. Polymer Chemistry, 1(9): 1374-1391, 2010.

179. Baek, S., Green, R.A. and Poole-Warren, L.A.: The biological and electrical trade-offs related to the thickness of conducting polymers for neural applications. Acta biomaterialia, 10(7): 3048-3058, 2014.

180. Forcelli, P.A., Sweeney, C.T., Kammerich, A.D., Lee, B.C.W., Rubinson, L.H., Kayinamura, Y.P., Gale, K. and Rubinson, J.F.: Histocompatibility and in vivo signal throughput for PEDOT, PEDOP, P3MT, and polycarbazole electrodes. Journal of Biomedical Materials Research Part A, 100(12): 3455-3462, 2012.

181. Green, R.A., Lovell, N.H., Wallace, G.G. and Poole-Warren, L.A.: Conducting polymers for neural interfaces: challenges in developing an effective long-term implant. Biomaterials, 29(24-25): 3393-3399, 2008.

182. Abidian, M.R., Kim, D.H. and Martin, D.C.: Conducting-polymer nanotubes for controlled drug release. Advanced Materials, 18(4): 405-409, 2006.

183. Boehler, C. and Asplund, M.: A detailed insight into drug delivery from PEDOT based on analytical methods: Effects and side effects. Journal of Biomedical Materials Research Part A, 103(3): 1200-1207, 2015.

184. Geetha, S., Rao, C.R., Vijayan, M. and Trivedi, D.: Biosensing and drug delivery by polypyrrole. Analytica Chimica Acta, 568(1-2): 119-125, 2006.

185. Krukiewicz, K., Jarosz, T., Zak, J.K., Lapkowski, M., Ruszkowski, P., Bobkiewicz-Kozlowska, T. and Bednarczyk-Cwynar, B.: Advancing the delivery of anticancer drugs: Conjugated polymer/triterpenoid composite. Acta biomaterialia, 19: 158-165, 2015.

186. Carpi, F. and Smela, E.: Biomedical applications of electroactive polymer actuators. John Wiley & Sons, 2009.

187. Romero, I.S., Bradshaw, N.P., Larson, J.D., Severt, S.Y., Roberts, S.J., Schiller, M.L., Leger, J.M. and Murphy, A.R.: Biocompatible Electromechanical Actuators Composed of Silk-Conducting Polymer Composites. Advanced Functional Materials, 24(25): 3866-3873, 2014.

188. Smela, E.: Conjugated polymer actuators for biomedical applications. Advanced Materials, 15(6): 481-494, 2003.

189. Xu, H., Wang, C., Wang, C., Zoval, J. and Madou, M.: Polymer actuator valves toward controlled drug delivery application. Biosensors and Bioelectronics, 21(11): 2094-2099, 2006.

190. Irimia-Vladu, M.: "Green" electronics: biodegradable and biocompatible materials and devices for sustainable future. Chemical Society Reviews, 43(2): 588-610, 2014.

191. Cheng, H. and Vepachedu, V.: Recent development of transient electronics. Theoretical and Applied Mechanics Letters, 6(1): 21-31, 2016.

192. Fu, K.K., Wang, Z., Dai, J., Carter, M. and Hu, L.: Transient electronics: Materials and devices. Chemistry of Materials, 28(11): 3527-3539, 2016.

193. Hwang, S.-W., Tao, H., Kim, D.-H., Cheng, H., Song, J.-K., Rill, E., Brenckle, M.A., Panilaitis, B., Won, S.M. and Kim, Y.-S.: A physically transient form of silicon electronics. Science, 337(6102): 1640-1644, 2012.

194. Moreno, S., Baniasadi, M., Mohammed, S., Mejia, I., Chen, Y., Quevedo-Lopez, M.A., Kumar, N., Dimitrijevich, S. and Minary-Jolandan, M.: Biocompatible collagen films as

substrates for flexible implantable electronics. Advanced Electronic Materials, 1(9), 2015.

195. Leskelä, M. and Ritala, M.: Atomic layer deposition (ALD): from precursors to thin film structures. Thin Solid Films, 409(1): 138-146, 2002.

196. Mundy, J.Z., Shafiefarhood, A., Li, F., Khan, S.A. and Parsons, G.N.: Low temperature platinum atomic layer deposition on nylon-6 for highly conductive and catalytic fiber mats. Journal of Vacuum Science & Technology A: Vacuum, Surfaces, and Films, 34(1): 01A152, 2016.

197. Mackus, A.J., Garcia-Alonso, D., Knoops, H.C., Bol, A.A. and Kessels, W.M.: Room-temperature atomic layer deposition of platinum. Chemistry of Materials, 25(9): 1769-1774, 2013.

198. Lee, J., Yoon, J., Kim, H.G., Kang, S., Oh, W.-S., Algadi, H., Al-Sayari, S., Shong, B., Kim, S.-H. and Kim, H.: Highly conductive and flexible fiber for textile electronics obtained by extremely low-temperature atomic layer deposition of Pt. NPG Asia Materials, 8(11): e331, 2016.

199. Moser, Y. and Gijs, M.A.: Miniaturized flexible temperature sensor. Journal of Microelectromechanical Systems, 16(6): 1349-1354, 2007.

200. Zribi, A., Barthès, M., Bégot, S., Lanzetta, F., Rauch, J.Y. and Moutarlier, V.: Design, fabrication and characterization of thin film resistances for heat flux sensing application. Sensors and Actuators A: Physical, 245: 26-39, 2016.

201. Li, S.-T., Chen, H.-C., Lee, N.S., Ringshia, R. and Yuen, D.: A Comparative Study Of Zimmer BioMend® And BioMend® Extend™ Membranes Made At Two Different Manufacturing Facilities. 2013.

202. Muratore, R., Akabas, T. and Muratore, I.B.: High-intensity focused ultrasound ablation of ex vivo bovine achilles tendon. Ultrasound in Medicine and Biology, 34(12): 2043-2050, 2008.

203. Lee, H.-B.-R. and Bent, S.F.: Microstructure-dependent nucleation in atomic layer deposition of Pt on TiO2. Chemistry of Materials, 24(2): 279-286, 2011.

204. Xu, R., Selvaraj, S.K., Jursich, G., Feinerman, A. and Takoudis, C.: Nucleation behavior-morphology-resistivity of atomic layer deposited Pt on atomic layer deposited yttria-stabilized zirconia films. ECS Journal of Solid State Science and Technology, 2(11): P452-P456, 2013.

205. Liang, G., Cheng, H., Zhiwei, Z., Wei, Z., Dongping, W. and Shili, Z.: Influence of surface preparation on atomic layer deposition of Pt films. Journal of Semiconductors, 33(8): 083003, 2012.

206. Li, P.-Y., Liu, H.-W., Chen, T.-H., Chang, C.-H., Lu, Y.-S. and Liu, D.-S.: Characterization of an Amorphous Titanium Oxide Film Deposited onto a Nano-Textured Fluorination Surface. Materials, 9(6): 429, 2016.

207. Lee, H.-B.-R., Pickrahn, K.L. and Bent, S.F.: Effect of O3 on growth of Pt by atomic layer deposition. The Journal of Physical Chemistry C, 118(23): 12325-12332, 2014.

208. Belbachir, K., Noreen, R., Gouspillou, G. and Petibois, C.: Collagen types analysis and differentiation by FTIR spectroscopy. Analytical and bioanalytical chemistry, 395(3): 829-837, 2009.

209. León-Mancilla, B., Araiza-Téllez, M., Flores-Flores, J. and Piña-Barba, M.: Physico-chemical characterization of collagen scaffolds for tissue engineering. Journal of applied research and technology, 14(1): 77-85, 2016.

210. Lu, N., Suo, Z. and Vlassak, J.J.: The effect of film thickness on the failure strain of polymer-supported metal films. Acta Materialia, 58(5): 1679-1687, 2010.

211. Ding, C., Zhang, M., Wu, K. and Li, G.: The response of collagen molecules in acid solution to temperature. Polymer, 55(22): 5751-5759, 2014.

212. Pohler, O.E.: Unalloyed titanium for implants in bone surgery. Injury, 31: D7-D13, 2000.

213. Wintermantel, E. and Ha, S.-W.: Medizintechnik: Life Science Engineering. Springer-Verlag, 2008.

214. Navarro, M., Michiardi, A., Castano, O. and Planell, J.: Biomaterials in orthopaedics. Journal of the Royal Society Interface, 5(27): 1137-1158, 2008.

215. Sivan, S., Kaul, S. and Gilbert, J.L.: The effect of cathodic electrochemical potential of Ti-6Al-4V on cell viability: voltage threshold and time dependence. Journal of Biomedical Materials Research Part B: Applied Biomaterials, 101(8): 1489-1497, 2013.

216. Keegan, G.M., Learmonth, I.D. and Case, C.: A systematic comparison of the actual, potential, and theoretical health effects of cobalt and chromium exposures from industry and surgical implants. Critical Reviews in Toxicology, 38(8): 645-674, 2008.

217. Spangehl, M.J., Younger, A., Masri, B. and Duncan, C.: Diagnosis of infection following total hip arthroplasty. Instructional course lectures, 47: 285-295, 1998.

218. Gilbert, J.: Electrochemical behavior of metals in the biological milieu. Comprehensive Biomaterials, 1: 1.103, 2011.

219. Jacobs, J.J., Gilbert, J.L. and Urban, R.M.: Current Concepts Review-Corrosion of Metal Orthopaedic Implants*. The Journal of Bone & Joint Surgery, 80(2): 268-82, 1998.

220. Gittens, R., Olivares-Navarrete, R., Tannenbaum, R., Boyan, B. and Schwartz, Z.: Electrical implications of corrosion for osseointegration of titanium implants. Journal of dental research, 90(12): 1389-1397, 2011.

221. Gilbert, J.L., Mehta, M. and Pinder, B.: Fretting crevice corrosion of stainless steel stem–CoCr femoral head connections: comparisons of materials, initial moisture, and offset length. Journal of Biomedical Materials Research Part B: Applied Biomaterials, 88(1): 162-173, 2009.

222. Ehrensberger, M.T., Sivan, S. and Gilbert, J.L.: Titanium is not “the most biocompatible metal” under cathodic potential: The relationship between voltage and MC3T3 preosteoblast behavior on electrically polarized cpTi surfaces. Journal of Biomedical Materials Research Part A, 93(4): 1500-1509, 2010.

223. Contu, F., Elsener, B. and Böhni, H.: A study of the potentials achieved during mechanical abrasion and the repassivation rate of titanium and Ti6Al4V in inorganic buffer solutions and bovine serum. Electrochimica Acta, 50(1): 33-41, 2004.

224. Gilbert, J.L., Zarka, L., Chang, E. and Thomas, C.H.: The reduction half cell in biomaterials corrosion: oxygen diffusion profiles near and cell response to polarized titanium surfaces. Journal of biomedical materials research, 42(2): 321-330, 1998.

225. Venugopalan, R., Weimer, J.J., George, M.A. and Lucas, L.C.: The effect of nitrogen diffusion hardening on the surface chemistry and scratch resistance of Ti-6Al-4V alloy. Biomaterials, 21(16): 1669-1677, 2000.

226. Haeri, M., Wöllert, T., Langford, G.M. and Gilbert, J.L.: Electrochemical control of cell death by reduction-induced intrinsic apoptosis and oxidation-induced necrosis on CoCrMo alloy in vitro. Biomaterials, 33(27): 6295-6304, 2012.

227. Haeri, M., Wöllert, T., Langford, G.M. and Gilbert, J.L.: Voltage-controlled cellular viability of preosteoblasts on polarized cpTi with varying surface oxide thickness. Bioelectrochemistry, 94: 53-60, 2013.

228. Haeri, M. and Gilbert, J.L.: Study of cellular dynamics on polarized CoCrMo alloy using time-lapse live-cell imaging. Acta biomaterialia, 9(11): 9220-9228, 2013.

229. Ciolko, A.A., Tobias, M. and Ehrensberger, M.T.: The effect of fretting associated periodic cathodic potential shifts on the electrochemistry and in vitro biocompatibility of commercially pure titanium. Journal of Biomedical Materials Research Part B: Applied Biomaterials, 2015.

230. Kalbacova, M., Roessler, S., Hempel, U., Tsaryk, R., Peters, K., Scharnweber, D., Kirkpatrick, J.C. and Dieter, P.: The effect of electrochemically simulated titanium cathodic corrosion products on ROS production and metabolic activity of osteoblasts and monocytes/macrophages. Biomaterials, 28(22): 3263-3272, 2007.

231. Ehrensberger, M.T. and Gilbert, J.L.: The effect of static applied potential on the 24-hour impedance behavior of commercially pure titanium in simulated biological conditions. Journal of Biomedical Materials Research Part B: Applied Biomaterials, 93(1): 106-112, 2010.

232. Clechet, P., Martelet, C., Martin, J. and Olier, R.: Photoelectrochemical behaviour of TiO 2 and formation of hydrogen peroxide. Electrochimica Acta, 24(4): 457-461, 1979.

233. Chiarugi, P., Pani, G., Giannoni, E., Taddei, L., Colavitti, R., Raugei, G., Symons, M., Borrello, S., Galeotti, T. and Ramponi, G.: Reactive oxygen species as essential mediators of cell adhesion the oxidative inhibition of a FAK tyrosine phosphatase is required for cell adhesion. The Journal of cell biology, 161(5): 933-944, 2003.

234. Evans, E. and Thomas, I.: The in vitro toxicity of cobalt-chrome-molybdenum alloy and its constituent metals. Biomaterials, 7(1): 25-29, 1986.

235. Gotman, I.: Characteristics of metals used in implants. Journal of endourology, 11(6): 383-389, 1997.

236. Van Noort, R.: Titanium: the implant material of today. Journal of Materials Science, 22(11): 3801-3811, 1987.

237. Williams, J. and Buchanan, R.: Ion implantation of surgical Ti-6Al-4V alloy. Materials Science and Engineering, 69(1): 237-246, 1985.

238. Yang, T.-S., Huang, M.-S., Wang, M.-S., Lin, M.-H., Tsai, M.-Y. and Wang, P.-Y.W.: Effect of Electrical Discharging on Formation of Nanoporous Biocompatible Layer on Ti-6Al-4V Alloys. Implant dentistry, 22(4): 374-379, 2013.

239. Kim, H., Kim, S., Kim, M., Lee, E., Oh, H., Oh, W., Park, S., Kim, W., Lee, G. and Choi, N.: Varying Ti-6Al-4V surface roughness induces different early morphologic and molecular responses in MG63 osteoblast-like cells. Journal of Biomedical Materials Research Part A, 74(3): 366-373, 2005.

240. Deligianni, D.D., Katsala, N., Ladas, S., Sotiropoulou, D., Amedee, J. and Missirlis, Y.: Effect of surface roughness of the titanium alloy Ti–6Al–4V on human bone marrow cell response and on protein adsorption. Biomaterials, 22(11): 1241-1251, 2001.

241. Mukherjee, S., Dhara, S. and Saha, P.: Enhancing the biocompatibility of Ti6Al4V implants by laser surface microtexturing: an in vitro study. The International Journal of Advanced Manufacturing Technology, 76(1-4): 5-15, 2015.

242. Patel, S.B., Hamlekhan, A., Royhman, D., Butt, A., Yuan, J., Shokuhfar, T., Sukotjo, C., Mathew, M.T., Jursich, G. and Takoudis, C.G.: Enhancing surface characteristics of Ti–6Al–4V for bio-implants using integrated anodization and thermal oxidation. Journal of Materials Chemistry B, 2(23): 3597-3608, 2014.

243. Saharudin, K.A., Sreekantan, S., Aziz, S.N.Q.A.A., Hazan, R., Lai, C.W., Mydin, R.B.S. and Mat, I.: Surface modification and bioactivity of anodic Ti6Al4V alloy. Journal of nanoscience and nanotechnology, 13(3): 1696-1705, 2013.

244. Yavari, S.A., van der Stok, J., Chai, Y.C., Wauthle, R., Birgani, Z.T., Habibovic, P., Mulier, M., Schrooten, J., Weinans, H. and Zadpoor, A.A.: Bone regeneration performance of surface-treated porous titanium. Biomaterials, 35(24): 6172-6181, 2014.

245. Bordji, K., Jouzeau, J., Mainard, D., Payan, E., Netter, P., Rie, K., Stucky, T. and Hage-Ali, M.: Cytocompatibility of Ti-6Al-4V and Ti-5Al-2.5 Fe alloys according to three surface treatments, using human fibroblasts and osteoblasts. Biomaterials, 17(9): 929-940, 1996.

246. Ku, C.-H., Pioletti, D.P., Browne, M. and Gregson, P.J.: Effect of different Ti–6Al–4V surface treatments on osteoblasts behaviour. Biomaterials, 23(6): 1447-1454, 2002.

247. Bruni, S., Martinesi, M., Stio, M., Treves, C., Bacci, T. and Borgioli, F.: Effects of surface treatment of Ti–6Al–4V titanium alloy on biocompatibility in cultured human umbilical vein endothelial cells. Acta biomaterialia, 1(2): 223-234, 2005.

248. Park, J.-W., Kim, H.-K., Kim, Y.-J., Jang, J.-H., Song, H. and Hanawa, T.: Osteoblast response and osseointegration of a Ti–6Al–4V alloy implant incorporating strontium. Acta biomaterialia, 6(7): 2843-2851, 2010.

249. Ross, A.P. and Webster, T.J.: Anodizing color coded anodized Ti6Al4V medical devices for increasing bone cell functions. International journal of nanomedicine, 8: 109, 2013.

250. Grotberg, J., Hamlekhan, A., Butt, A., Patel, S., Royhman, D., Shokuhfar, T., Sukotjo, C., Takoudis, C. and Mathew, M.T.: Thermally oxidized titania nanotubes enhance the corrosion resistance of Ti6Al4V. Materials Science and Engineering: C, 59: 677-689, 2016.

251. Del Pino, A.P., Fernández-Pradas, J., Serra, P. and Morenza, J.: Coloring of titanium through laser oxidation: comparative study with anodizing. Surface and Coatings Technology, 187(1): 106-112, 2004.

252. Van Gils, S., Mast, P., Stijns, E. and Terryn, H.: Colour properties of barrier anodic oxide films on aluminium and titanium studied with total reflectance and spectroscopic ellipsometry. Surface and Coatings Technology, 185(2): 303-310, 2004.

253. Yang, C.-l., Chen, F.-l. and Chen, S.-w.: Anodization of the dental arch wires. Materials Chemistry and Physics, 100(2): 268-274, 2006.

254. Karambakhsh, A., Afshar, A. and Malekinejad, P.: Corrosion resistance and color properties of anodized Ti-6Al-4V. Journal of Materials Engineering and Performance, 21(1): 121-127, 2012.

255. Cunha, A., Zouani, O.F., Plawinski, L., do Rego, A.M.B., Almeida, A., Vilar, R. and Durrieu, M.-C.: Human mesenchymal stem cell behavior on femtosecond laser-textured Ti-6Al-4V surfaces. Nanomedicine, 10(5): 725-739, 2015.

256. Ravichandran, R., Ng, C.C., Liao, S., Pliszka, D., Raghunath, M., Ramakrishna, S. and Chan, C.K.: Biomimetic surface modification of titanium surfaces for early cell capture by advanced electrospinning. Biomedical materials, 7(1): 015001, 2012.

257. Lin, Z., Wang, Y., Wang, D.-n., Zhao, B.-h. and Li, J.-c.: Porous structure preparation and wettability control on titanium implant. Surface and Coatings Technology, 228: S131-S136, 2013.

258. Ponsonnet, L., Reybier, K., Jaffrezic, N., Comte, V., Lagneau, C., Lissac, M. and Martelet, C.: Relationship between surface properties (roughness, wettability) of titanium and titanium alloys and cell behaviour. Materials Science and Engineering: C, 23(4): 551-560, 2003.

259. Rosales-Leal, J., Rodríguez-Valverde, M., Mazzaglia, G., Ramon-Torregrosa, P., Diaz-Rodriguez, L., Garcia-Martinez, O., Vallecillo-Capilla, M., Ruiz, C. and Cabrerizo-Vilchez, M.: Effect of roughness, wettability and morphology of engineered titanium surfaces on osteoblast-like cell adhesion. Colloids and surfaces A: Physicochemical and Engineering aspects, 365(1): 222-229, 2010.

260. Köunönen, M., Hormia, M., Kivilahti, J., Hautaniemi, J. and Thesleff, I.: Effect of surface processing on the attachment, orientation, and proliferation of human gingival fibroblasts on titanium. Journal of biomedical materials research, 26(10): 1325-1341, 1992.

261. Lausmaa, J., Mattsson, L., Rolander, U. and Kasemo, B.: Chemical composition and morphology of titanium surface oxides. in *MRS Proceedings*. 1985. Cambridge Univ Press.

262. Varghese, O.K., Gong, D., Paulose, M., Grimes, C.A. and Dickey, E.C.: Crystallization and high-temperature structural stability of titanium oxide nanotube arrays. Journal of Materials Research, 18(1): 156-165, 2003.

263. Bai, Y., Park, I.S., Park, H.H., Lee, M.H., Bae, T.S., Duncan, W. and Swain, M.: The effect of annealing temperatures on surface properties, hydroxyapatite growth and cell behaviors of TiO2 nanotubes. Surface and Interface Analysis, 43(6): 998-1005, 2011.

264. Kim, H.M., Miyaji, F., Kokubo, T. and Nakamura, T.: Preparation of bioactive Ti and its alloys via simple chemical surface treatment. Journal of biomedical materials research, 32(3): 409-417, 1996.

265. Nishiguchi, S., Kato, H., Fujita, H., Oka, M., Kim, H.-M., Kokubo, T. and Nakamura, T.: Titanium metals form direct bonding to bone after alkali and heat treatments. Biomaterials, 22(18): 2525-2533, 2001.

266. MAZĂRE, A., VOICU, G., TRUSCĂ, R. and Ioniţă, D.: Heat treatment of TiO2 nanotubes, a way to significantly change their behaviour. 2011.

267. Sarraf, M., Zalnezhad, E., Bushroa, A., Hamouda, A., Rafieerad, A. and Nasiri-Tabrizi, B.: Effect of microstructural evolution on wettability and tribological behavior of TiO 2 nanotubular arrays coated on Ti–6Al–4V. Ceramics International, 41(6): 7952-7962, 2015.

APPENDICES

Appendix A

PERMISSION TO USE PREVIOUSLY PUBLISHED MATERIALS

JVST A

Chapters 2.2 were previously published in Journal of Vacuum Science & Technology A (JVST). JVST is published by American Vacuum Society (AVS) through AIP. JVST journal (American Institute of Physics (AIP)) permits authors to use their paper in thesis. The following statement is given in AIP webpage:

https://publishing.aip.org/authors/copyright-reuse

AIP permits authors to include their published articles in a thesis or dissertation. It is understood that the thesis or dissertation may be published in print and/or electronic form and offered for sale, as well as included in a university's repository. Formal permission from AIP is not needed. If the university requires written permission, however, we are happy to supply it."

As a member of AIP, AVS also follows AIP's policies. The following statement is taken from JVST webpage:

https://avs.scitation.org/jva/authors/webposting

“As a Member Society of the American Institute of Physics (AIP) and as a close partner, AVS adheres to the policies outlined by AIP in their statement of ethics and responsibilities of authors submitting to AVS Journals."

J Bio Tribo Corros

Appendix B1 was previously published as " Human Osteoblast Cell-Ti6Al4V Metal Alloy Interactions Under Varying Cathodic Potentials: A Pilot Study" in Journal of Bio- and Tribo-Corrosion. Written permission for the use of tables and figures & text from Springer Science+Business Media, which controls the copyright, is given in the next pages (Figure 27).

SPRINGER NATURE LICENSE
TERMS AND CONDITIONS

Apr 02, 2018

This Agreement between Mr. Arghya Kamal Bishal ("You") and Springer Nature ("Springer Nature") consists of your license details and the terms and conditions provided by Springer Nature and Copyright Clearance Center.

License Number	4313810232776
License date	Mar 21, 2018
Licensed Content Publisher	Springer Nature
Licensed Content Publication	Journal of Bio- and Tribo-Corrosion
Licensed Content Title	Human Osteoblast Cell-Ti6Al4V Metal Alloy Interactions Under Varying Cathodic Potentials: A Pilot Study
Licensed Content Author	Arghya K. Bishal, John Grotberg, Cortino Sukotjo et al
Licensed Content Date	Jan 1, 2017
Licensed Content Volume	3
Licensed Content Issue	3
Type of Use	Thesis/Dissertation
Requestor type	academic/university or research institute
Format	electronic
Portion	full article/chapter
Will you be translating?	no
Circulation/distribution	<501
Author of this Springer Nature content	yes
Title	Human Osteoblast Cell-Ti6Al4V Metal Alloy Interactions Under Varying Cathodic Potentials: A Pilot Study
Instructor name	Dr. Christos G Takoudis
Institution name	University of Illinois at Chicago
Expected presentation date	May 2018
Requestor Location	Mr. Arghya Kamal Bishal 851 S Morgan St 218 SEO UIC Bioengineering (MC 063) CHICAGO, IL 60607 United States Attn: Mr. Arghya Kamal Bishal
Billing Type	Invoice
Billing Address	Mr. Arghya Kamal Bishal 851 S Morgan St 218 SEO UIC Bioengineering (MC 063) CHICAGO, IL 60607 United States Attn: Mr. Arghya Kamal Bishal
Total	0.00 USD
Terms and Conditions	

Figure 27: Permission for use of the material in Appendix B. 1. Section, previously published in Journal of Bio- and Tribo-Corrosion.

Appendix B

OTHER COMPLETED PROJECTS

B. 1. Biocompatibility of Ti-6Al-4V under cathodic potentials

This section was previously published as "Human Osteoblast Cell-Ti6Al4V Metal Alloy Interactions under Varying Cathodic Potentials: A Pilot Study" in Journal of Bio- and Tribo-Corrosion.

B. 1. 1. Introduction

Metallic biomaterials are used extensively in the body to improve and restore the functions of different body parts(212; 213). In particular, metals are widely used in dental and orthopedic implants for their superior mechanical properties, e.g., toughness and hardness, over any other class of materials(214). However, many factors contribute to the success of a metallic implant like its ability to bear the cyclic load, minimize corrosion and resist wear conditions(215). Metallic implants also face different challenges including lack of osseointegration(216), infection(217) and corrosion(218; 219). Among these, osseointegration, the ability of the surrounding tissue to integrate with the surface of the metal implant, is one of the biggest concerns for metallic biomaterial(220). Corrosion also plays a significant role in the biocompatibility of the metal alloy since surrounding cells are very sensitive to electrochemical reactions and the products generated during corrosion. Generally, metallic implants start corroding when they get exposed to cyclic load along with the corrosive environment inside the body. This may cause an adverse effect on the osseointegration and also on the mechanical stability of the implant (219-221). Ultimately, the implant may fail from aseptic loosening due to the metal ion and wear debris released

during corrosion. In order to improve the performance of metallic implants overcoming these modes of failure, a better understanding of the electrochemistry of corrosion and its effect on biocompatibility is very important.

Corrosion is a natural phenomenon by which the refined metals try to go back to their more stable form. In this process, a metal chemically reacts with the environment and thus gradually loses materials (metal oxide, metal ions). Therefore, higher resistance to corrosion is one of the most desired properties for a biocompatible metallic implant. Titanium and its alloys are widely used in dental and orthopedic implants due to their remarkable biocompatibility with bone tissue. Higher corrosion resistance is one of the main contributing factors behind this excellent biocompatibility of titanium and its alloys. Upon exposure to solution/air environment, a thin passive oxide layer is formed spontaneously on the top of these metal surfaces. This thin oxide film on its surface acts as a kinetic barrier to prevent corrosion(222). However, this protective oxide layer may abrade away mechanically by adjacent bone or metal during fretting. Consequently, the metal surface tries to repassivate by protective oxide layer formation and this repassivation process induces many electrochemical events including a shifting of open circuit potential (OCP) of titanium (lies between -250 to -100 mV vs Ag/AgCl) to more cathodic potentials(222). Previous reports showed that the OCP of titanium and its alloy could drop to as low as -850 to -1000 mV vs. SCE or lower under conditions of severe mechanical abrasion (223-225). Such electrical polarization may have negative effects on the surrounding tissue. Therefore, it is important to know the influence of cathodic potentials on the biocompatibility of titanium alloy.

Metal/Alloy	Cell type	Polarizing potentials (mV) vs Ag/AgCl	Significant findings	References
cpTi, grade 4	MC3T3-E1 pre-osteoblast	-1000 to +1000	-600 to -1000mV dramatically reduced spreading and viability of cells	Ehrensberger et al 2009(222)
CoCrMo	MC3T3-E1 pre-osteoblast	-1000 to +500	Below -400mV apoptotic cell death reported	Haeri et al 2012(226)
cpTi, grade 4 (bare and anodized)	MC3T3-E1 pre-osteoblast	-400 and -500	On anodized sample cells showed higher viability at -400 and -500mV compared to bare sample	Haeri et al 2013(227)
Ti-6Al-4V	MC3T3-E1 pre-osteoblast	-600 to -300mV	-400mV is voltage threshold for cell viability, cell died below this potential, and this killing effect is also time dependent	Sivan et al. 2013(215)
CoCrMo	MC3T3-E1 pre-osteoblast	-100, -400, -1000 and +500	For -1000mV cell death can occur very quickly (~15min) whereas for +500 and -400 it can take hours	Haeri et al 2013(228)
cpTi, grade 2	MC3T3-E1 pre-osteoblast	-750 and -1000	Cell viability was reduced significantly at -1000mV, while cells were viable at -750mV	Ciolko et al 2015(229)

TABLE VI**:** Previous studies on effect of cathodic potentials on biocompatibility of metal implant materials

Previously, people have studied MC3T3 pre-osteoblast cell response on electrically polarized CoCrMo alloy(226; 228), commercially pure titanium (cpTi)(222; 229), anodized cpTi(227) and Ti-6Al-4V(215) surface as presented in TABLE VI. They reported a significant reduction in biocompatibility when those metal/alloys are held at cathodic potentials. Ehrensberger et al. showed that application of a static cathodic potential of -600 and -1000mV vs. Ag/AgCl over 24 hr caused ~85% reduction in spreading and viability of preosteoblast cells cultured on the cpTi surface(222). Haeri et al. reported a reduction below 5% in the viability of preosteoblast cells cultured on cpTi held at static cathodic potentials of -400 or -500mV vs. Ag/AgCl(227). Another work by Sivan et al. reported the voltage threshold and time dependence of Ti-6Al-4V biocompatibility. In their work, they showed that cell death of preosteoblast cells resulted within 4hr at the cathodic polarization of -600 and -1000mV vs. Ag/AgCl while cell death occurred in 10-24hr at -400mV vs. Ag/AgCl(215). Recently, Ciolko et al. examined the effect of applying periodic cathodic potential on the biocompatibility of cpTi, and they found significant reduction in viability and morphology of preosteoblast at -1000mV vs. Ag/AgCl enforced periodically over 24hr while no deleterious effect on cellular response at periodic polarization of -750mV vs. Ag/AgCl(229). In our study, we investigated for the first time the behavior of human osteoblast MG63 cell line, on mirror finished smoother Ti-6Al-4V surface electrically polarized at three different potentials. We studied changes in cell morphology with the shifting of OCP towards more cathodic potentials. Also, we measured different electrochemical parameters to understand the correlation between cell behavior and cathodic polarization.

B. 1. 2. Material and Methods

B. 1. 2. 1. Sample preparation

Ti-6Al-4V alloy discs of 15 mm diameter and 3 mm thickness (Mac-Master Carr, Elmhurst, IL) were mechanically wet-ground using a series of abrasive pads (#320, #400, #600 and #800) (Carbimet 2, Buehler, Lake Bluff, IL). Samples were then polished using diamond paste (MetaDi 9-micron, Buehler, Lake Bluff, IL) with lubricant (MetaDi Fluid, Buehler, Lake Bluff, IL) on polishing cloth (TexMet polishing cloth, Buehler, Lake Bluff, IL), and brought to mirror finish using colloidal silica polishing suspension (MasterMet, Buehler, Lake Bluff, IL) on polishing cloth (Chemomet I, Buehler, Lake Bluff, IL). Samples were then washed with deionized water and sonicated in 70% ethanol. After that samples were autoclaved followed by a wash with 70% ethanol prior to cell culture.

B. 1. 2. 2. Osteoblast cell culture

MG63 human osteoblasts cells were cultured in Dulbecco's Modified Eagle Medium (DMEM) (Gibco) with 10% fetal bovine serum (FBS) (Gibco) and 1% antibiotic (Gibco) until roughly 80% confluence in a cell culture incubator at 37° C and 5% CO_2. Cells were then trypsinized using 0.25% trypsin (Sigma) and subcultured for experimentation. Cells were seeded on the titanium alloy discs at a density of 1.15×10^5 cells per disc (with 1.13 cm^2 of available exposed area inside corrosion chamber) for 1 day prior to electrochemical testing.

B. 1. 2. 3. Electrochemical tests

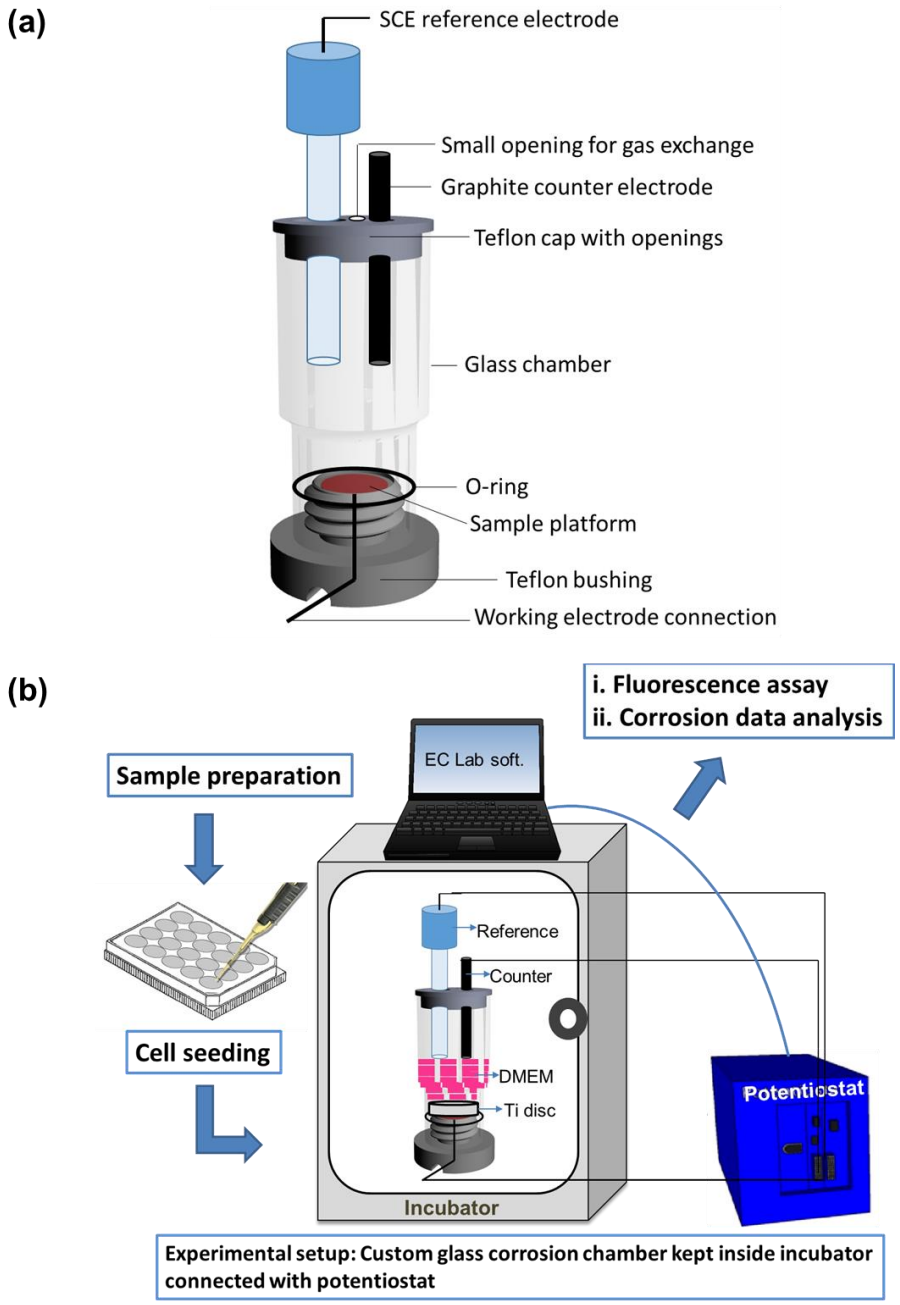

Figure 28**:** (a) Schematic of custom-made glass electrochemical chamber, (b) schematic of the experimental setup

Each titanium alloy disc seeded with cells was transferred to a custom glass corrosion apparatus (Figure 28a). The disc was mounted at the bottom of this chamber. A stainless-steel screw was connected to the underside of the titanium alloy disc and passed through the Teflon threaded bushing to serve as an external electrical contact to the sample. A sterile O-ring was used in the threading between glass and Teflon bushing to achieve a water tight seal around the titanium alloy surface. 1.13 cm^2 of exposed area of the sample to the interior of the chamber is achieved in this setup. Another Teflon cap was used to seal the chamber from the top. This cap had openings for graphite counter electrode: CE, reference electrode: RE (in this case, Saturated Calomel Electrode or SCE) and for proper gas exchange from incubator environment. The sample served as the working electrode. Right after mounting the disc with the cell, the glass chamber was filled with 12 ml of cell culture DMEM media to avoid any stress or shock to cells. Here the cell culture media served as the electrolyte for corrosion study, and the pH was 7.5 at room temperature. The entire experiment was performed inside an incubator at 37° C to simulate physiologic temperature of the human body (Figure 28b).

Electrochemical impedance spectroscopy (EIS) were performed at a range of 100k-0.005 Hz, prior to 24 hours of potentiostatic polarization. A potentiostat (SP-240, BioLogic, Claix, France) was used for application of static potentials. Two different cathodic potentials were examined during this study, i.e., -300mV vs. SCE, -600mV vs. SCE, and open circuit potential (no applied potential) was used as a control (Figure 29a). Since previous reports (TABLE VI) indicated that -400mV might be a viability threshold and below that (i.e., < -400mV) a dramatic reduction of cell spreading and viability for MC3T3-E1 mouse pre-osteoblast cells seeded on Ti and its alloy surface would take place, the two

potentials -300 and -600 mV were chosen for MG63 human osteoblast cell responses. For our case, OCP was between -250mV and -135mV vs. SCE. Finally, after 24 hours of potentiostatic polarization, EIS were performed again at the above-mentioned frequency range and at OCP. The sequence of corrosion protocol is displayed in Figure 29b.

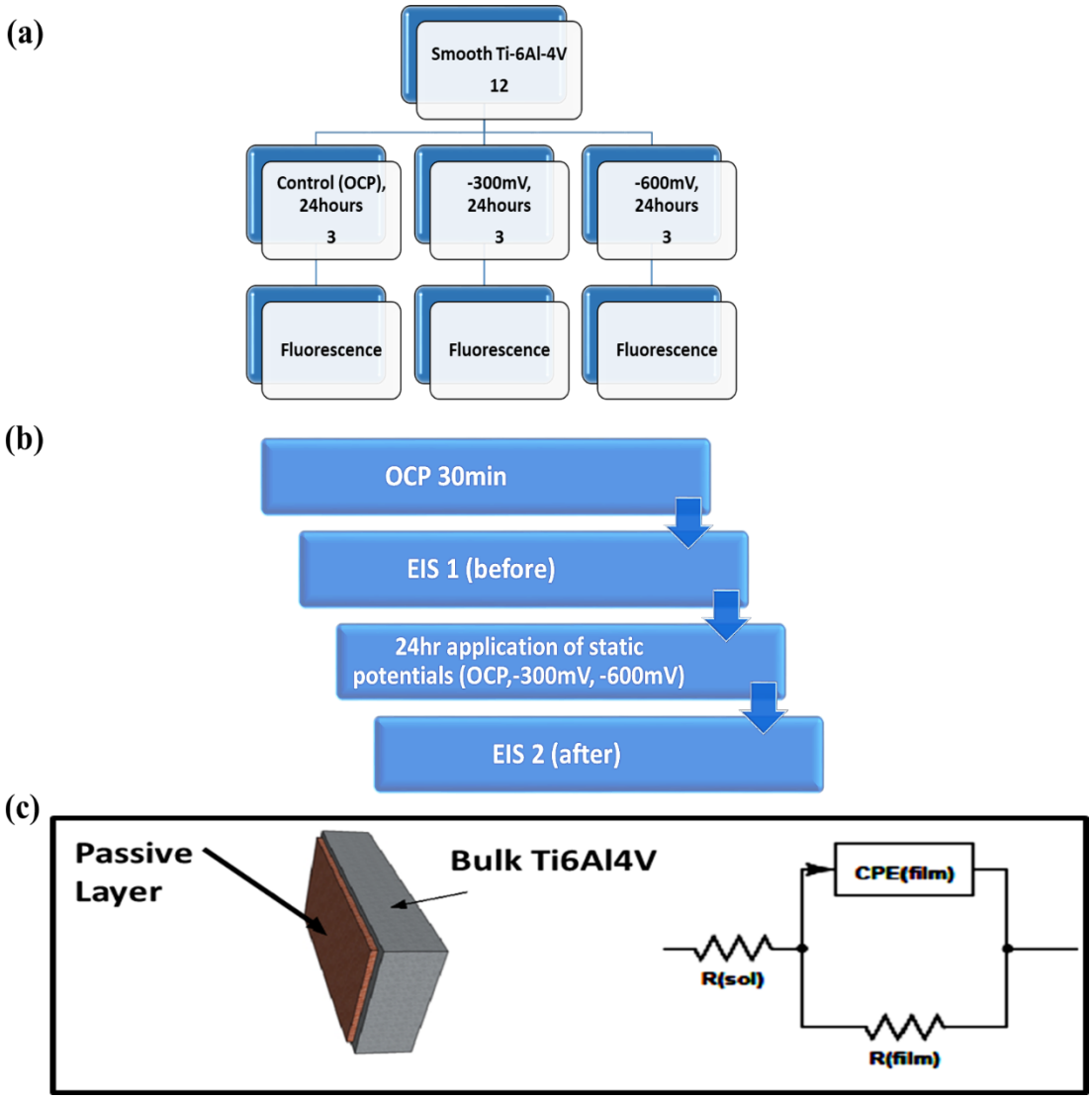

Figure 29**:** (a) Schematic of experimental design, (b) diagram of corrosion protocol used, (c) schematic of modified Randle's circuit used for modelling electrochemical impedance, where R(sol) represents the resistance of the solution and CPE(film) and R(film) represent the capacitance and resistance of the native oxide film respectively

Additionally, EIS data were used to estimate total polarization resistance and capacitance using constant phase element (CPE) equivalents. A modified Randle's circuit (Figure 29c) was used to model the impedance. EC-Lab v. 10.23 software was used to perform the z-fit analysis of this equivalent circuit model over a range of 1000-0.01 Hz. Bode and Nyquist plots were used to calculate the solution resistance (R_s), polarization resistance (R_p or R film), constant phase element (CPE) and alpha (n). All these values were measured before and after 24hours of potentiostatic polarization. Following the electrochemical test, the electrodes were disconnected from the potentiostat and then the samples were prepared for fluorescence assay.

B. 1. 2. 4. Fluorescence assay

Cell morphology on each sample group was assessed after 24 hours of electrochemical tests using fluorescent dye based reagent labeling (Molecular Probes™, ThermoFisher Scientific) and fluorescence microscopy. Cells were imaged with a fully automated inverted microscope (Leica DMI6000 B, Leica Microsystem, Germany) and post-processing of the images was performed using LAS AF software (Leica, Germany). Prior to imaging, cells were first fixed in 3.7% Formaldehyde, permeabilized with 0.1 % Triton X-100 and stained in phosphate-buffered saline (PBS). Actin and nuclei were stained with ActinRed™ 555 ReadyProbes® Reagent (Molecular Probes™, ThermoFisher Scientific) and NucBlue® Fixed Cell ReadyProbes® Reagent (Molecular Probes™, ThermoFisher Scientific) respectively.

B. 1. 3. Results

B. 1. 3. 1. Cell morphology

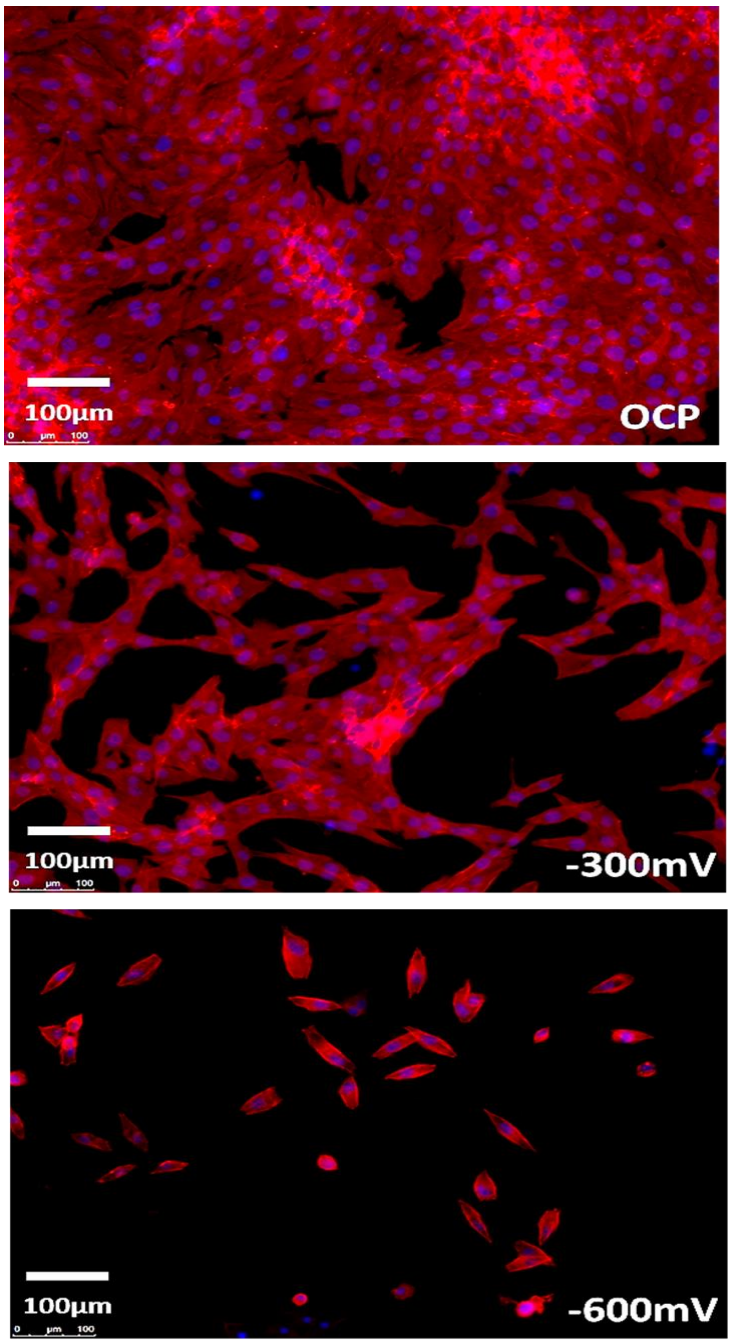

Figure 30**:** Fluorescence image of cell morphology after 24 hours of different potential application

Fluorescence images of MG63 cells cultured on Ti-6Al-4V alloy samples, electrically polarized at the three different potentials (OCP, -300, -600 Vs. SCE) for 24 hours, are displayed in Figure 30. Cellular morphology was found to be affected by cathodic voltages depending on their magnitude. The morphology of cells cultured on control sample maintained freely at OCP were well spread and higher in density compared to the other two potentials shown in Figure 30. The size of the cells cultured at -300mV did not differ from the cells maintained at OCP. In spite of being less dense compared to OCP, the cells cultured at -300mV remained elongated and well spread with clear evidence of flattened actin and presence of nuclei. However, a stark difference in the morphology of cells cultured at -600mV was observed from the cell morphology at -300mV and OCP. Cells cultured on the samples polarized at -600mV were rendered small, balled-up and fewer in number. Thus Figure 30 reveals clear differences in cell morphology of MG63 cells due to the application of different potentials.

B. 1. 3. 2. Electrochemical current density

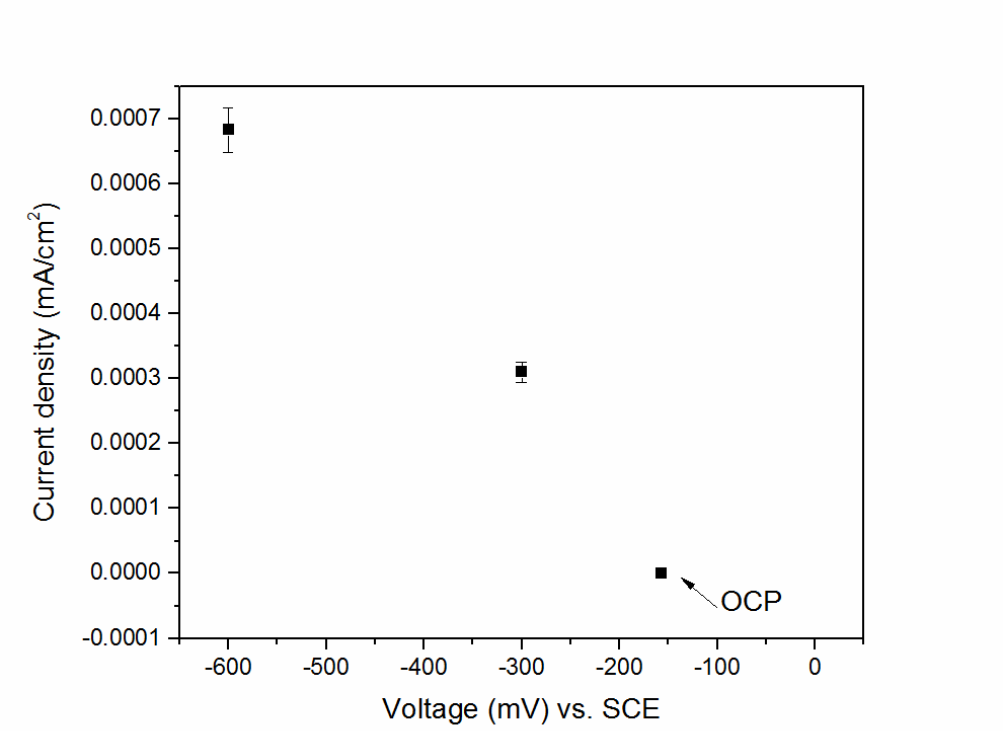

Figure 31**:** Current evolution due to application of potentials for 24 hours

The average current densities the MG63 cells experienced over a period of 24hr when they were cultured on Ti-6Al-4V polarized at different potentials, is presented in Figure 31. These cathodic current densities were found to be increased with the cathodic shift of the applied potential. Current values measured at -300mV were ~3×10^{-4} mA cm^{-2}. Larger

current values of ~6.8×10^{-4} mA cm^{-2} were measured at -600mV and cells became small size and balled up at this low reduction current density.

B. 1. 3. 3. Electrochemical impedance analysis

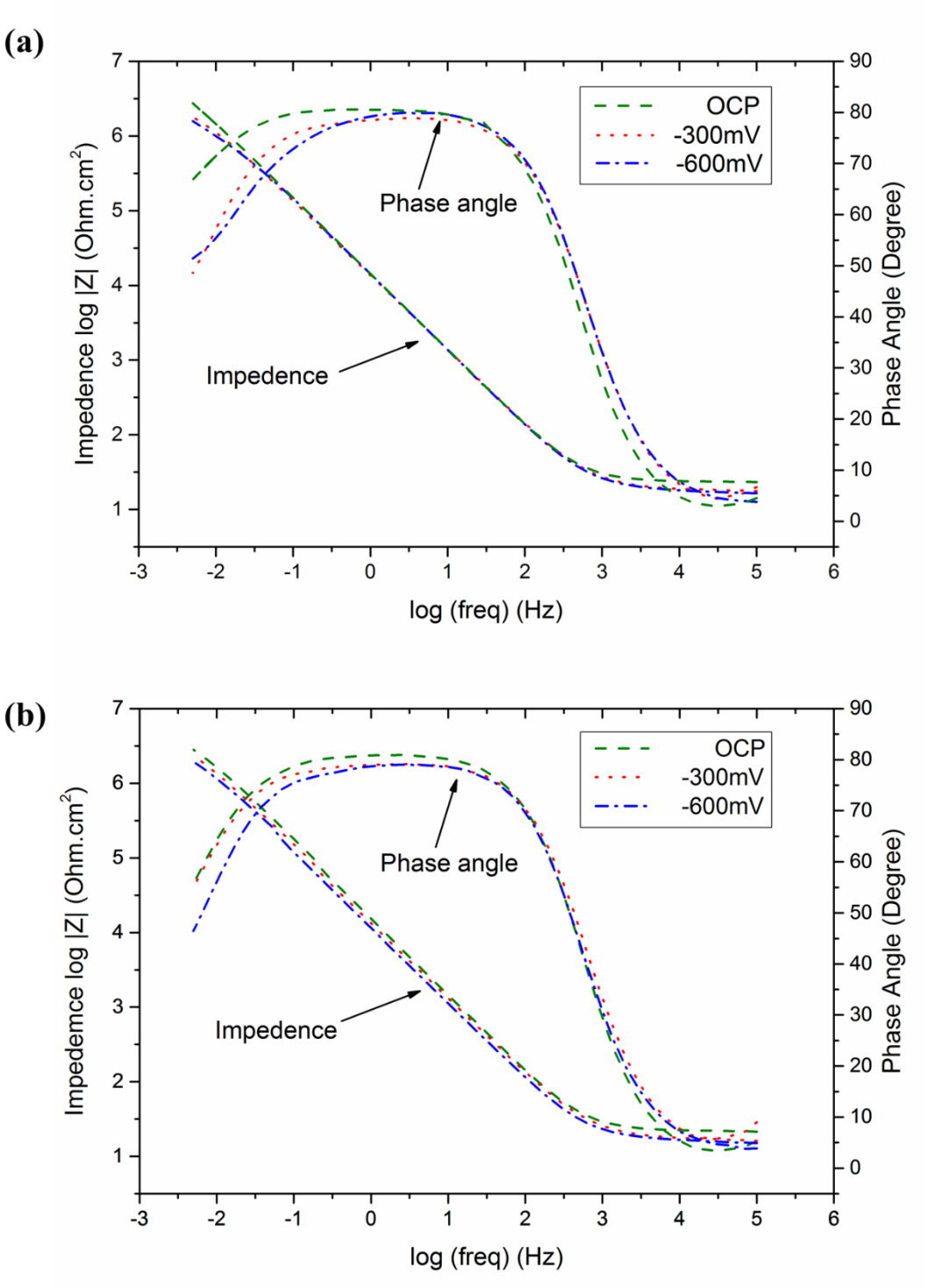

Figure 32**:** Bode plot before (a) and after (b) 24 hours of polarization.

To analyze the electrochemical events at the surface oxide layer and to find a correlation of the observed cellular responses with those events, electrochemical impedance spectroscopy (EIS) was employed. Impedance spectra were recorded before and after 24 hours of polarization and the EIS results at OCP, -300mV and -600mV vs. SCE have been presented as Bode plots (phase angle vs. frequency and impedance |z| vs. frequency) in Figure 32a, Figure 32b and as Nyquist plot (real Z vs. img Z) in Figure 33. For each experimental condition, all the representative Bode plots showed single time constant behavior. No significant change in the impedance spectra and in the phase angles was observed before 24hr or at the start of polarization among the three potentials used. However, changes were observed after 24hr of polarization with static potentials. As shown in Figure 32b, the impedance drops with shifting toward more cathodic potentials from OCP. The phase angle was also found to get lowered with a cathodic shift of potentials at frequency ranges from 1-100 Hz. Bode plots did not show the drop of impedance very clearly though.

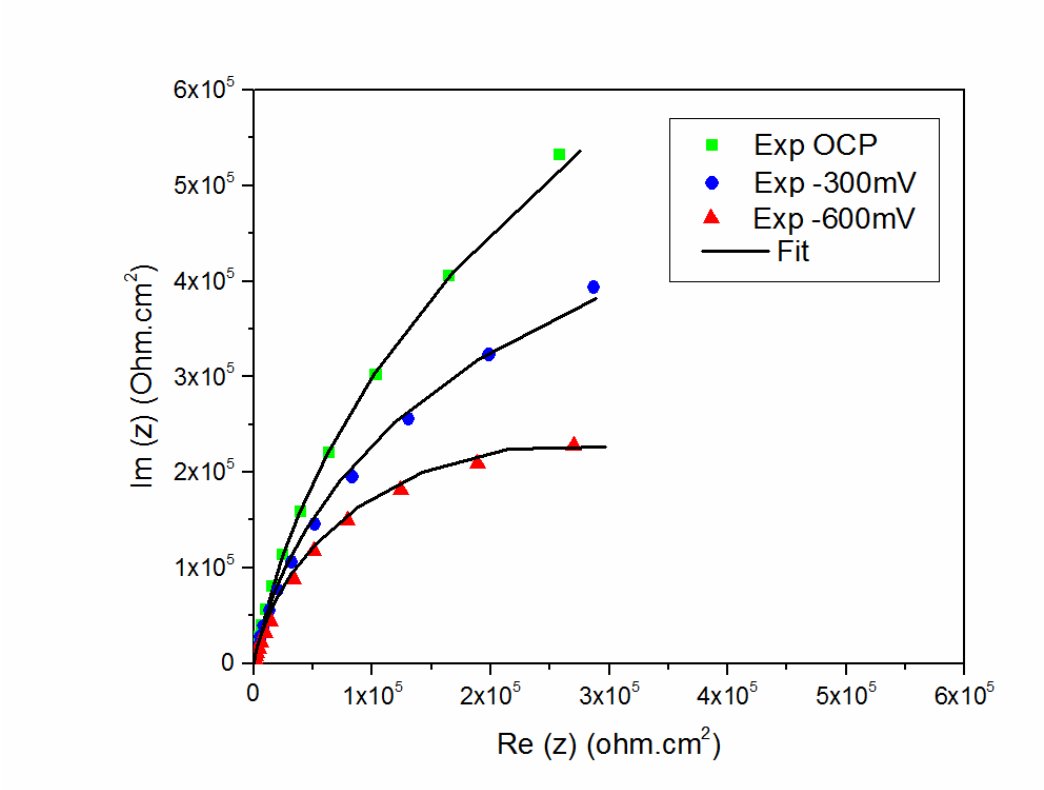

Figure 33**:** Nyquist plot of three potentials with fitted curve after 24hr of polarization

A significant drop in impedance is observed more clearly in Nyquist plot (Figure 33) with the cathodic shift in potentials. The Nyquist plots for all the three potentials were subsequently fit to a modified Randles circuit. The values of total polarization resistance

(R_p or R film), constant phase element (CPE or capacitance) and alpha for samples at OCP, -300mV and -600mV vs. SCE were displayed in Figure 34.

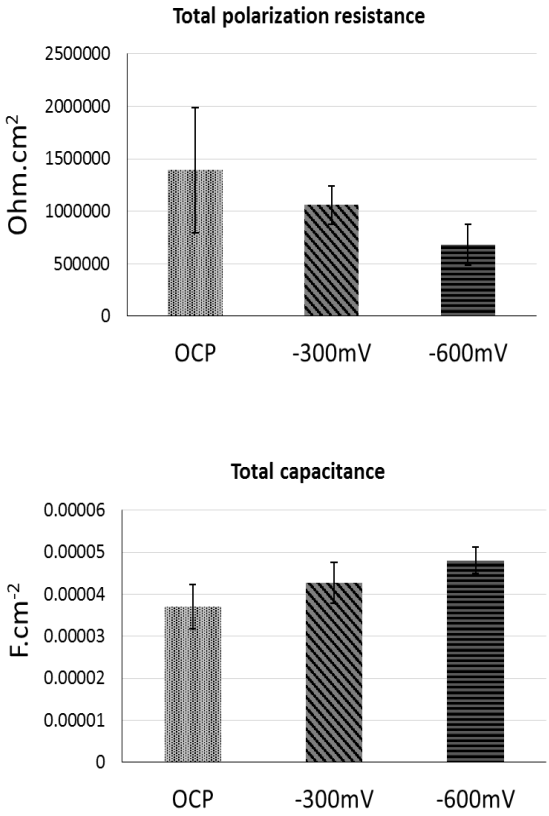

Potential conditions	R_p ($\Omega.cm^2$)	CPE ($F.cm^{-2}$)	Alpha
OCP	$13.93\pm5.97\times10^5$	$3.7\pm0.52\times10^5$	0.929±0.014
-300mV	$10.58\pm1.79\times10^5$	$4.27\pm0.48\times10^5$	0.874±0.007
-600mV	$6.8\pm1.93\times10^5$	$4.8\pm0.31\times10^5$	0.892±0.012

Figure 34**:** EIS fitting results: polarization resistance (top left), total capacitance (top right), and summary of resistance, capacitance and alpha values at different potential conditions (bottom)

There was a noticeable reduction in R_p after 24hr for the samples statically polarized at -300mV and -600mV vs. SCE compared to the samples maintained at OCP. On the other hand, the capacitance values determined for the samples at -300mV and -600mV vs. SCE was larger compared to the OCP. The alpha value (CPE exponent) for the samples polarized at -300 and -600mV vs. SCE was smaller than the alpha value of the sample maintained at OCP. The resistance of the solution (R_s) did not change significantly across all the potentials, and it remained ~15.7Ωcm^2.

B. 1. 4. <u>Discussion</u>

The results of this study have demonstrated that static cathodic potentials have a negative impact on the MG63 cell morphology cultured on the smooth Ti-6Al-4V surface within 24 hr. The cell morphology observed at OCP can be related to the cell condition in the normal cell cycle where the cells are well spread and healthy. Shifting of OCP towards more cathodic voltages resulted in a reduction of the cell morphology and viability. -300mV vs. SCE voltage range seemed to be the border-line between healthy, fully spread cells and unhealthy, balled up cells. Significant reduction in cell spreading was observed at -600mV vs. SCE where the cells became small and rounded. This reduced biocompatibility of MG63 cells observed due to the application of static cathodic potential is consistent with previous reports for different cell types. Shivan S et al. and Ehrensberger et al. (215; 222) reported a similar trend in the reduction of biocompatibility for MC3T3 pre-osteoblast cell lines cultured on the Ti-6Al-4V surface and cpTi surface, held at static cathodic potentials for 24 hr. The periodic cathodic polarization of cpTi was also reported to reduce viability and morphology of MC3T3 pre-osteoblast significantly over 24 hr(229). This negative effect of cathodic potential on preosteoblast cellular behavior is not only limited to titanium

and its alloys. In the case of CoCrMo alloy (OCP lies between -200 to -400mV vs. Ag/AgCl), it has also been reported that MC3T3 pre-osteoblast cells became rounding-up, reduced-size, and finally non-viable below -400mV (Ag/AgCl)(226).

This observed cellular viability throughout the voltage range can be correlated with the cathodic current densities. Low current density (3×10^{-4} mA cm^{-2}) was recorded for voltages within a viable range where cells are well spread. At -600mV vs. SCE, a relatively larger cathodic current density (6.8×10^{-4} mA cm^{-2}) was measured which likely attributed to the significant reduction in cell spreading. Ciolko et al. reported that the large cathodic current density increases oxygen consumption in the adjacent microenvironment of the polarized metal surface, as oxygen reduction is the dominant cathodic half-cell reaction for these experimental conditions(229). Gilbert et al. also reported a reduction in cell spreading and viability as consequence of a local depletion of oxygen adjacent to the cathodically polarized cpTi surface at -1000mV vs. Ag/AgCl(224). Therefore, the observed reduction in cell spreading in our study could be due to depletion of oxygen. Additionally, Kalbacova et al. have shown that production of intracellular reactive oxygen species (ROS) increases by application of cathodic current densities ranging from -0.5 to -5 $\mu A/cm^2$ to Ti-6Al-4V for 24 hr and this ROS reduces metabolic activity of osteoblast-like cells(230). This could be another contributing factor to the reduction in cell spreading on the cathodically polarized Ti-6Al-4V surface.

The electrochemical conditions and properties of the surface were also found to be closely followed by the cellular response of MG63 on the polarized Ti-6AL-4V surface. For all the sample groups, the film resistance (R_p) and capacitance (CPE) values changed significantly after 24 hr of application of cathodic potentials. The impedance outcome of

this study demonstrated that the sample held at static -600mV vs. SCE potential had relatively small R_p value ($6.8\pm1.93\times10^5\Omega.cm^2$) as compared to the film resistance values of the samples kept at OCP and -300mV vs. SCE. On the other hand, capacitance value ($4.8\pm0.31\times10^5$ $F.cm^{-2}$) was highest at -600mV vs. SCE compared to all the other experimental conditions. This decreased resistance and increased capacitance conditions of the sample held at -600mV clearly indicate the high conductivity of the surface oxide and thereby thinning of surface oxide film over time. The resistance and capacitance of an oxide can also be determined from the following general equations(229):

Resistance of oxide (R_{ox}) = $\frac{L\rho}{A}$ and Capacitance of oxide (C_{ox}) = $\frac{k\epsilon_0 A}{L}$,

where L is oxide thickness, ρ is oxide resistivity, A is a cross-sectional area, k is dielectric constant, and ϵ_0 is the permittivity of free space. Considering the titanium dioxide resistivity value as ~$10^8\Omega\cdot$cm and from the measured resistance values of the oxide, the calculated thickness values of the surface oxide film for OCP, -300mV and -600mV are 0.16mm, 0.12mm and 0.07mm respectively. Therefore, these equations show the thinning of oxide layer due to a decrease in resistance and increase in capacitance, as we found for the sample at -600mV. This finding is consistent with previous reports on different cell lines, where they showed the generation of an electrochemical interface with lower resistance and higher capacitance as a result of applying cathodic potentials(222; 229; 231). This unstable thin oxide layer could be another contributing factor to the deleterious cell response of MG63 at -600mV vs. SCE. However, OCP and -300mV had relatively higher R_p and lower capacitance which offered a stable, biocompatible surface oxide layer favorable for healthy and well-spread cell morphology (Figure 35).

Cathodic potentials may also induce reduction reactions and thereby generation of toxic compounds like hydrogen peroxide(215; 226). Generation of hydrogen peroxide was reported on titanium oxide surface under cathodic voltage in an oxygen containing aqueous solutions(232). This hydrogen peroxide generation can lead to oxidative stress which can affect cell functionality like cellular adhesion(233). Therefore, either one of this mentioned reaction or the cumulative contribution of all can be responsible for such deleterious effect on our MG63 cell morphology cultured on the cathodically polarized Ti-6Al-4V surface.

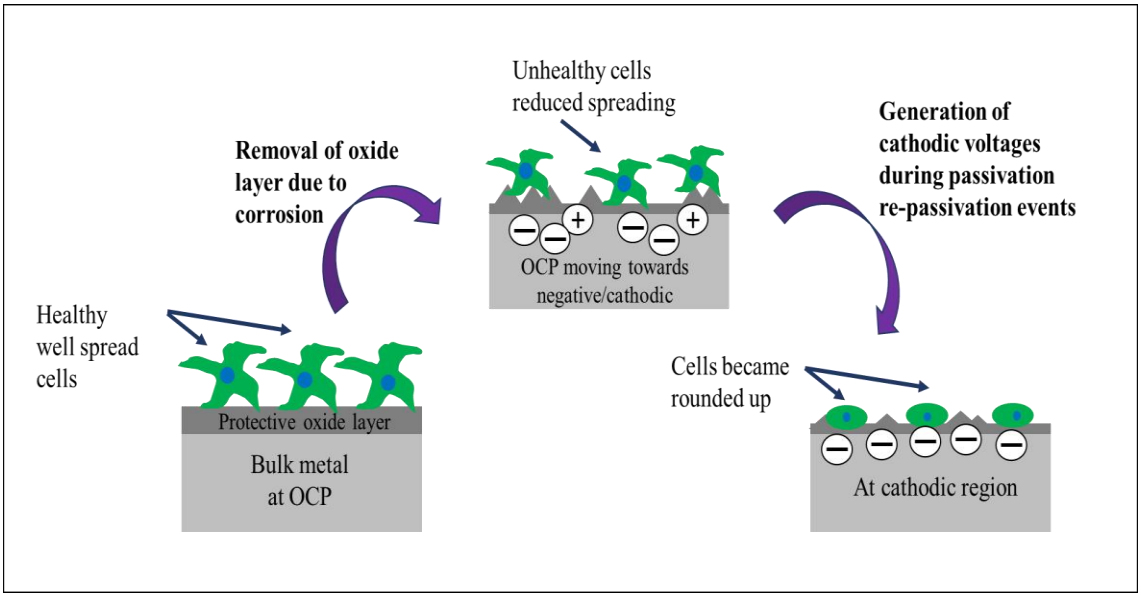

Figure 35**:** Schematic diagram of corrosion induced cathodic potentials' impact on cell spreading. At early stage, metal surface has a protective and biocompatible native oxide layer on the surface keeping the cells viable and well-spread; with the removal of oxide layer due to corrosion OCP of the metal starts decreasing towards more cathodic region causing reduction in cell spreading, i.e., unhealthy cells

Now, apart from the electrochemical reasons behind cell death, the biological pathway or the mechanism responsible for cell death may also be an important factor for consideration. Haeri et al. described the cell death by two distinguishable mechanisms, either through apoptosis where modification in internal cell signaling pathway causes death or through necrosis where disruption mediated cell death happens from sudden injury(226). They mentioned the high concentration release of capacase 3 and 9 protein as an indicator of cell death when MC3T3 pre-osteoblast were a culture on cathodically polarized (-400 and -500mV) CoCrMo alloy surface. In our case, we observed the shrunken, oval shaped, small cells at -600mV and which may also be an indication of an apoptosis process.

B. 1. 5. Conclusion

We investigated the impact of the cathodic shift in potential of mirror finished Ti-6Al-4V surfaces on human osteoblast MG63 cells. We observed healthy well-spread cells on Ti-6Al-4V surfaces held at OCP and -300mV vs. SCE, while at -600mV vs. SCE the cells started shrinking and becoming smaller in number and finally becoming balled-up due to a remarkable reduction in cell spreading. The cellular behavior closely followed electrochemical events at the surface. At -600 mV, the observed highest capacitance, and lowest resistance suggested an unstable surface oxide layer attributed to a reduction in cell morphology. At -600mV, we also observed relatively large cathodic current density which might be another factor contributing to the reduction of cell spreading. This apparent deleterious effect of the cathodically polarized surface on cell morphology could be apoptotic in nature. However, there could be a lot of other factors responsible for cell death. This type of cellular response on the electrically polarized surface may also not be limited to particular cell type or metal type. Further investigation is required for an in-depth

understanding of the dominating mechanism behind the reduction in cell spreading and survivability. As Ti-6Al-4V is a widely used alloy in orthopedic and dental clinical practices, our finding has a promising clinical significance in addressing the challenges related to in-vivo osseointegration.

B. 2. Biocompatibility of surface treated Ti-6Al-4V alloy

B. 2. 1. Introduction

The most commonly used materials for surgical implants are probably metal and alloys(234). In the beginning, stainless steel (type 316L austenitic) and Co-Cr alloys were widely used for implants followed by titanium and titanium alloys(235). In the early 1940s, titanium was first introduced into the medical field and later became an important alloying element with other metals(236). Among titanium alloys, Ti-6Al-4V (alloy composition is in weight per cent) have received the most clinical interest as it possesses most of the desirable properties of a surgical implant material(237). It is alpha+beta phase alloy(238). Addition of aluminium and vanadium to titanium acts as alpha and beta-stabilizer, respectively, which depressed the alpha-beta transition temperature and thus facilitates the co-existence of alpha and beta forms at room temperature(236). Due to its excellent corrosion resistance and biocompatibility, higher fatigue and tensile strength, good ductility, low density and low elastic modulus, the Ti-6Al-4V alloy became well established metallic biomaterial for making dental implants and load-bearing orthopedic implants(237; 238).

Like other implant biomaterials, Ti-6Al-4V surface characteristics play an important role on their biocompatibility and osseointegration(238). Factors that directly and/or indirectly affect biocompatibility of Ti-6Al-4V, are surface roughness(239; 240), surface wettability, surface morphology, surface free energy(241; 242), surface oxide film properties(238), active surface area(243), surface porosity(244), and protein adsorption rate on the surface(241). Therefore, by tuning these surface properties, we can alter the

biocompatibility of this Ti-alloy. A variety of studies have been performed to functionalize Ti-6Al-4V surface for better cellular response. Some of the examples are listed here in TABLE VII.

Surface treatments	**Biological consequences**
Glow discharge nitrogen implantation, plasma nitriding and titanium nitride deposition(245)	Nitrogen implantation no effect, osteoblast and fibroblast cell viability reduced after two nitriding treatments
Production of different surface roughness by polishing with metallographic paper(240)	Increased human bone marrow stromal cell attachment and protein adsorption on rough surface than smooth
Nitric acid passivation and aging treatment(246)	Higher human osteoblast (MG-63) and mature osteoblast (SaOS-2) cell proliferation on aged sample
Air furnace and plasma treatment(247)	Treated sample showed better biocompatibility for human umbilical vein endothelial cell (HUVEC) than control
Surface roughness by sandblasting(239)	Better osteoblast like cell (MG-63) proliferation, gene expression on rough surface
Incorporation of strontium(Sr) by hydrothermal treatment(248)	Improved osseointegration of human osteoblast (MG-63) on Sr containing surface

Anodization in sulfuric acid followed by anodization in hydrofluoric acid(249)	Increased human osteoblast cellular adhesion, proliferation
Anodization and annealing treatment for creating anodic nanotube(243)	Improved bone marrow stromal cell viability and adhesion
Electrical discharge machining (EDM)(238)	EDM at 15A peak current showed better MG63 cellular adhesion, proliferation
Anodization and thermal oxidation(242)	Better mouse osteoblast (MC3T3-E1) cell density on anodized-annealed
Acid-alkali, acid-alkali-heat treatment, and anodizing-heat treatment(244)	Anodizing-heat treatment improved human periosteum-derived(hPDC) cell response
Laser surface microtexturing treatment(241)	Sample-microgroove created by lowest wavelength and highest duty cycle improved MG63 cell viability and spreading

TABLE VII: Different surface treatments to improve biocompatibility of Ti-6Al-4V

Therefore, it is a good indication from the previous studies that by modifying the Ti-6Al-4V surface, its biocompatibility along with other surface properties can be improved. Here we performed a comparative study of human stem cell response among different surface treated groups of Ti-6Al-4V. We performed annealing and anodization treatment on our sample surface and after that we performed different biological assay to understand the stem cell behavior on these different surfaces. We hypothesized that the high temperature

annealing could have a higher impact on the biocompatibility of different Ti-6Al-4V surface.

B. 2. 2. Materials and Methods

B. 2. 2. 1. Sample preparation

Sample preparation protocol was same as reported before. (250) Briefly it was described as follow:

B. 2. 2. 1. 1. Polishing protocol

Ti-6Al-4V alloy discs of 15 mm diameter and 3 mm thickness (Mac-Master Carr, Elmhurst, IL) were mechanically wet-ground using a series of abrasive pads (#320, #400, #600 and #800) (Carbimet 2, Buehler, Lake Bluff, IL). Samples were then polished using diamond paste (MetaDi 9-micron, Buehler, Lake Bluff, IL) with lubricant (MetaDi Fluid, Buehler, Lake Bluff, IL) on polishing cloth (TexMet polishing cloth, Buehler, Lake Bluff, IL), and brought to mirror finish using colloidal silica polishing suspension (MasterMet, Buehler, Lake Bluff, IL) on polishing cloth (Chemomet I, Buehler, Lake Bluff, IL). Samples were then divided into 4 groups for experimental manipulation: smooth (as control), TO (formation of rutile/anatase by thermal oxidation at 600° C for 3h), Ad (formation of amorphous TNTs by electrochemical anodization at 60V for 2h) and Ad+TO (formation of rutile/anatase TNTs by 60V, 2h anodization followed by 600° C, 3h thermal oxidation).

B. 2. 2. 1. 2. Thermal oxidation protocol

The thermal oxidation process of the annealed sample group were performed in a Single-zone Quartz Furnace (Lindberg, S# 54032) in air at ambient pressure. The samples were then ultrasonically cleaned in ethanol and dried with nitrogen gas prior to annealing. Once

the target temperature of 600° C is obtained, samples were loaded 5 cm per 5 minutes into the region closest to the thermocouple to ensure gradual temperature change within the samples, avoiding micro-cracks from thermal shock, and to ensure the accuracy of final sample temperature. The samples were kept at the final position in the furnace for 3 hours, and then were removed 5 cm per 5 minutes to ensure gradual cooling.

B. 2. 2. 1. 3. Electrochemical anodization protocol

For the electrochemical anodization process, samples were ultrasonically cleaned in acetone for 30 minutes prior to anodization. Ti-6Al-4V were connected to a dc voltage source (Hoefer Scientific Instrument PS500X DC Power Supply) as the working electrode while a carbon rod was used as the counter electrode. The two-electrode system were submerged in electrolyte containing 4.0 vol. % DI-water (3.85 ml), 0.2 wt. % NH4F (0.21 g), and ethylene glycol (EG, 96.15 ml). Samples were anodized at 60 V at room temperature for 2 hours. After anodization, samples were washed with DI-water, ethanol then air-dried and wrapped in sterile tissue (Kimwipe, Kimtech Science) and stored in a glass petri dish (KIMAX® Petri Dish).

B. 2. 2. 1. 4. Electrochemical anodization followed by thermal oxidation protocol

For the Ad+TO sample group, both of the aforementioned processes were used. Samples were first subjected to the electrochemical anodization protocol of 60V for 2 hours in same electrolyte, followed by the thermal oxidation protocol of 600° C for 3 hours in air.

B. 2. 2. 2. Sample characterization

After surface treatments, sample surfaces were analyzed with high resolution Field Emission scanning electron microscope (FESEM JEOL JSM-6320F, JEOL USA, Inc.) to

know about surface features. X-ray diffraction spectroscopy (XRD) was performed on all the sample groups to investigate the crystallinity of the surface using Bruker AXS D2 Phaser 2nd Gen x-ray diffractometer (Bruker Corporation, USA).

B. 2. 2. 3. Cell culture

Human mesenchymal stem cells (MSCs) were used to evaluate the proliferation resulting from the surface modifications of Ti-6Al-4V. MSCs were cultured in Dulbecco's Modified Eagle Medium (DMEM) (Gibco) with 10% fetal bovine serum (FBS) (Gibco) and 1% antibiotic (Gibco) until roughly 80% confluence in a cell culture incubator at 37° C and 5% CO_2. Cells were then trypsinized using 0.25% trypsin (Sigma) and subcultured for experimentation.

For proliferation study, once seeded on the titanium alloy discs, cells were cultured in osteogenic medium comprised of the same culture conditions supplemented with ascorbic acid, dexamethasone, and β-glycerophosphate (Sigma).

B. 2. 2. 4. Fluorescence assay

Cell structure on each sample group was assessed using fluorescent dye based reagent labelling (Molecular Probes™, ThermoFisher Scientific) and fluorescence microscopy. Cells were imaged with a fully automated inverted microscope (Leica DMI6000 B, Leica Microsystem, Germany) and post-processing of the images were performed using LAS AF software (Leica, Germany). For this assay, 1.15×10^4 cells were seeded on each type of disc and fluorescence images were taken at two time point i.e. after day 1 and day 7. Prior to imaging, cells were first fixed in 3.7% Formaldehyde, permeabilized with 0.1 % Triton X-100 and stained in phosphate-buffered saline (PBS). Actin and nuclei were stained with

ActinRed™ 555 ReadyProbes® Reagent (Molecular Probes™, ThermoFisher Scientific) and NucBlue® Fixed Cell ReadyProbes® Reagent (Molecular Probes™, ThermoFisher Scientific), respectively.

B. 2. 2. 5. Scanning Electron Microscopy

In order to understand cell morphology on the different groups of samples, the cells were imaged using SEM. Images were taken using a high resolution Field Emission SEM (JEOL JSM-6320F, JEOL USA, Inc.). Prior to SEM investigation, at harvest, the culture media was removed, samples were washed two times in PBS, and then fixed with 2 % glutaraldehyde. After fixation, samples were rinsed with PBS for two times, then dehydrated through successive ethanol baths (with 30%, 50%, 70%, 90% and 100%). Then the samples were kept in Hexamethyldisilazane (HMDS) for 15 minutes and dried under the hood. Finally, they were gold-coated using a sputter coater right before SEM.

B. 2. 2. 6. Proliferation assay or MTT assay

MSCs were cultured on top of the titanium alloy discs in 24-well culture plates at a density of 13.175×10^4 cells/well, with one disc per well, in the osteogenic growth media. Cell proliferation/attachment were evaluated at two time points, after 1 day of incubation, and after 7 days of incubation, to investigate the effects of short-term and long-term attachment and proliferation on the treated surfaces. CellTiter 96® (Promega) assay were used for analysis. After the aforementioned incubation periods, the pre-optimized dye solution were added for the conversion of tetrazolium into formazan product. After an additional 4 hours of incubation at 37° C, the solubilization solution/stop mix were added to the 24-well plates to solubilize the formazan product. The cell culture media from the 24-well plates were

then transferred to a 96-well plate and analyzed for absorbance changes. Absorbance was taken at 570 nm. Measurements were performed in triplicate.

B. 2. 2. 7. Statistical analysis

Water contact angle (WCA) and MTT assay data were evaluated statistically by one-way analysis of variance (ANOVA) and pair-wise comparison between treatment groups was performed by Tukey test. A critical significance level of $p < 0.05$ was used for all test. All the statistical test were performed using SPSS version 22 software (IBM, NY, USA).

B. 2. 3. Results

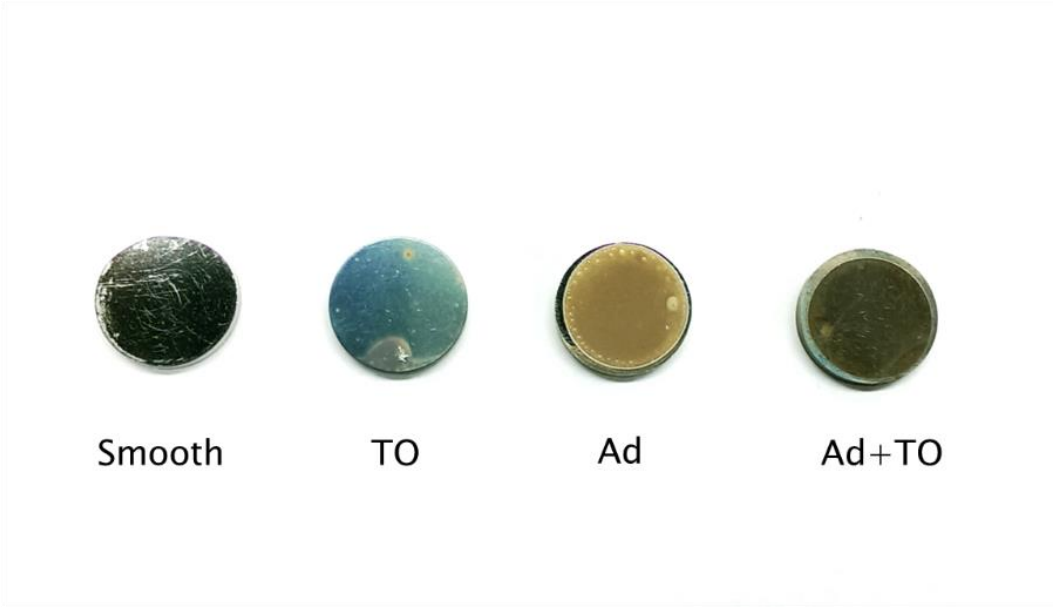

Figure 36: Samples showing different colors after surface treatments

After surface treatments samples developed different colors as shown (Figure 36). Interestingly, four different surface treatments had four distinct colors. Smooth discs had

color like a shiny steel color, thermally oxidized group became bluish, after anodization the sample surface turned into brownish muddy color, while the anodized then annealed sample had dark brown color. This difference in color after different surface treatments can also be used for color coding purposes. This type of color creation is directly related to surface oxide. When light interferes with the transition oxide layer of titanium, color change takes place(251; 252). With the change in oxide layer thickness, the color also changes(253). Recently Karambakhsh et al reported color changes of Ti-6Al-4V surface by changing anodic oxide thickness using different anodization voltages(254).

Surfaces of our samples were characterized after surface treatments. Firstly, the surface morphology was proved using scanning electron microscopy. Surface morphology changed after different surface treatments (Figure 37). The initially smooth surface (Figure 37; smooth) became uneven, granular due to thermal oxidation treatment (Figure 37; TO). Nanotubular, porous surface was observed from the anodization treatment (Figure 37; Ad). Finally, nanotubes seemed to collapse to a less porous surface when the anodized surface was thermally oxidized (Figure 37; Ad+TO).

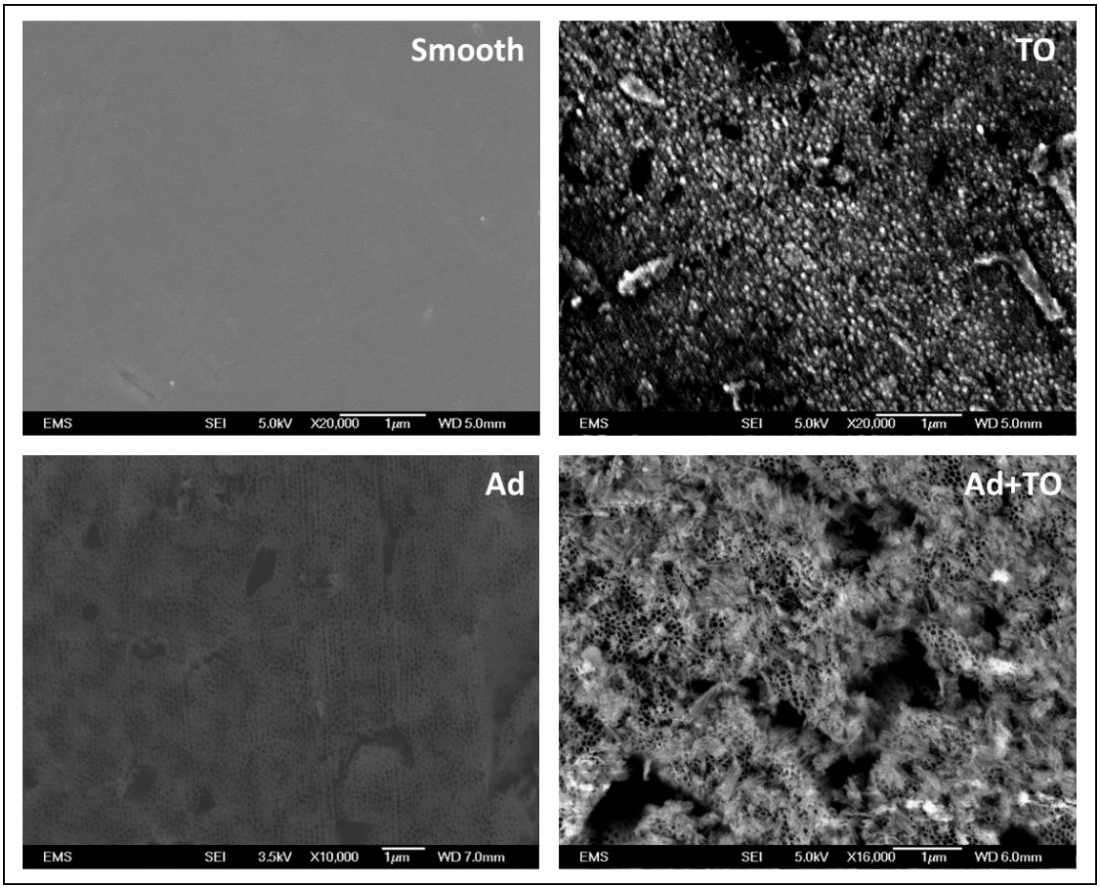

Figure 37: SEM micrograph of four different surface groups: Smooth (top left), TO (top right), Ad (bottom left), Ad+TO (bottom right).

Wettability of the sample was also studied. Contact angle measurements were performed at two time points, day 1 and day 7 after the surface treatments. In between day 1 and day 7, samples were wrapped in kimwipes and stored in plastic vail (lab air ambience). Water contact angle data are presented in Figure 38.

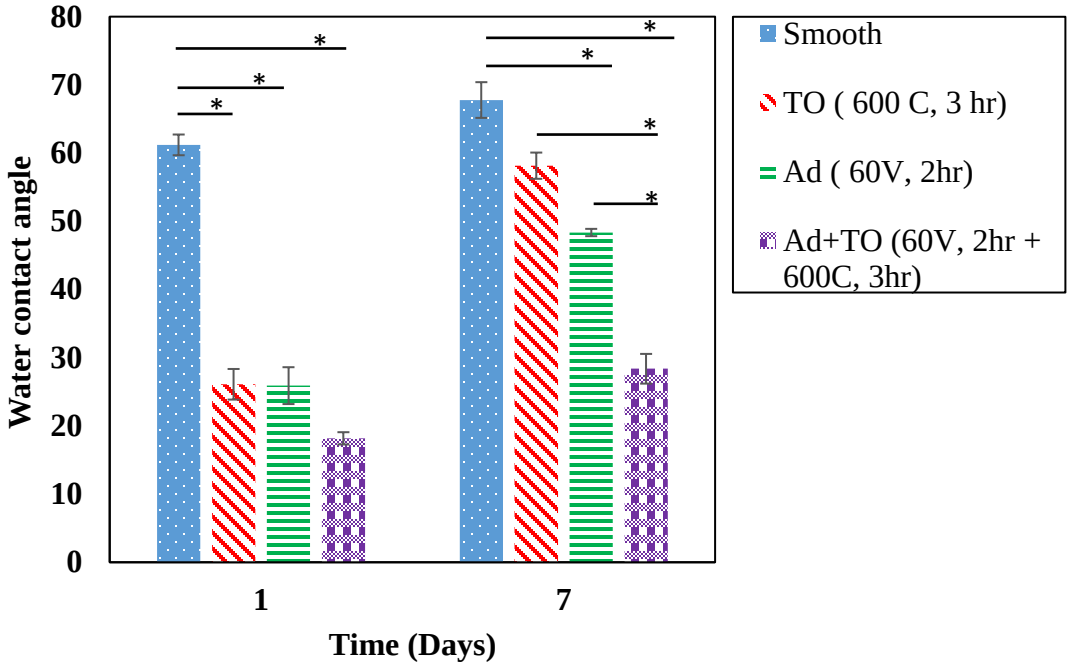

Figure 38: Water contact angle on day 1 and day 7 after surface treatments, * $p < 0.05$ (reproduced from Grotberg et al. (250))

It can be observed that there was a wettability difference among the sample groups and also between day 1 and day 7. The smooth sample group had the highest water contact angle values which indicated the hydrophobic nature of this surface. On day 1, both TO and Ad groups showed similar wettability which is significantly hydrophilic compared to smooth group. While all gained hydrophobicity with time, TO and Ad still they offered better wettability than smooth surfaces. The Ad+TO group was found to have significantly

more hydrophilic surface both on day 1 and day 7 among all groups. Similar kind of trend in wetting behavior of surface treated Ti-6Al-4V was reported by Sweetu et al(242), although their treatment parameters and aging duration were different from ours. Their thermal oxidation was done at 450°C while ours was at 600°C. For anodization, they used 60V for 4 hours while we used for 2 hours only. Still, after ~3 weeks of aging, their wettability trend (Ad+TO wca < Ad wca < TO wca < smooth wca) was similar to ours for 7 days-aged samples.

	Smooth	**TO**	**Ad**	**Ad+TO**
Roughness (µm)	0.015 ± 0.0005	0.031 ± 0.0026	6.84 ± 0.1888	3.39 ± 0.1186

TABLE VIII: Average surface roughness values of the four different sample group

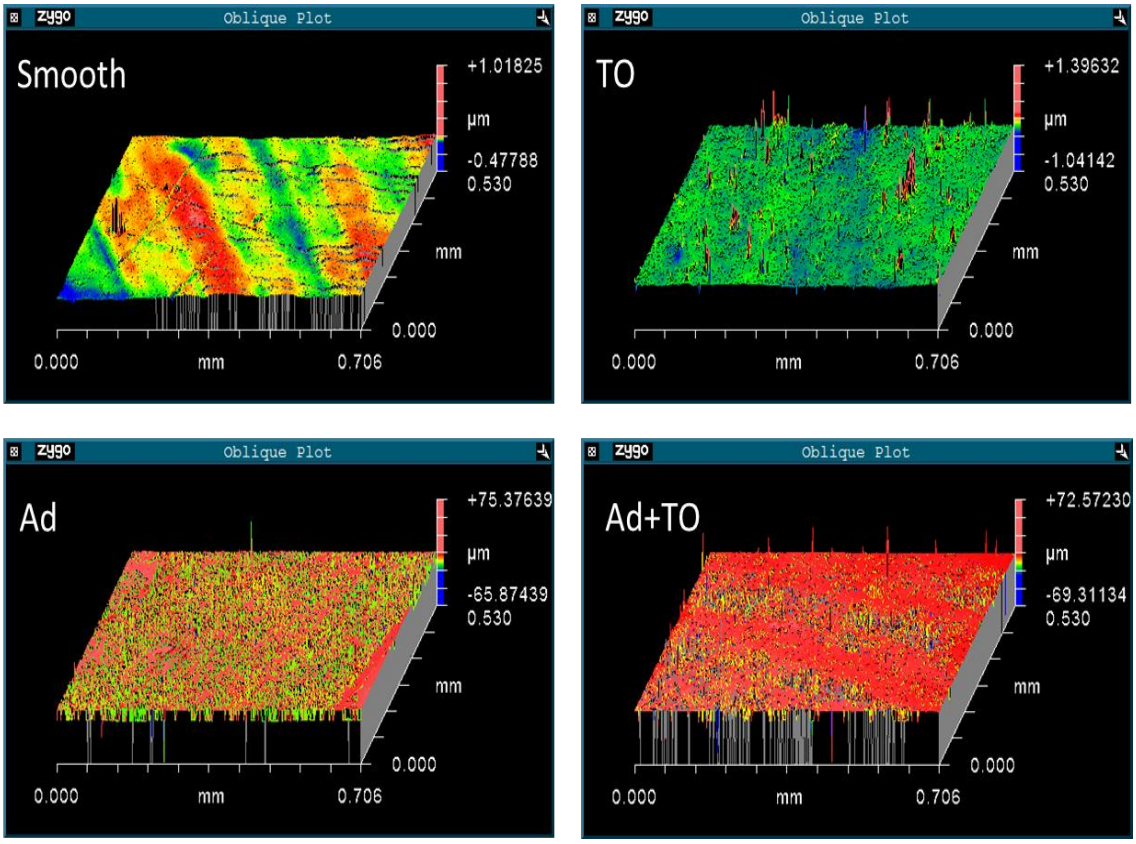

Figure 39: Surface roughness profile (oblique plot) of smooth, To, Ad and Ad+TO group

Surface roughness were also measured (TABLE VIII, Figure 39). From the surface roughness data, the smooth had the lowest surface roughness. After thermally oxidized the smooth surface gained roughness, but it was still quite smooth. Large differences were observed on Ad and Ad+TO sample groups. They both were much rougher (by more than 2 orders of magnitude) than the smooth and TO ones. Ad had the highest surface roughness due to the presence of porous nanotube on their surface. The Ad+TO group had slightly less surface roughness than that of Ad. For the Ad+TO group, it seems thermal oxidation might smoothen the surface a bit.

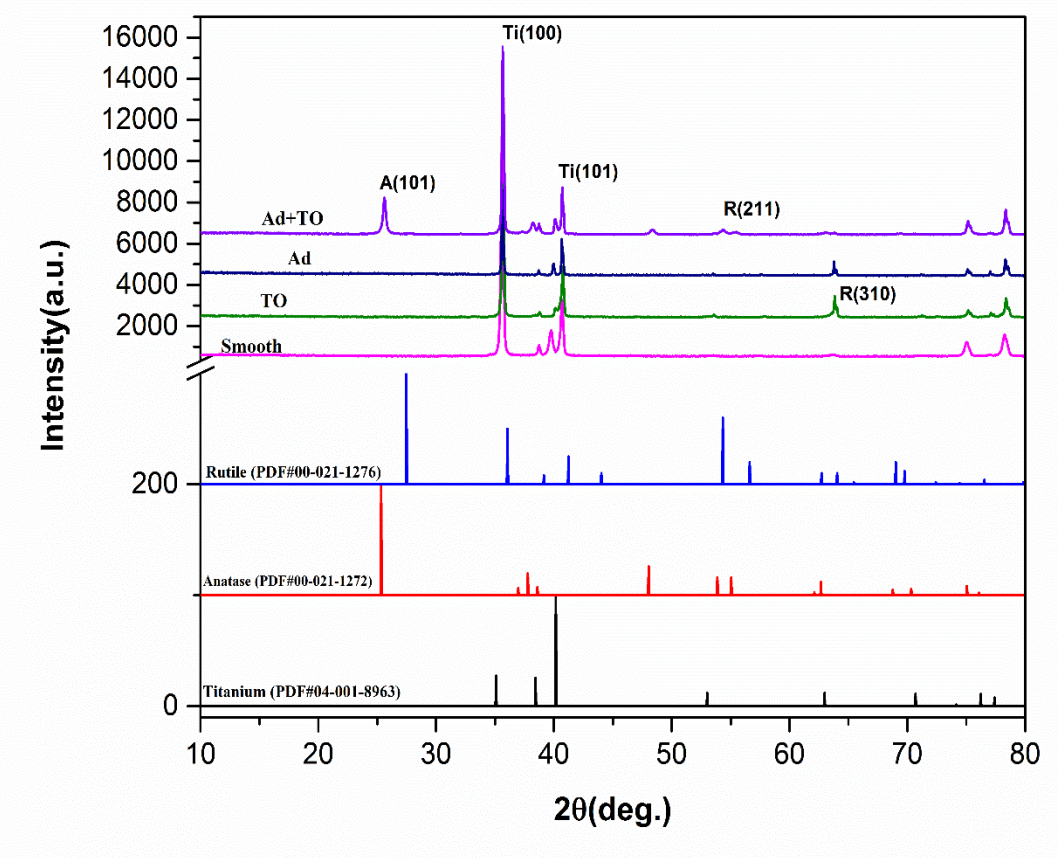

Figure 40: XRD of smooth, TO, Ad and Ad+TO. XRD baselines for rutile TiO_2 (R), anatase TiO_2 (A) and titanium (Ti) are also included.

XRD spectrum of smooth, TO, Ad and Ad+TO samples are presented in Figure 40. Titanium peaks are observed at 2-theta of 35° (100) and 40° (101). For TO the 2-theta feature of 64° is attributed to rutile (310). For Ad+TO, a rutile (211) peak appeared at 2-theta of 54.3, while the feature at 2-theta of 25.28 (101) was attributed to anatase. These XRD data indicated the crystallization of amorphous TiO_2 into anatase and/or rutile due to thermal oxidation.

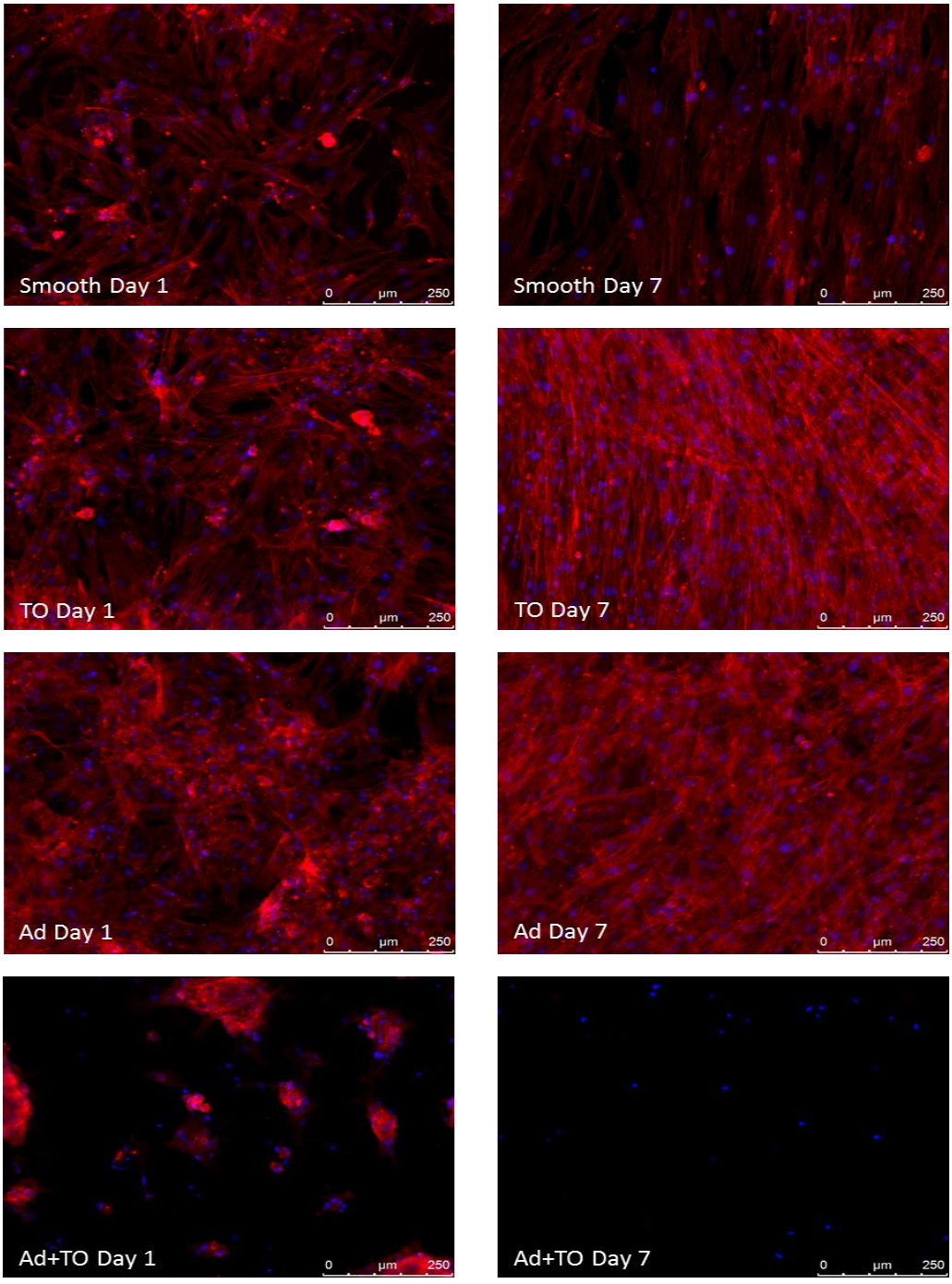

Figure 41: Fluorescence assay images for smooth, thermally oxidized (TO), anodized (Ad) and anodized then thermally oxidized (Ad+TO) samples at two different time points day 1 and day 7.

From fluorescence assay (Figure 41) we saw the cells became confluent and elongated from day 1 to day 7 for smooth, TO and Ad sample groups. For the smooth surface, the cells are elongated at day 7 but not very confluent compared to day 1. On the other hand, for both TO and Ad group cells are well spread on the sample and much more confluent at day 7 compared to day 1. The result indicated, among the 4 groups TO surface had the better cell response. But for the Ad+TO group the cells became round shaped from day 1 itself and on day 7, there was no cell on the Ad+TO sample group. It indicated this surface is not favorable for the cells.

To investigate the cellular behavior furthermore on this 4 different sample groups, MTT assay was performed (Figure 42). MTT assay is a measure of cell viability. Our results indicated, TO sample had the highest cell response whereas Ad+TO group showed significantly poor cellular response among all these 4 groups. This result also supports the result we got in our fluorescence assay.

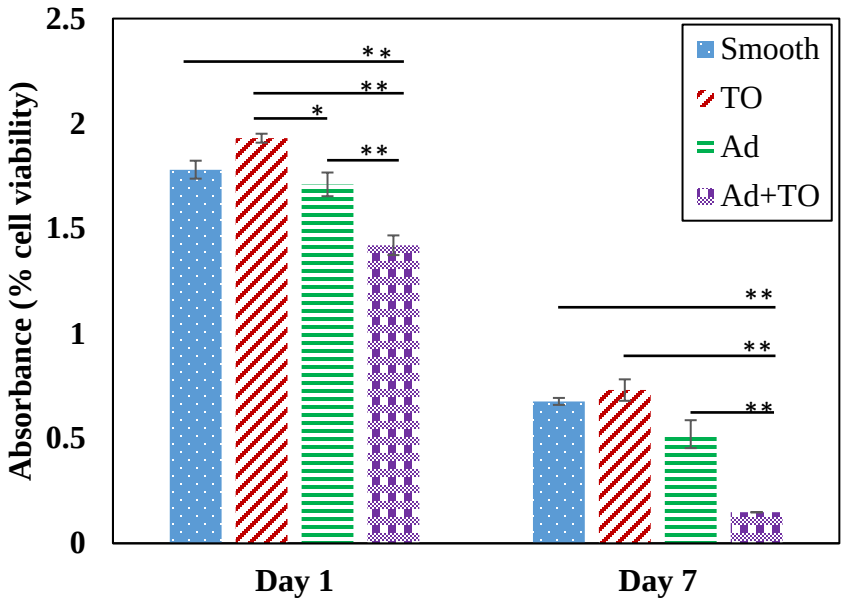

Figure 42: Cell proliferation assay for smooth, TO, Ad, and Ad+TO sample groups at two different time point day 1 and day 7 (* $p < 0.05$, ** $p < 0.001$).

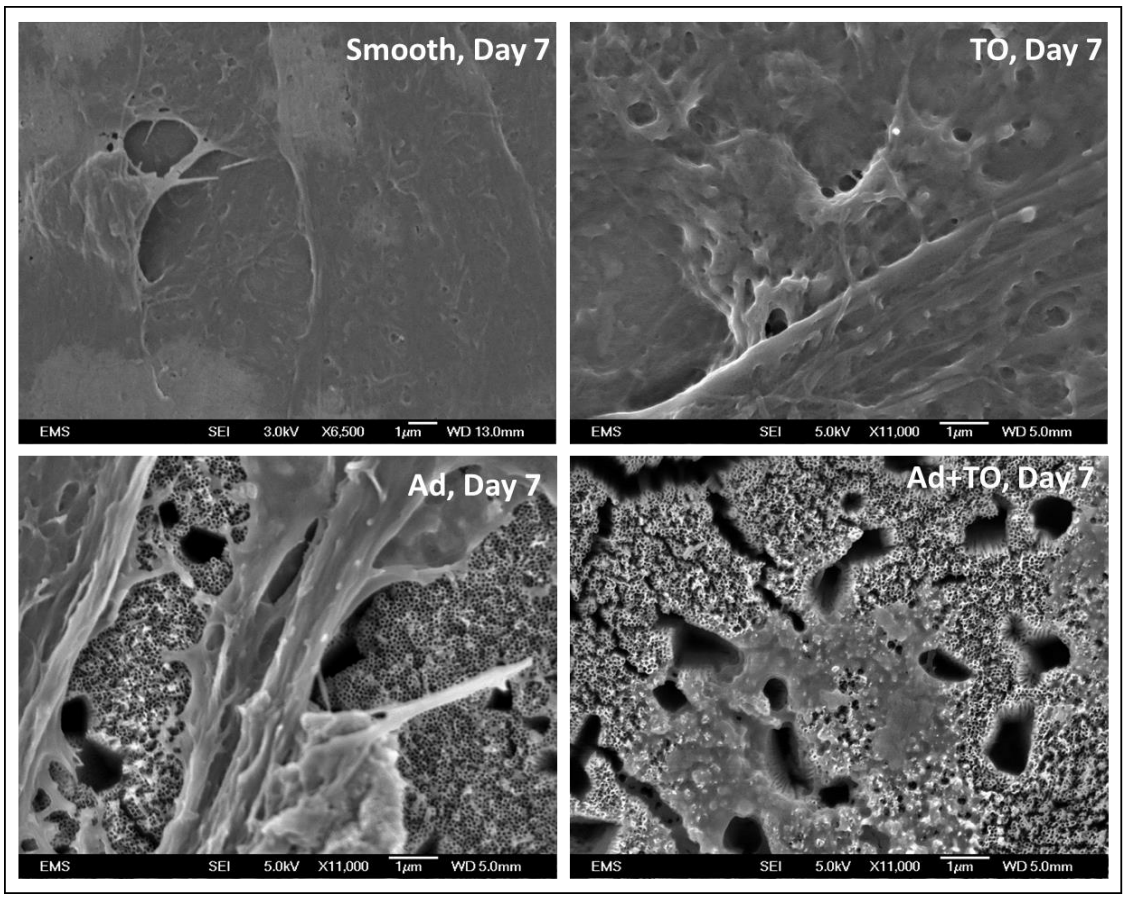

Figure 43: SEM micrograph of hMSC on smooth, TO, Ad and Ad+TO surface after Day 7

To better understand the cell morphology on different surfaces, SEM images were taken (Figure 43). SEM micrographs supported our observations made through fluorescence microscopy. After day 7 of culturing, smooth surface was mostly covered with cells and

there was not much change of cell morphology. Cells were denser and much proliferated for the TO group after day 7. Well spread, elongated, stretched cells were observed on the nanotubular surface of the Ad group. But no cell was found on Ad+TO group. Therefore, the hMSC morphology apparently depends on the surface properties of the Ti-6Al-4V alloy.

B. 2. 4. Discussion

Ti-6Al-4V alloy surface itself is fairly biocompatible(245; 248). Surface treatment can improve this biocompatibility. First the Ti-6Al-4V samples were polished to bring mirror finish and these polished "smooth" group was considered as control. Good cell response was expected on this biocompatible, smooth surface of Ti-6Al-4V alloy. Though this group was not the best, all our results corroborated the good biocompatibility of this smooth surface. Cunha et al and Ravichandran et al also found this type of good cellular response on polished smooth Ti-6Al-4V surface for hMSCs (255; 256).

Wettability of surface plays a major role towards cell behavior on titanium and titanium alloy. Previous reports showed that better wetting behavior of the hydrophilic surface of titanium and its alloy resulted in better cellular adhesion (257-259). In our study, smooth surface was less hydrophilic TO and Ad. There was not much difference in wetting behavior of TO and Ad on both day 1 and day 7, and we observed similar kind of good cell response for both these sample groups. On the other hand, Ad+TO in spite of being the most hydrophilic surface, it did not exhibit good cellular response. Therefore, wetting behavior may not be the leading reason behind the differences in cell behavior on the four different surfaces investigated.

Another important reason behind different cell response could be the surface roughness of these samples. Surface roughness also greatly influences the cell response on titanium and its alloy (239; 240; 258; 259). Rough Ti-6Al-4V surface proved to be better for higher protein adsorption(240), cell differentiation and attachment(239) compared to smooth surface. TO is rougher than smooth and this could be one reason behind better cell differentiation observed on TO compared to smooth. Ad was the roughest due to presence of nanotube grown through anodization and here also well stretched elongated cells were found over the surface of nanotube. Saharudin et al also reported improved cellular behavior of bone marrow stromal cell lines on nanotubes grown on Ti-6Al-4V surface(243). While Ad+TO is also rough compared to smooth and TO group, that could be the reason behind retaining its hydrophilicity. Although surface roughness of Ad+TO still did not result in enhanced biocompatibility.

In spite of being the most hydrophilic and a rough surface, Ad+TO did not show better cell response among the four groups studied. To investigate the reason behind the apparent cytotoxicity of the Ad+TO group and its surface oxide properties, one of the most important parameter in this case, should be considered. Moreover, the surface oxide present on Titanium and its alloy surface contributes the most towards their excellent biocompatibility (245; 260; 261). Now, the properties of this surface oxide get altered through different surface treatments. Thermal treatment can directly alter different properties of surface oxide causing structural, morphological and chemical changes of the surface oxide layer (243). Crystalline structure of titanium oxide is temperature dependent and with different temperature they have 3 different phase anatase, rutile and mixed (both anatase and rutile) (262). Lower temperature (around 450-500^{o}C) offers mostly anatase or mixed but

temperature around 600°C only offers purely rutile structure (263). Rutile TiO_2 achieved through thermal oxidation at around 600°C was reported to improve bioactivity (264; 265). In our case also we found our TO group showed the best cell response indicating the success of heat treatment in improving biocompatibility to a greater extent.

On the other hand, this high temperature (600°C) thermal oxidation on TiO_2 nanotube surface had an adverse effect on its biocompatibility. Ad group containing titania nanotube on its surface had better biocompatibility (improved osseointegration, well stretched cell) due to their morphology. But in case of Ad+TO group, high temperature treatment turned this surface cytotoxic. With increase in temperature (400-600°C) the nanotube wall gets thicker and consequently the nanotube diameter decreases (243; 266). Mazare et al reported 35.65% increase in wall thickness and around 34.43% decrease in nanotube diameter for thermal treatment of titania nanotube at 500°C for 2 hours (266). At 600°C the titania nanotubes turned into nanorod losing all the porous surface morphology (243). Saraf et al also reported that nanotube got collapsed due to annealing at higher temperature (600-700°C) and turned into rutile nanorod like structure (267). These drastic changes of surface morphology might turned the Ad+TO group highly non-favorable for cells and consequently most cells died on this surface. Additionally, one of the major component of this alloy is Aluminum whose melting point is around 650-660°C very close to our annealing temperature. Therefore, the release of aluminum may also influence the cell viability negatively though we did not use higher annealing temperature than the melting point of aluminum.

B. 2. 5. Conclusion

We engineered four different types of surface for Ti-6Al-4V alloy and then we studied their response towards cellular behavior for hMSC cell line. Our result showed thermally oxidized sample surface had the better biocompatibility among the all four surface groups. On anodized surface cells were well stretched. But anodization followed by thermally oxidation at 600°C turned the surface toxic to cells likely due to the change of surface oxide properties and surface morphology. Therefor we can conclude high temperature annealing may improve and/or deteriorate the biocompatibility of Ti-6Al-4V depending on the surface morphology. Further investigation is required to get deeper understanding underlying this different cell response. We hope this result will contribute to the surface enhancement and functionalization of metallic implants.

B. 3. SALD of ZrO_2

Area selective deposition on material surfaces is required to cater to the demands of different thin film based applications. Typically, photolithography is used commonly in semiconductor industries for fabricating necessary patterns on the surface. However, it involves numerous processing steps and thereby increasing both processing time and cost in case of using photolithography techniques to form such patterns on the surface. In this era of device miniaturization as photolithography is reaching its limit, an alternative more efficient technique needs to be developed for deposition of nano-pattern of metal/metal oxides on surface. For nano-patterning selective ALD is becoming popular. As ALD reaction occurs based on the availability of surface reactive groups/nucleation sites, successful selective ALD can be achieved by modifying the surface groups of substrates prior to performing the ALD process. Preliminary studies were conducted with the objective of performing SALD of zirconium oxide (ZrO_2) on SiO_2/Si substrates. Firstly, Tetrakis(dimethylamino)zirconium(IV) (TDMAZ) precursor and ethanol oxidizer was used at reaction temperature of 200°C. Poor nucleation (no ZrO_2 film) was detected on SiO_2/Si substrates. TDMAZ containing bubbler temperature was increased starting from 65°C till 90°C, and effect of different oxidizers such as ozone and oxygen was also investigated. However, in any of the case no film was detected. The uniform heating of TDMAZ containing bubbler and/or prolonged pre-heating (at least 3 hours prior to any ALD run) of TDMAZ bubbler with slow ramp of temperature might be useful to try for successful ALD of ZrO_2 from TDMAZ precursor. Afterwards, ALD of ZrO_2 on SiO_2/Si was also attempted using Tris(dimethylamino)cyclopentadienyl Zirconium (ZyALD) precursor and ethanol as oxidizer at reaction temperature of 200°C. ZrO_2 thin film with thickness of 12.8±1.7 nm was achieved on SiO_2/Si samples. Although the deposited film

is very uniform (±0.5 nm) for each sample surface like a typical ALD process, the growth rate is not consistent for all the samples and it keep increasing from 1st ALD run to consecutive runs. Additionally, some unreacted excess precursor was also found inside reactor chamber. Higher flow-rate (37 mL/min) of inlet precursor carrier gas most likely the reason behind such observation. Efforts are being made to tune the flow rate for avoiding such problem. Bubbler without any deep tube in the inlet section (flow over delivery system) might also help to resolve this problem.

VITA

Arghya Kamal Bishal

Education

Ph.D., Bioengineering

University of Illinois at Chicago, USA

May 2018

B.Tech., Biotechnology

Haldia Institute of Technology,

West Bengal University of Technology, India

May 2013

Experience

Validation Engineer

TechnoPro Solutions Inc., USA

Jun 2017 – Aug 2017

Patents

Sukotjo, C., Takoudis, C. G., Bishal, A.K. Biofunctionalization of Collagen Membrane with thin film of TiO_2 deposited using Atomic Layer Deposition technique to accelerate bone formation process, in the process of filing U.S. Patent (2017)

Sukotjo, C., Bishal, A.K., Takoudis, C. G. Conductive collagen a novel material for green transient electronics, in the process of filing U.S. Patent (2017)

Publications

Bishal A. K., Sukotjo C., Takoudis C. G.: Room temperature TiO_2 atomic layer deposition on collagen membrane from a titanium alkylamide precursor, Journal of Vacuum Science & Technology A: Vacuum, Surfaces, and Films, 35(1):01B134 (2017)

Publications

Bishal A. K., Butt A., Selvaraj S. K., Joshi B., Patel S. B., Huang S., Yang B., Shukohfar T., Sukotjo C., Takoudis C. G.: Atomic Layer Deposition in Bio-Nanotechnology: A Brief Overview, Critical Reviews™ in Biomedical Engineering, 43(4) (2015)

Bishal A. K., Grotberg J., Sukotjo C, Mathew M. T., Takoudis C. G.: Human Osteoblast Cell-Ti6Al4V Metal Alloy Interactions under Varying Cathodic Potentials: A Pilot Study, Journal of Bio Tribo-Corrosion, 1;3(3):40 (2017)

Bishal A. K., Sukotjo C., Wee A. G., Barão V. A. R., Yuan J., Landers R., Takoudis C. G.: Color stability of maxillofacial prosthetics silicone functionalized with oxide nano coating, under review with Journal of Prosthetics Dentistry.

Bishal A. K., Sukotjo C., Takoudis C.G.: In-vitro Bioactivity of Collagen Membrane Functionalized with Room Temperature ALD-TiO_2, Submitted.

Bishal A. K., Sukotjo C., Takoudis C. G.: Highly Conductive and Flexible Biomaterial Achieved by Low Temperature Atomic Layer Deposition of Platinum on Collagen, Submitted.

Selvaraj S. K., Chang S., Bishal A. K., Butt A. and Takoudis C. G.: Photoactivated disinfection of titanium dental implants coated with atomic layer deposited tin doped titanium oxide, Submitted.

Darwish G., Huang S., Bishal A. K., Barão V. A. R., Sukotjo C., Takoudis C. G., Yang B.: Improving Polymethyl methacrylate Resin Using a Novel Nano-ceramic Coating, Accepted for publication with Journal of Prosthodontics.